QUANTIFICATION OF RAIL SEAT LOAD DISTRIBUTIONS ON CONCRETE CROSSTIES

BY

MATTHEW J. GREVE

THESIS

Submitted in partial fulfillment of the requirements
for the degree of Master of Science in Civil Engineering
in the Graduate College of the
University of Illinois at Urbana-Champaign, 2015

Urbana, Illinois

Advisors:

Professor Christopher P.L. Barkan
Senior Lecturer J. Riley Edwards

ABSTRACT

As higher demands are placed on North American railroad infrastructure by heavy haul traffic, it is increasingly important to understand the factors affecting the magnitude and distribution of load imparted to concrete crosstie rail seats. The rail seat load distribution is critical to the analysis of failure mechanisms associated with rail seat deterioration (RSD), the degradation of the concrete surface at the crosstie rail seat. RSD can lead to wide gauge, cant deficiency, and an increased risk of rail rollover, and is therefore of primary concern to Class I Freight Railroads in North America. As part of a larger study aimed at improving concrete crossties and fastening systems, researchers at UIUC are attempting to characterize the loading environment at the rail seat using matrix-based tactile surface sensors (MBTSS). This instrumentation technology has been implemented in experimentation utilizing both field conditions and laboratory facilities, and has provided valuable insight to further previous RSD research. This thesis will examine the results of experimentation with MBTSS to quantify the distribution of rail seat loads on concrete crossties, and consider several factors which affect the distribution of load at concrete crosstie rail seats. These findings will then be applied to new design metric, which is proposed to evaluate the uniformity of the rail seat load distribution. The findings of this thesis will ultimately lead to an improved understanding of the distribution of load on concrete crosstie rail seats, and will lead to crosstie and fastening system designs which are inherently resistant to RSD.

to my friends and family,

for your undying support and encouragement

ACKNOWLEDGEMENTS

This thesis could not have been completed without the contributions of a number of individuals, both in the railroad industry and beyond. Their support has made this research and my entire graduate school experience much more than it could have ever been without them.

I would like to start by thanking Amsted RPS for funding my graduate studies and research assistant position, and for providing critical resources necessary to conduct laboratory experimentation. I would also like to thank the Federal Railroad Administration for funding RailTEC's crosstie and fastening system research project through the 2010 Broad Agency Announcement, and especially Cam Stuart and Hugh Thompson for their guidance and support for the project. Thanks to the Transportation Technology Center, Inc. for funding research utilizing their artificial RSD facility, and for their support during field experimentation at their facilities. Thank you also to Michael and Jean Franke and AREMA Committee 30 (Ties) for your financial support through the AREMA Scholarship program.

Next, I would like to thank the individuals in the railroad industry who have supported this research. Thank you to our FRA Tie and Fastener BAA industry partners for their support and insight: Union Pacific Railroad; BNSF Railway; National Railway Passenger Corporation (Amtrak); Amsted RPS / Amsted Rail, Inc.; GIC; Hanson Professional Services, Inc.; and CXT Concrete Ties, Inc., an LB Foster Company. For providing advice, direction, and support, I would also like to thank Jose Mediavilla and Chase Nelson from Amsted RPS, Al Cloutier, Mike Trosino, and Joe Smak from Amtrak, Darwin Schafer from Benesch, John Bosshart from BNSF Railway (ret.), Dave Davis and Mike McHenry from the Transportation Technology Center, Inc., John Jeambey from TTX Company, and Brian Marquis and Theodore Sussmann from the Volpe National Transportation Systems Center. Thank you also to the members of AREMA Committee 30 (Ties) for the encouragement and advice that you have provided to my peers and me. Your support has helped our research leave a lasting impact on the industry.

Thank you to the students, faculty, and staff at RailTEC. For providing comments, support, experience, and input, I would especially like to thank Thiago Bizarria do Carmo, Sam Chadwick, Donovan Holder, Alexander Lovett, Andrew Scheppe, Marcelo Suarez, Sihang Wei, Brent Williams, and

Henry Wolf. Thanks to Douglas Capuder, Matt Csenge, Zachary Ehlers, Zachary Jenkins, and Daniel Rivi for their assistance with data collection and analysis. Thanks also to Mauricio Gutierrez, Ryan Kernes, Chris Rapp, and Tristan Rickett for their guidance and for kindling my interest in railroad research when I was an undergraduate. Thank you to Conrad Ruppert and Dr. Don Uzarski for providing invaluable insight and contributions as industry experts and classroom instructors, and for instilling in me that there is no one-size-fits-all answer: as Dr. Uzarski would say, "it depends." Thanks also to Tim Prunkard, Marc Killion, and the entire Newmark Structural Engineering Laboratory Machine Shop for their assistance with experimental setup and in preparing and calibrating instrumentation.

There are not enough words to adequately express my thanks to those who have had an advisory role in my graduate research. Thank you to Professor Chris Barkan for providing oversight of my work, and for always challenging me to find the clearest, most concise way to effectively present my data. Thank you to Riley Edwards for making time to provide positive and constructive guidance and encouragement in all matters academic, research, and personal from the first time I set foot on the UIUC campus. Thank you also to Senior Research Engineer Marcus Dersch and Research Engineers Ryan Kernes (now with GIC) and Yu Qian for always challenging me to take my research one step further.

Thank you to the faculty at UIUC, Indian Springs School, and Hilltop Montessori not only for expanding my knowledge, but also for helping me grow as a person. I would also like to thank you for investing your time and effort in all of their students, making the world a better place.

Lastly, and most importantly, I would like to thank my family and friends who have not otherwise been mentioned here. Thank you to my mother, Helen, and father, Mark, for the tireless and unwavering support, encouragement, and guidance that you have provided my entire life. Thank you to my sister, Christine, for being a friend and source of encouragement. And thank you to Will Carlson, Brennan Caughron, Joel Hurneman, Jonathan Lee, Tyler Perona, Christian Poole, Jesse Strode, Mike Wnek, and especially Isaac Grant, James Jordan, and Aurora Uncia for your support and friendship.

TABLE OF CONTENTS

CHAPTER 1: INTRODUCTION

1.1. Background

As the demand in North America for high-performance, low-maintenance railroad infrastructure continues to grow, concrete crossties and elastic fastening systems are becoming increasingly common. Concrete crossties are typically used in areas of high curvature and steep grades on lines that experience high-speed, higher-speed, or heavy-axle load traffic, and as of 2010, 25 million crossties are in service in North America (Zeman 2010). Because of the increasingly frequent use of concrete crossties and elastic fastening systems in these demanding environments, it is important to understand the factors leading to common performance failures of concrete crossties and fastening systems.

One of the most common failures of concrete crossties is the degradation of the concrete material directly below the rail, in the area of the crosstie known as the rail seat. This degradation is commonly referred to as rail seat deterioration (RSD), or formerly as rail seat abrasion (RSA) (AREMA 2014). Figure 1.1 illustrates an extreme instance of RSD, with the depth of wear increasing towards the field side of the rail seat. More common examples of RSD can be shown in Figure 1.2, showing the variety of ways in which this determination mechanism manifests itself. RSD has become a problematic failure for concrete crossties since it was first observed on Canadian National in the 1980's, and is most common on routes with steep grades, high curvature, and in the presence of moisture (Zeman 2010). If left untreated, RSD may lead to accelerated wear of the fastening system, wide gauge, excessive rail cant, and an increased risk of derailment due to rail rollover, as in the cases of two Amtrak passenger trains, one near Sprague, Washington in 2006 and the other near Home Valley, Washington in 2005 (Zeman 2010, FRA 2006, and NTSB 2006).

FIELD

GAUGE

Figure 1.1 Extreme rail seat deterioration (RSD) wear pattern (NTSB 2006)

FIELD

(a) Moderate tangent RSD

(b) Severe tangent RSD

(c) Light curve RSD

(d) Severe curve RSD in track

GAUGE

Figure 1.2 Other typical RSD wear patterns

In order to understand the severity of concrete crosstie and fastening system failures, and to evaluate research needs as perceived by the railroad industry, researchers at the University of Illinois at Urbana-Champaign (UIUC) conducted a survey of North American railroad industry experts, representing railroads, crosstie and fastening system manufacturers, and research institutions. The findings of the survey showed that RSD is considered the most critical problem with concrete crossties and fastening systems in North America. Additionally, RSD was ranked as the area of crosstie and fastening system research most in need of research (Van Dyk 2014). It is therefore apparent that there is a need for research examining the causes and failure mechanisms of RSD on concrete crossties and fastening systems.

1.2. Previous Research on RSD

Extensive research has been conducted in the past to identify potential failure mechanisms of RSD and determine the feasibility of these mechanisms. Initial research performed at UIUC by Tatiana Bakharev (1997) compared the microstructure of field-worn RSD to that of wear generated by specific, potential failure mechanisms expected to result in RSD. Bakharev identified similarities between damage to the rail seat from RSD and damage to laboratory specimens from abrasion, freeze-thaw cracking, and an analytical model of hydraulic pressure cracking (Bakharev 1997). She concluded that a combination of the three aforementioned failure mechanisms may generate RSD. Her work was furthered by John Zeman (2010), who identified six potential failure mechanisms by which RSD may be initiated: abrasion, crushing, freeze-thaw cracking, hydraulic pressure cracking, hydro-abrasive erosion, and cavitation erosion. Zeman further investigated the effect of moisture on these failure mechanisms. He determined that cavitation erosion was not a feasible failure mechanism in field conditions, and that hydraulic pressure cracking, though feasible, had a relatively insignificant effect compared to other failure mechanisms (Zeman 2010).

Ryan Kernes (2013) later expanded on Zeman's work, focusing on the complex mechanisms of abrasion. Kernes conducted extensive laboratory tests examining the effect of relative slip and coefficient of friction at the rail-pad interface. He developed a novel laboratory testing procedure, the Large-Scale

Abrasion Test, which was designed to replicate component interactions at the rail pad assembly-rail seat interface. Specimens of representative materials for both the rail pad assembly and rail seat were subjected to small, repeated displacements at contact pressures ranging from 400 to 1,800 pounds per square inch (psi). Due to the presence of abrasion at all tested load magnitudes, Kernes concluded that abrasion should be considered the critical RSD failure mechanism against which concrete crossties and fastening systems are designed (Kernes 2013).

Research conducted by Chris Rapp (et al. 2013) at UIUC utilizing matrix-based tactile surface sensors (MBTSS) has highlighted the effect of rail pad modulus and fastening system type on the loading environment at the rail seat. Rapp's findings indicated that while rail pads with a lower flexural modulus distribute rail seat loads over a higher contact area, resulting in lower pressures, they allow for greater rail rotation than a rail pad with a higher flexural modulus. Similarly, while rail pads with a higher flexural modulus restrict rail rotation, which improves track geometry conditions, they are not able to distribute the rail seat load over a large area, and therefore result in higher pressures at the rail seat. The results indicated that a more common two-part rail pad assembly, consisting of both low- and high-flexural modulus components, provides the combined benefits of both single-component rail pads tested. Further, Rapp's findings showed that the design of the clip can affect the shape of the rail seat load distribution, but that the pressures observed under the tested fastener types did not vary significantly (Rapp et al. 2013).

In addition to research at UIUC, the John A. Volpe National Transportation Systems Center (hereafter referred to as "Volpe") has modeled RSD to evaluate its consequences on track geometry. Following the derailment of two passenger trains due to severe RSD, Volpe utilized analytical modeling to understand the loading environment at the crosstie rail seat as a factor contributing to the failure mechanisms associated with RSD (Choros et al. 2007). By utilizing concepts from the design of foundation footings, Volpe was able to estimate the distribution of load as trapezoidal when the resultant of the reaction on the rail base from the crosstie rail seat was located within the middle third of the rail base (i.e. the absolute value of the distance from the resultant force to the centerline of the rail was less

than one-sixth the width of the rail base), and triangular when this resultant force was located outside this middle third of the rail base. After obtaining input loads from a NUCARS™ model representing train characteristics and track geometry representative of the derailment cases in question, Volpe's findings suggested that pressures exerted on the crosstie rail seat may exceed 16,000 psi (Choros et al. 2007).

1.3. Instrumentation Technology

To characterize the distribution of load at the crosstie rail seat, researchers at UIUC have utilized MBTSS. The MBTSS system used by UIUC is manufactured by Tekscan® Inc. and consists of rows and columns of conductive ink which, when pressed together by a load applied normal to the contact plane, output a change in resistivity at each intersection of a row and a column. This output, termed a "raw sum", can be interpreted as the pressure exerted on the sensor at a given intersection when given the total applied load. MBTSS simultaneously outputs the area over which this load is applied. This is termed the "contact area" of the load and is calculated from the number of sensing locations that indicate an applied load. Data are collected from the entire sensing area at a maximum rate of 100 Hz. The data are calibrated during analysis using a known or assumed input load.

Previous experimentation at the University of Kentucky (UK) and UIUC have shown that MBTSS are susceptible to shear and puncture damage (Stith 2005, Rapp et al. 2012). To protect the sensors, layers of biaxially-oriented polyethylene terephthalate (BoPET) and polytetrafluoroethylene (PTFE) are secured to both sides of a sensor that has been trimmed to fit the rail seat. The assembly is then installed between the rail pad assembly and the concrete crosstie rail seat (Figure 1.3) (Rapp et al. 2012).

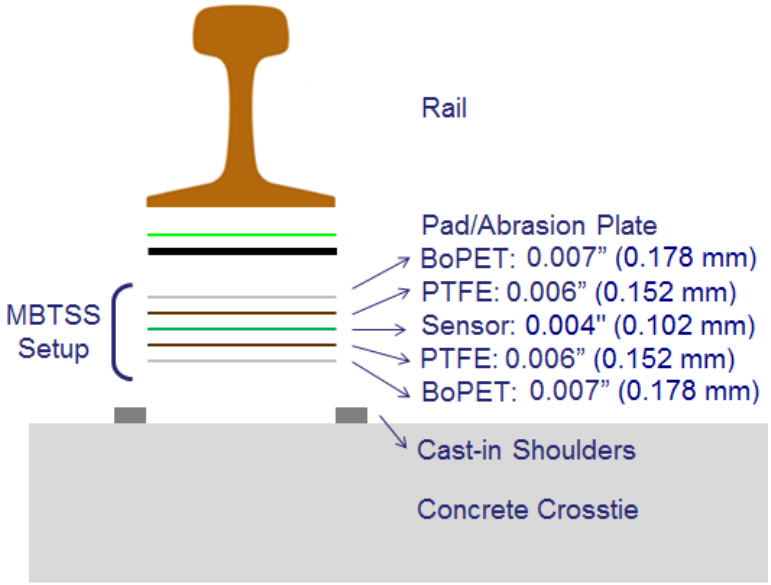

Figure 1.3 MBTSS layers and thicknesses (adapted from Rapp et al. 2012)

1.4. Motivation for Research

Recently, researchers at UIUC have undertaken a project, funded by the Federal Railroad Administration (FRA), to investigate common failures with concrete crossties and elastic fastening systems. As part of this project, further investigation of the causes and failure modes associated with RSD was desired, with the goal of incorporating the findings therein with other FRA-funded research to generate a framework for the mechanistic design of concrete crossties and their fastening systems. In this design philosophy, components are designed from expected outputs and relationships based on projected critical inputs, rather than from simple empirical equations. It is believed that such a design approach would establish a clearer procedure for designing crossties and fastening systems, resulting in fewer service failures and higher reliability of the track structure and its components (RailTEC 2015).

In order to effectively address RSD, it is important to first understand the causes associated with RSD and the failure mechanisms by which it is initiated and propagated. Table 1.1 summarizes the relationships between commonly identified causes of RSD and the five failure mechanisms proposed by Zeman (2010). Of these failure mechanisms, four are affected by "high stresses at the rail seat", which can be directly attributed to the distribution of loads at the rail seat. While extensive research has been

conducted examining the effect of moisture (Zeman 2010) and relative motion (Kernes 2013), which similarly contribute to four of five RSD failure mechanisms, relatively little research has been conducted concerning the rail seat load distribution. It is therefore apparent that in order to further our understanding of RSD failure mechanisms, there is a great need for research quantifying the rail seat load distribution on concrete crossties and examining the factors that affect it.

Table 1.1 Relevance of the causes of RSD to potential concrete failure mechanisms (adapted from Zeman 2010)

	Concrete Failure Mechanisms				
Causes	Abrasion	Crushing	Freeze-Thaw	Hydraulic Pressure	Hydro-Abrasive
High stresses at rail seat	✓	✓		✓	✓
Relative motion at rail seat	✓	✓		✓	✓
Presence of moisture	✓		✓	✓	✓
Presence of abrasive fines	✓				✓

1.5. Thesis Scope

This study will quantify rail seat pressures on concrete crossties and consider factors which affect the distribution of load at concrete crosstie rail seats. The effect of loading environment, fastener health, rail seat deterioration, and particle intrusion will be examined through targeted laboratory and field experimentation. This data will be used to support the development of a new design metric that quantifies the uniformity of the rail seat load distribution. The research detailed in this thesis will facilitate the design of concrete crossties and elastic fastening systems which are more inherently resistant to rail seat deterioration.

1.6. Thesis Organization

This thesis is comprised of six chapters, including an introduction, conclusion, and four sections within the body of the thesis. These chapters within the body of the thesis will address the following questions concerning the distribution of loads at the concrete crosstie rail seat:

1. How do input load and fastener health affect the magnitude of rail seat pressures? (Chapter 2)

2. How does the presence and severity of RSD affect the distribution of loads at the crosstie rail seat? (Chapter 3)
3. Is crushing a feasible failure mechanism by which RSD may be initiated? (Chapter 4)
4. How can the findings of this thesis be applied to further the design methodology for crossties and fastening systems in the context of a framework for mechanistic design? (Chapter 5)

CHAPTER 2: ANALYSIS OF THE EFFECT OF LOADING ENVIRONMENT AND FASTENER WEAR ON RAIL SEAT LOAD DISTRIBUTIONS[1]

2.1. Introduction

As described in Chapter 1 of this thesis, previous research into characteristics of RSD relied on analytically-calculated rail seat pressures. Studies conducted by Volpe and UIUC had previously determined typical rail seat pressures using empirical methods further described in the body of this chapter. As part of research funded by the FRA to improve the design of concrete crossties and their fastening systems, researchers at UIUC conducted field experimentation to measure forces, strains, and displacements associated with the North American heavy haul freight loading environment. Rail seat load distributions captured using MBTSS were analyzed to quantify the effect of the loading environment on rail seat pressures. The data were compared to the analytical models used by Volpe and UIUC to augment the knowledge gained from their findings, and to further explore the role of the rail seat load distribution in the formation of RSD.

While the conditions represented by data collected from field experimentation are representative of those in revenue service, they introduce inherent variability due to component wear, crosstie support conditions, and repeatability of load application. Additional data were therefore collected from laboratory experimentation to complement the data from field experimentation, allowing for comparison to a more controlled setting. Preliminary results indicated that the wear experienced by the fastener clips in the field may have had a significant impact on the distribution of loads at the rail seat. Therefore, data from the laboratory were analyzed to further explore the effect of fastener wear.

[1] Much of Chapter 2 was originally published in the Proceedings of the 2014 Joint Rail Conference in Colorado Springs, Colorado, USA (Greve et al. 2014) and the Proceedings of the 2015 Joint Rail Conference in San Jose, California, USA (Greve et al. 2015b)

2.2. Field Experimentation

Field experimentation was performed at the Transportation Technology Center (TTC) in Pueblo, Colorado, USA; a railroad research and testing facility that consists of 48 miles (77.2 km) of track with variable geometries and operating conditions. A section of 15 new concrete crossties with Safelok I shoulders and fastening systems was installed on the 13.5 mile (21.7 km) Railroad Test Track (RTT) in a section of tangent track. Eight rail seats, on five crossties, at this site were instrumented with MBTSS, as shown in Figure 2.1. Five consecutive rail seats (located on the near rail, rail seats 1N through 5N) were chosen in an attempt to fully capture the vertical load distribution, and to investigate the effect and variability of support conditions in a group of crossties. Additionally, three consecutive rail seats on the opposite rail (located on the far rail, rail seats 2F through 4F) were selected to provide further information on load transfer, and to examine the variability of support conditions across a single crosstie.

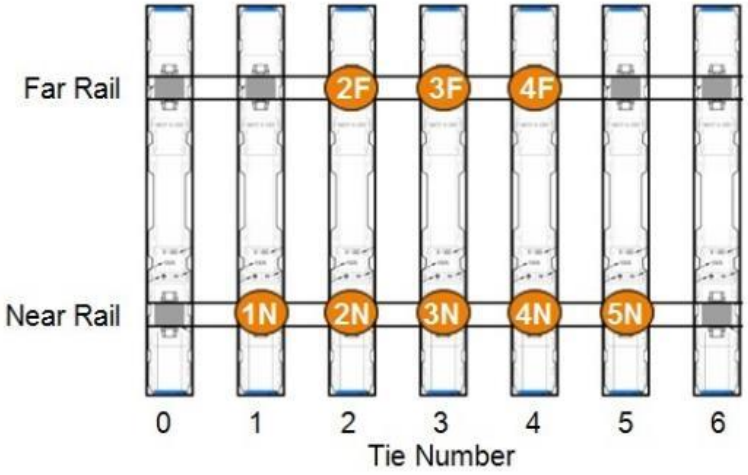

Figure 2.1 Plan view of MBTSS field installation at TTC

Although the rail pad assemblies and insulators were replaced prior to field experimentation, the clips were not. At the time of experimentation, the clips had been subjected to 5 million gross tons (MGT) of traffic and three cycles of removal and reapplication. It was hypothesized that the wear of the clips, especially due to the three reapplications, significantly reduced the applied toe load. This reduced the ability of the fastening system to resist rail rotation under lateral load, which may affect this distribution of rail seat loads.

2.3. Laboratory Instrumentation

Laboratory experimentation was performed at the Research and Innovation Laboratory (RAIL) at Schnabel, a facility owned by UIUC, operated by the Rail Transportation and Engineering Center (RailTEC), and used for conducting research on railroad infrastructure systems and components. Experiments were conducted using the Track Loading System (TLS), a loading frame which can accommodate a 22 foot (6.7 m) section of track with full depth substructure, shown in Figure 2.2. A track segment of 11 concrete crossties with Safelok I shoulders was constructed to Class I specifications and instrumented to replicate field conditions. Figure 2.3 shows a plan view of the MBTSS installation on the TLS. Five consecutive rail seats on the TLS were instrumented with MBTSS to fully capture the vertical load distribution and investigate the variability of support conditions.

Figure 2.2 Track loading system (TLS) installation during experimentation

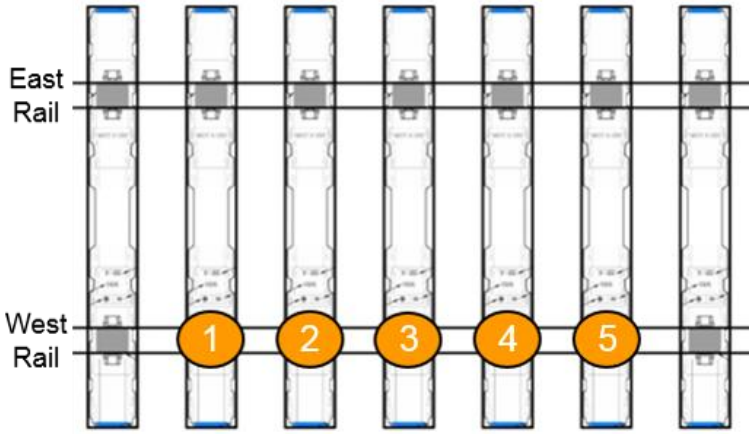

Figure 2.3 Plan view of MBTSS lab installation on the TLS

During laboratory experimentation, any clips that were removed were replaced with new clips to maintain an unworn condition. Although other sources of variation exist between the TLS and the RTT, it is believed that the health of the fastening system had the greatest effect of the possible variables between laboratory and field rail seat load distribution results for identical loading environments.

During data analysis, rail seats 3 and 5 were observed to have significantly lower rail seat loads than those recorded on rail seats 1, 2, and 4. Although the entire track structure was tamped using a pneumatic hand tamper prior to experimentation, gaps measuring several millimeters in height had developed under rail seats 3 and 5, resulting in poor load transfer at the crosstie-ballast interface. This resulted in significant skewing of the data when results from all five rail seats were averaged, leading to an underestimation of the rail seat pressures. The data from rail seats 3 and 5 were therefore excluded from further analysis; the analysis subsequently presented in this chapter is based on averaged data from rail seats 1, 2, and 4, the properly-supported crossties.

2.4. Experimentation Loading Environment

The application of loads during field experimentation was accomplished using the Track Loading Vehicle (TLV). The TLV is owned by the Association of American Railroads (AAR) and operated by the Transportation Technology Center, Inc. (TTCI). The TLV can be used to study a variety of scenarios including wheel climb derailments, vertical modulus, lateral track strength, gage widening, and wheel/rail force relationships (Schust et al. 1997). An instrumented wheelset is attached to vertically- and laterally-

oriented actuators, which are attached to the frame of a modified rail car. The TLV's ability to apply controlled vertical and lateral loads to the rail using realistic loading conditions and application made it an ideal tool for the purposes of this experimentation.

The application of loads during laboratory experimentation was accomplished using the TLS. For this experimentation, vertical loads were applied using two hydraulic actuators, and the lateral loads were applied using a single manually-operated hydraulic jack as shown in Figure 2.2. The vertical loads were applied to both journals of a standard 36 inch (91.4 cm) wheelset through standard journal adaptors, and the lateral loads were applied towards the West (instrumented) Rail.

The testing procedure in both the field and the lab consisted of applying loads to both rails with the loading axle centered above each instrumented crosstie. Vertical loads were applied to each rail at increasing magnitudes from 0 to 40,000 lbf (178 kN) at 5,000 lbf (22.2 kN) increments. In the field, gauge-widening lateral forces were applied at a 20,000 lbf (88.9 kN) vertical load, resulting in Lateral over Vertical (L/V) force ratios ranging from 0.0 to 0.6 at 0.1 increments, and at a 40,000 lbf (178 kN) vertical load, resulting in L/V force ratios ranging from 0.0 to 0.5 at 0.1 increments, followed by a final increment of 0.05, resulting in a final L/V force ratio of 0.55. In the lab, lateral forces were applied at 10,000 lbf (44.5 kN), 20,000 lbf (88.9 kN), 30,000 lbf (133 kN), and 40,000 lbf (178 kN) vertical loads, resulting in L/V force ratios ranging from 0.0 to 0.6 at 0.1 increments at all four vertical loads.

2.5. Modeling Rail Seat Load Eccentricity

To better understand the cause of RSD's signature triangular wear pattern, Volpe modeled the effect of lateral load on the rail seat load distribution (Choros et al. 2007). The rail and rail seat are assumed to be infinitely stiff bodies, and concepts from the design of building footings are used to describe the change in load distribution as lateral load increases. Volpe considered the eccentricity of the overturning moment about the center of the rail base, and determined that if the eccentricity is within the middle third of the base (i.e. the absolute value of the eccentricity is less than or equal to one-sixth the width of the rail base), the load distribution is trapezoidal, with pressures at the gauge and field sides of the rail base calculated as:

$$p_g = \frac{P}{b} \times (1 - \frac{6e}{b})$$

and

$$p_f = \frac{P}{b} \times (1 + \frac{6e}{b})$$

where, p_g = Pressure on gauge side of rail base

p_f = Pressure on field side of rail base

P = Centerline vertical load

b = Rail base width

e = Eccentricity, the applied moment divided by the vertical load (M/P)

If the eccentricity is beyond the middle third of the rail base, the distribution is triangular, with the pressure at the field side of the rail base calculated as:

$$p_f = \frac{2P}{3 \times (\frac{b}{2} - e)}$$

where, p_f = Pressure on field side of rail base

P = Centerline vertical load

b = Rail base width

e = Eccentricity, the applied moment divided by the vertical load (M/P) (Choros et al. 2007)

The expression for eccentricity can now be redefined in terms of the applied lateral and vertical loads and the lever arms with which they act, relative to the centerline of the rail base. As described above, the critical eccentricity at which the gauge side of the rail seat becomes unloaded is one-sixth the width of the rail base. It is assumed that when critical eccentricity is achieved, both the lateral and vertical loads are applied directly above the rail seat at the gauge face of the rail. Therefore, at critical eccentricity:

$$e_{crit} = \frac{b}{6} = \frac{M}{P} = \frac{L_{\text{crit}} \times h_g - V_{\text{crit}} \times \frac{w_h}{2}}{V_{\text{crit}}}$$

where, e_{crit} = Critical eccentricity resulting in triangular load distribution

b = Rail base width

M = Applied moment relative to rail base center

P = Centerline vertical load

L_{crit} = Critical lateral wheel load

V_{crit} = Critical vertical wheel load

h_g = Height from rail base to gauge face

w_h = Width of rail head

Although Choros et al. did not specify an equation to convert lateral load into an overturning moment, they did state that they assumed that the rail pad assembly did not distribute the rail seat load and that the fasteners provided no contribution to the moment (i.e. through clamping force applied to the rail base) (Choros et al. 2007). Thus, it can be assumed that the only contributions to the moment are the lateral and vertical load eccentricities, as described above. The equation for the critical eccentricity can therefore be rearranged to obtain an expression for the critical L/V force ratio:

$$\frac{L}{V}_{crit} = \frac{L_{\text{crit}}}{V_{\text{crit}}} = \frac{\frac{b}{6} + \frac{w_h}{2}}{h_g}$$

where, L/V_{crit} = Critical L/V force ratio resulting in triangular load distribution

L_{crit} = Critical lateral wheel load

V_{crit} = Critical vertical wheel load

b = Rail base width

h_g = Height from rail base to gauge face

w_h = Width of rail head

If the dimensions of a 136RE rail section, the rail size used in field experimentation at TTC, are used, the critical L/V force ratio can be calculated as 0.37. At this L/V force ratio, the gauge side of the rail seat will become unloaded, and the load distribution will develop a significant concentration on the field side of the rail seat.

This calculated critical L/V force ratio can be compared to results from field experimentation with MBTSS. All eight instrumented rail seats experience a loss of contact area at a "threshold" L/V ratio. When a 40,000 lbf (178 kN) vertical load is applied, this threshold L/V occurs between 0.3 and 0.4, which agrees with the calculated critical L/V force ratio derived from the Volpe model (Figure 2.4). However, when the vertical load is reduced to 20,000 lbf (88.9 kN), this threshold L/V occurs between 0.2 and 0.3: the predicted critical L/V now overestimates this threshold (Figure 2.5).

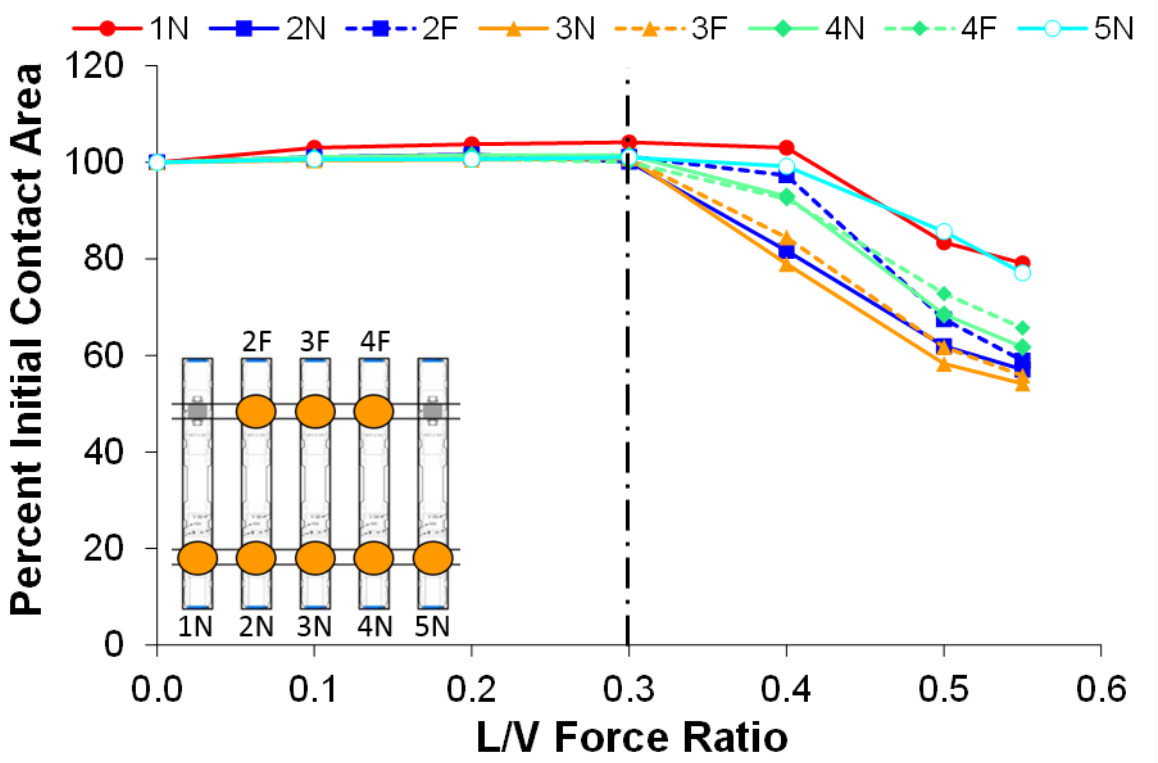

Figure 2.4 Loss of contact area under 40,000 lbf (178 kN) vertical wheel load

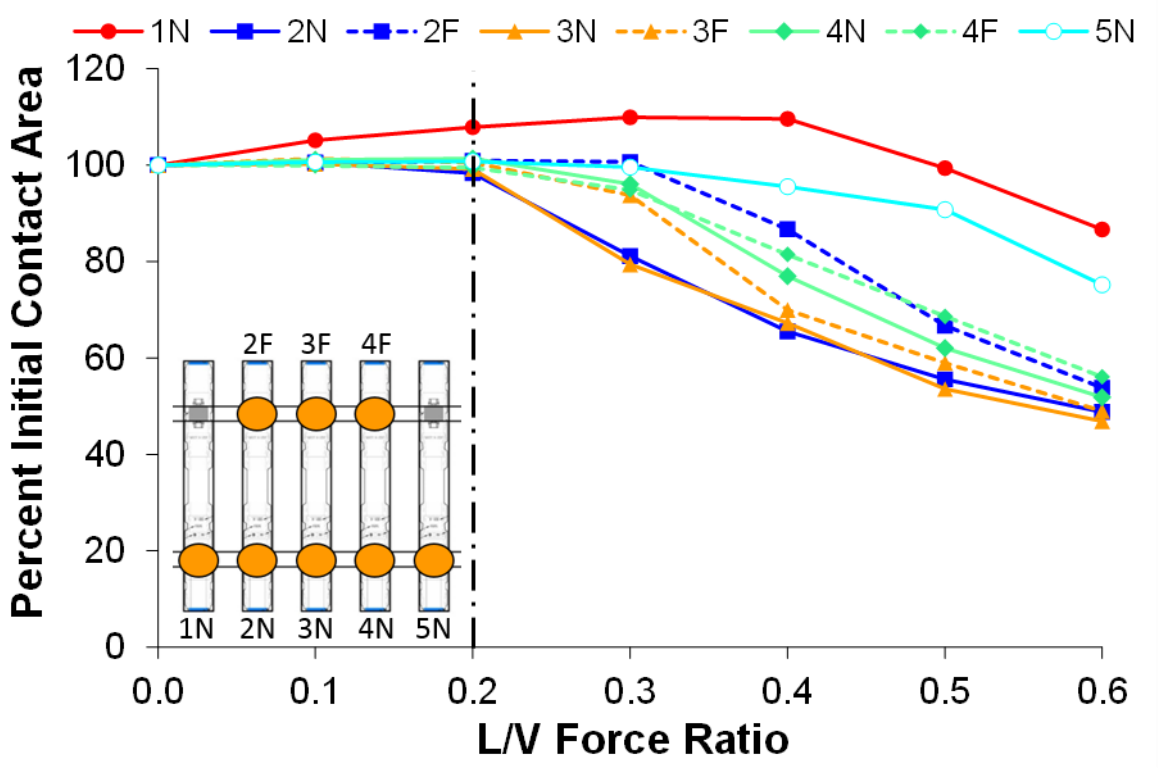

Figure 2.5 Loss of contact area under 20,000 lbf (88.9 kN) vertical wheel load

This behavior of the contact area may be a result of the reaction against the lateral load. A higher vertical force would increase the available frictional force at the rail base-rail pad interface, which counter the lateral wheel load. At the critical L/V force ratio, the lateral load may overcome this frictional force, causing the rail to slip to bear against the insulator post and cast-in shoulder. Once this slip occurs, this new bearing point may become a pivot about which the rail can rotate. A lower vertical wheel load would reduce the capacity of the rail pad frictional force, resulting in slip at a lower lateral load.

A second contributing factor could be the location of the wheel/rail contact patch. Below the threshold L/V, the contact patch is located on the head of the rail rather than the gauge face, and only shifts once the lateral load overcomes frictional forces at the wheel/rail interface. Under a 20,000 lbf (88.9 kN) vertical load, these frictional forces would be reduced, meaning that less lateral load is required to cause the wheel to slip laterally. This slip relative to the head of the rail would reduce the lever arm with which the vertical load acts to resist the overturning moment. More detailed analysis of the resisting

moments applied by the vertical wheel load and fastening system toe loads could further refine this model.

2.6. Contact Pressure and Abrasion

Researchers at UIUC conducted several representative experiments to examine the effect of abrasion on interactions at the rail pad-rail seat interface. These experiments involved the construction of a bi-axial loading frame which could apply vertical and lateral loads to specimens representing rail pads of varying material and rail seats. To establish a loading regime, they calculated the average pressure on a rail seat, assuming uniform load distribution over the entire rail seat. This value was estimated to be between 400 psi and 1,800 psi (2.76 MPa and 12.41 MPa, respectively), depending on the applied vertical load. Their findings indicated that in all loading cases, a specimen of nylon 6-6 (a typical rail pad material) will produce abrasion given repeated, small-displacement slip at the rail pad-rail seat interface (Shurpali et al. 2013).

To compare this assumption to data from field experimentation, we will examine the average change in rail seat pressure observed during field experimentation. It is assumed that each rail seat supports half of the vertical wheel load applied directly above it, and that the other half is distributed across the four crossties closest to the point of loading (i.e. two crossties to either side of the center crosstie). This approximation is derived from both experimental field data and literature on rail seat load magnitudes (RailTEC 2015). Therefore, for a 40,000 lbf (178 kN) vertical wheel load, we can approximate the total rail seat load as 20,000 lbf (88.9 kN), which will remain constant as the L/V force ratio increases.

This analysis will consider three different quantifications of pressure: uniform, average, and maximum. Uniform pressure is calculated by assuming a uniform distribution of the rail seat load across the entire area of the rail seat, the same method as was used to determine input loads for the previously mentioned abrasion tests. Average pressure is calculated by distributing the rail seat load over the observed contact area, the actual portion of the rail seat engaged in load transfer during a given test. Maximum pressure is calculated by determining the conversion factor between the total raw sum recorded

by MBTSS and the input load, and then applying this conversion factor to the sensing location with the highest raw sum.

Figure 2.6 illustrates the change in uniform, average, and maximum pressure due to increasing L/V force ratio at a constant vertical wheel load. By definition, the uniform pressure is unaffected by the change in L/V and remains constant at 556 psi (3.83 MPa), because it assumes that the contact area does not change. Below the previously observed threshold L/V force ratio (between 0.3 and 0.4), average pressure plots very close to the uniform pressure, indicating that the entire rail seat is loaded. Beyond the threshold L/V force ratio, average pressure increases 45% to 817 psi (5.63 MPa), or 47% greater than the uniform pressure. The maximum pressure is considerably higher than both the uniform and average pressures, starting at 1,179 psi (8.13 MPa), or 112% greater than the uniform pressure. It increases to 1,996 psi (13.76 MPa) at 0.5 L/V, a 69% increase from the 0.0 L/V case, or 259% higher than the uniform pressure. Though not illustrated in Figure 2.6, the location of the maximum pressure trends toward the field side of the rail seat as the L/V ratio increases; this coincides with a shift in the centroid of loading from the center of the rail seat 1.88 in (47.78 mm) toward the field side, or 1.25 in (31.75 mm) from the field side shoulder at 0.5 L/V.

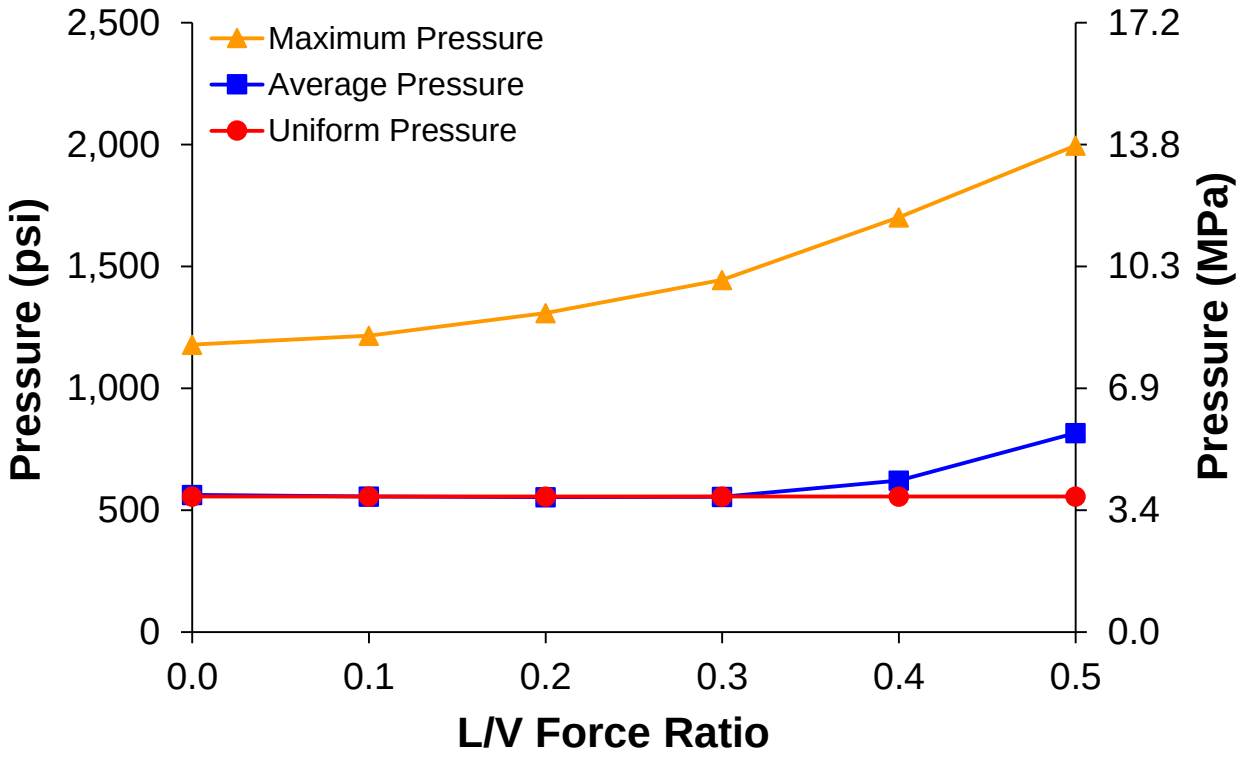

Figure 2.6 Change in rail seat pressures at 40,000 lbf (178 kN) vertical wheel load

Figure 2.6 shows that the assumed range of 400 to 1,800 psi (2.76 MPa and 12.41 MPa) used in the abrasion experimentation at UIUC adequately bounds the average pressure exerted on the rail seat under typical loads for North American heavy-axle freight traffic. However, it does not capture the maximum pressures observed at high lateral loads (above 0.4 L/V force ratio). Wear patterns of mild or newly-formed RSD suggest that RSD first develops at these areas of extreme pressure, expanding as the loss of material becomes more severe. More detailed analysis of the characteristics of abrasion at higher pressures, perhaps exceeding 2,000 psi (13.79 MPa), and how they differ from the characteristics of lower-pressure abrasion could lead to a better understanding of abrasion as a failure mechanism for RSD.

2.7. Effect of Fastener Wear

Figure 2.7 compares the qualitative effect of L/V force ratio under a constant 40,000 lbf (178 kN) vertical load for three separate cases. The first case represents the common design assumption that the rail seat load is distributed uniformly across the entire rail seat. By definition, this distribution is not affected by

L/V force ratio. The second case represents a typical rail seat load distribution for a rail seat with new fasteners, as illustrated by data from experimentation on the TLS. Although there is some concentration of load on the field side of the rail seat, the fasteners are able to restrict rail rotation to 0.31 degrees or less. This results in very little change in rail seat load distribution. The final case represents a typical rail seat load distribution for a rail seat with worn fasteners, as illustrated by data from field experimentation on the RTT using the TLV. The ability of the clips to restrict rail rotation is reduced, allowing rail rotations up to 0.52 degrees, which results in significant concentration of the rail seat load along the field side of the rail seat. Further, this excessive rail rotation results in a complete unloading of the gauge side of the rail seat at L/V force ratios above the previously mentioned threshold L/V force ratio of 0.4. Figure 2.7 also shows the change in pressures exerted on the rail seat: the increased rail rotation in the worn fastener case results in higher pressures than the new fastener case, as illustrated by the accompanying pressure scale.

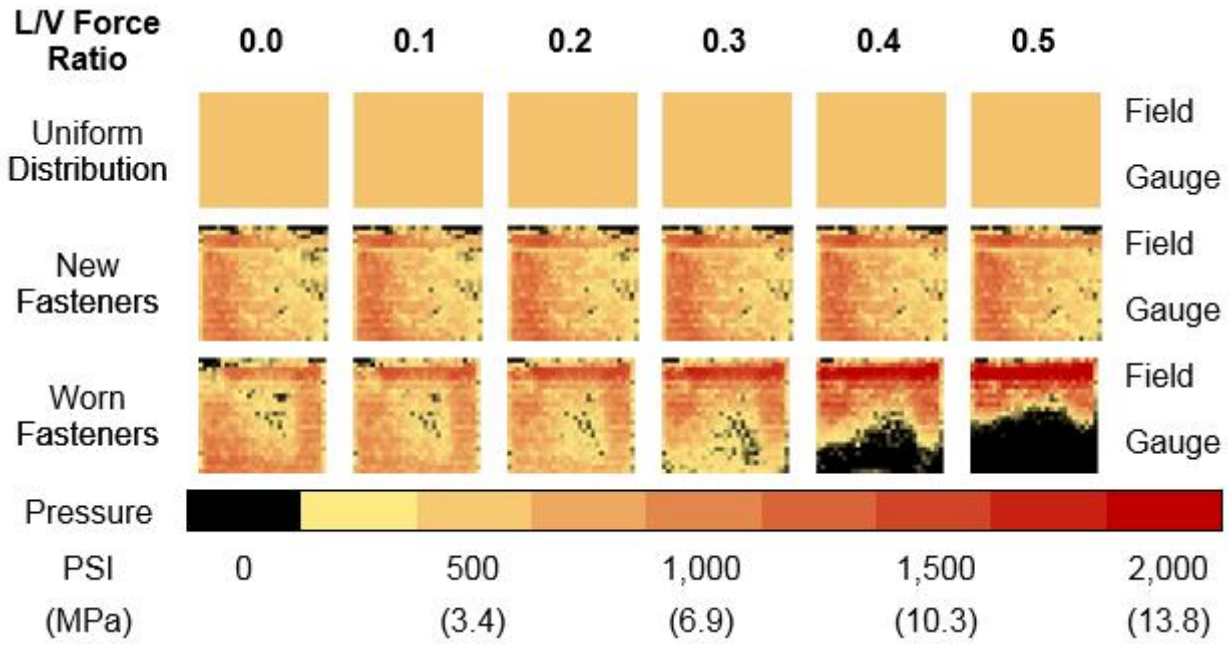

Figure 2.7 Qualitative effect of L/V force ratio on rail seat load distributions under 40,000 lbf (178 kN) vertical wheel load

Figure 2.8 illustrates the quantitative effect of L/V force ratio and fastener health on contact area, the area of the rail seat that is engaged in load transfer. The data has been normalized to the contact area seen under a 40,000 lbf (178 kN) vertical and 0 lbf lateral wheel load combination. Therefore, the percent of contact area at 0.0 L/V force ratio describes the effect of vertical load, while the change in percent contact area for each data series describes the effect of L/V force ratio for each vertical load magnitude. The use of new fasteners results in a consistent increase in contact area for all vertical load magnitudes of between 0.58% and 1.75%. It is hypothesized that this increase is due to deformation of the rail pad assembly as the rail rotates under higher L/V force ratios. By contrast, the worn fastener case exhibits a loss of up to 42% of initial contact area once the L/V force ratio exceeds the aforementioned critical "threshold" value. These data support the hypothesis that the ability of the worn fasteners to restrict rail rotation was reduced, which resulted in the observed lower contact areas under worn fasteners.

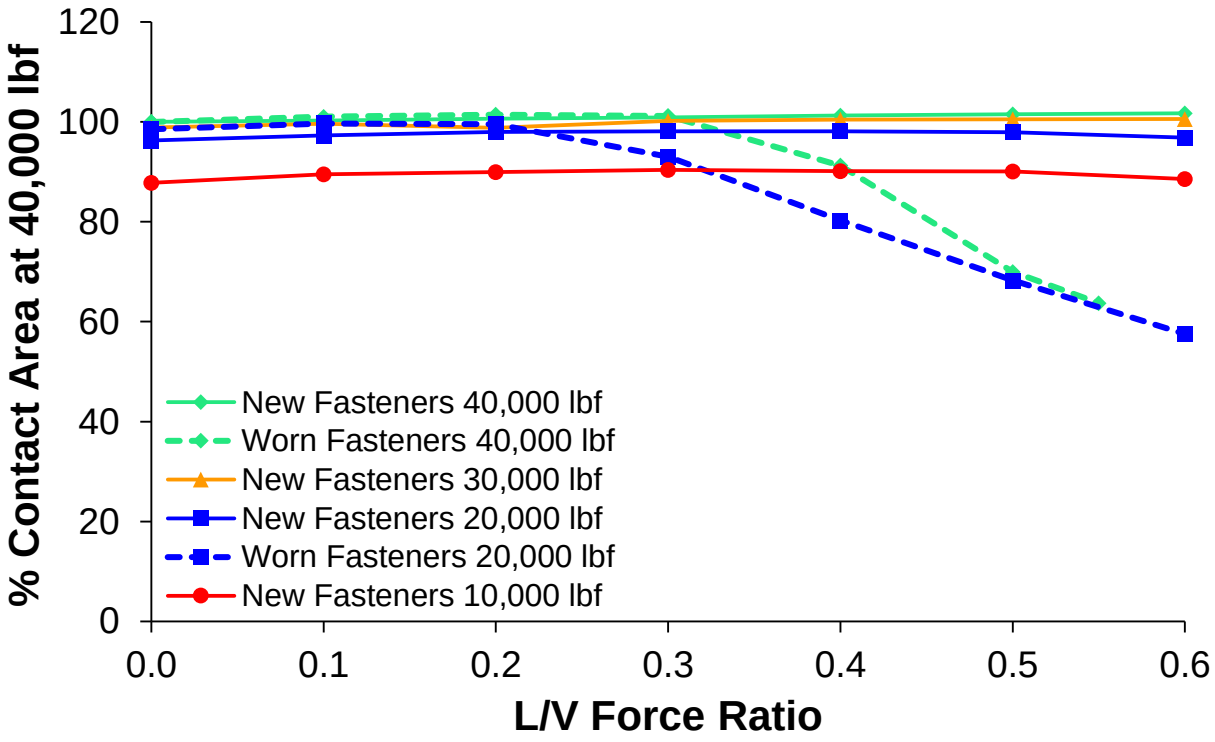

Figure 2.8 Quantitative effect of L/V force ratio on contact area

In order to examine the effect of fastener wear and loading environment on pressures, it is necessary to determine the total load applied to each rail seat. For the new fasteners investigated in the

laboratory, the rail seat load was calculated from internal strain gauges embedded below the crosstie rail seat. For the worn fastener case (data collected in the field), these embedment gauges were not present on rail seats instrumented with MBTSS. It was therefore necessary to estimate the rail seat load directly below the point of loading. The rail seat load in this case was estimated to be half of the vertical wheel load, based on both an extensive literature review (RailTEC 2015) and data acquired from strain gauges used in conjunction with field experimentation.

Figure 2.9 compares the uniform, average, and maximum pressures for the new and worn fastener cases under a 20,000 lbf (88.9 kN) vertical load, and Figure 2.10 compares the uniform, average, and maximum pressures for the same cases under a 40,000 lbf (178 kN) vertical load. In both figures, the new fastener average pressures plot within 50% of the theoretical uniform pressure, even under L/V force ratios as high as 0.6. This indicates that almost all of the contact area is utilized in load transfer. The worn fastener average pressures plot close to the theoretical uniform pressure below the aforementioned "threshold" L/V force ratio. Above this critical point, the reduction of contact area increases these pressures by up to 80% of their original value.

The maximum pressures observed for the new fastener case were approximately 325% higher than the theoretical uniform pressure under a 20,000 lbf (88.9 kN) vertical wheel load, experiencing no net change from 0.0 to 0.6 L/V. Under a 40,000 lbf (178 kN) vertical wheel load, the new fastener maximum pressures are inversely related to L/V force ratio, ranging from 211% to 177% higher than the theoretical uniform pressure. By contrast, the maximum pressures observed in the worn fastener case for both vertical wheel load magnitudes exhibited strong positive correlation with L/V force ratio. Again, the magnitude of maximum pressure relative to the theoretical uniform pressure is greater under the 20,000 lbf vertical load, ranging from 285% to 540% greater than the theoretical uniform pressure, than under the 40 kip vertical wheel load, ranging from 155% to 325% greater than the theoretical uniform pressure.

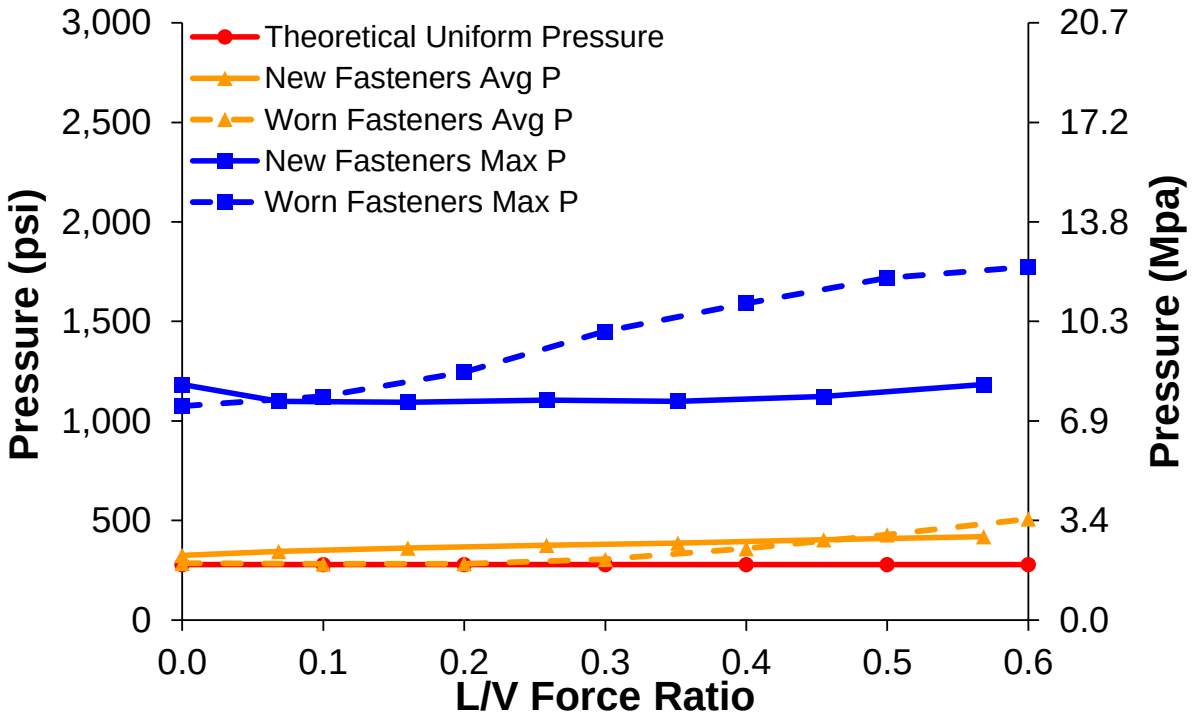

Figure 2.9 Effect of L/V force ratio on rail seat pressures (20,000 lbf (88.9 kN) vertical wheel load)

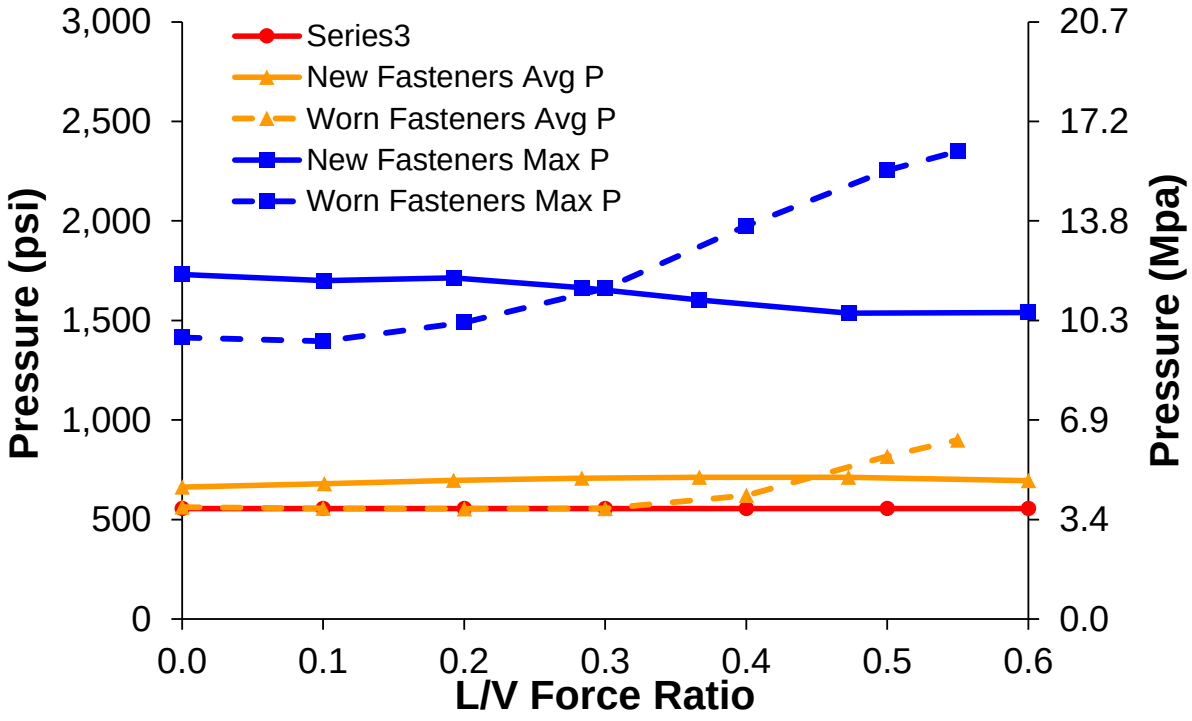

Figure 2.10 Effect of L/V force ratio on rail seat pressures (40,000 lbf (178 kN) vertical wheel load)

It is important to note that although none of the observed pressures approach the design compressive strength of the concrete (i.e. 7,000 psi (AREMA 2014)), the increase in pressure will change the characteristics of failure mechanisms associated with RSD (e.g. increased frictional force leading to more severe abrasion). It is hypothesized that RSD first develops in regions of extreme pressure and then spreads as the loss of material becomes more severe. Figures 2.9 and 2.10 show a higher maximum pressure for the new fastening system case than was observed in the worn fastener case at low L/V force ratios. During laboratory experimentation, several rail seats exhibited vertical rail seat loads in excess of the assumed 50% vertical wheel load distribution used to calculate rail seat loads for field experimentation. It is hypothesized that this is due primarily to increased rail seat load on the instrumented rail seats resulting from stiffer support conditions relative to adjacent crossties. These higher rail seat loads are hypothesized to be the cause for the initial elevation of the new fastener maximum pressure relative to the worn fastener maximum pressure.

2.8. Conclusions and Future Work

The findings of this analysis show that as lateral load increases, the rail seat becomes more irregularly loaded, and the load distribution concentrates on the field side of the rail seat. At a critical L/V force ratio, the rail seat begins to experience a reduction in contact area. The contact area continues to reduce as lateral load is increased beyond the critical L/V force ratio; at 0.5 L/V force ratio it can be seen that the gauge side of the rail seat can be completely unloaded in the presence of worn fasteners. This further concentrates the rail seat load onto the field side, which could explain the shape of the telltale triangular RSD wear pattern.

Although the modeling work performed by Volpe is relatively basic and relies on several worst-case assumptions, when comparing it to the field results presented in this paper, it provides an acceptable initial estimate for the critical L/V force ratio for a loading environment representative of North American heavy-axle load freight traffic. However, at lower vertical wheel loads, the calculated critical L/V tends to overestimate data obtained from field experimentation. With further refinement, the footing model proposed by Volpe could provide a good basis for a mechanistic calculation of the rail seat load.

Consideration should be given for the effect of the vertical wheel load and elastic fastener clamping force in resisting the overturning moment created by the lateral wheel load.

The previous research conducted at UIUC provides insight into the causes, effects, and mitigation of abrasion between the rail pad and rail seat. Although the range of pressures chosen for their experimentation sufficiently bound the observed average pressure on a rail seat, it did not capture the maximum pressures observed, occurring at 0.4 L/V force ratio and above in the case of worn fasteners. Further experimentation at these higher pressures may yield more information on the initial formation of RSD. Consideration should be given to conducting similar tests to those already performed, at higher loads and reduced contact areas to simulate these high L/V scenarios.

Data from this experimentation have shown that the health of the fastening system has a significant effect on the rail seat load distribution in concrete crossties. Data collected from laboratory experimentation on a track structure with new fasteners were compared to data from field experimentation under identical loading scenarios on a track structure with fasteners that had been subjected to both 5 MGT of traffic and, more importantly, three fastening system reapplication cycles. This wear on the fasteners resulted in an average reduction of contact area by 40%, an increase in average pressure by 71%, and an increase in maximum pressure by 60%, relative to the performance of new fasteners. Further, it was shown that under the worn fastener case, the portion of the rail seat load distributed within one inch of the field side shoulder was the most sensitive to changes in L/V force ratio, accounting for up to half of the total rail seat load under high L/V force ratios. It is therefore important to consider the effect of fastening system wear when evaluating the long-term performance of concrete crossties and fastening systems. Further experimentation to quantify the effect of traffic on fastening system wear, and therefore rail seat load distribution, would therefore be beneficial to understanding the parameters critical to preventing RSD. The load distribution at the rail seat is critical to four of the five RSD failure mechanisms proposed by researchers at UIUC. Therefore, it is critical to further understand how it is affected by changes in the loading environment and track structure. Further analysis could consider the effects of crosstie support conditions, fastening system type, and RSD-induced wear of the rail seat.

These findings may provide guidance in controlling the behavior of the load distribution which, in turn, could mitigate the effects of RSD.

CHAPTER 3: EXAMINATION OF THE EFFECT OF CONCRETE CROSSTIE RAIL SEAT DETERIORATION ON RAIL SEAT LOAD DISTRIBUTIONS[2]

3.1. Introduction

As discussed in Chapter 1 of this thesis, a recent survey of North American railroads and suppliers revealed that RSD was ranked as the most critical problem with concrete crossties and fastening systems (Van Dyk 2014). In addition, it was also ranked as the concrete crosstie and fastening system topic that was most in need of research (Van Dyk 2014). Therefore, researchers at UIUC conducted research funded by the United States Department of Transportation (US DOT) FRA and TTCI to characterize the distribution of rail seat loads in the presence of RSD.

RSD is a self-perpetuating failure mechanism: in the absence of maintenance, the wear magnitude will become more severe. As the rail seat is worn away and the effective height of the rail base relative to the cast-in shoulders is reduced, RSD also results in reduced clamping force from the fastening system. As further detailed in Chapter 2 of this thesis, reduced clamping force (in the form of fastener fatigue) has been shown to significantly affect the rail seat load distribution. Therefore, it is reasonable to expect that the loading environment at the rail pad-rail seat interface in the presence of RSD will significantly differ from that on an unworn rail seat. This chapter will therefore focus on the analysis of data gathered from MBTSS experiments designed to explore the effect of manufactured RSD on the load distribution and pressure magnitude at the rail seat.

3.2. Experimentation Plan

Field experimentation was conducted at TTC in Pueblo, Colorado, USA. Untreated concrete crosstie rail seats, one per crosstie, were ground to simulate common RSD wear profiles, and installed in a section of a service track that is a part of the Facility for Accelerated Service Testing (FAST). All three sections were tamped following installation of the crossties in 2013, and had experienced less than 1 MGT of traffic between tamping and the date of this experimentation. When testing was not being conducted, steel

[2] Much of Chapter 3 has been accepted for publication in the Transportation Research Record: Journal of the Transportation Research Board, and was originally published in the Proceedings of the 2015 Annual Meeting of the Transportation Research Board of the National Academics in Washington, D.C., USA (Greve et al. 2015a)

plates were inserted on the worn rail seats as a safety procedure to restore the original cant. The crossties were arranged in three sections of twenty crossties, each section with a specified target wear depth. The wear depth was gradually increased from both ends of each section until the target depth was achieved at the center of the section. Figure 3.1 illustrates the wear depth profile of each section; the target wear depth of Section 1 was 1/4 in (6.35 mm), the target wear depth of Section 2 was 3/8 in (9.53 mm), and the target wear depth of Section 3 was 3/4 in (19.05 mm). Though not illustrated in Figure 3.1, Section 1 was located in a section of tangent track, and Sections 2 and 3 were located in 8.9-degree (195 m) and 3.9-degree (445 m) curves, respectively, with the ground rail seats installed on the high rail of the curve. The rail seats of each section were also ground to specific wear profiles, as illustrated in Figure 3.2. Rail seats in Section 1 were ground to a uniform wear depth (emulating RSD typically associated with tangent track), preserving the design cant of the rail seat of 1:40 (Figure 3.2a) while rail seats in Sections 2 and 3 were ground to simulate triangular wear across the entire rail seat (emulating reverse rail cant), beginning at the original plane of the rail seat at the gauge side shoulder and increasing to the prescribed wear depth at the field side shoulder (Figure 3.2b). The Safelok I fastening system was used for all three sections.

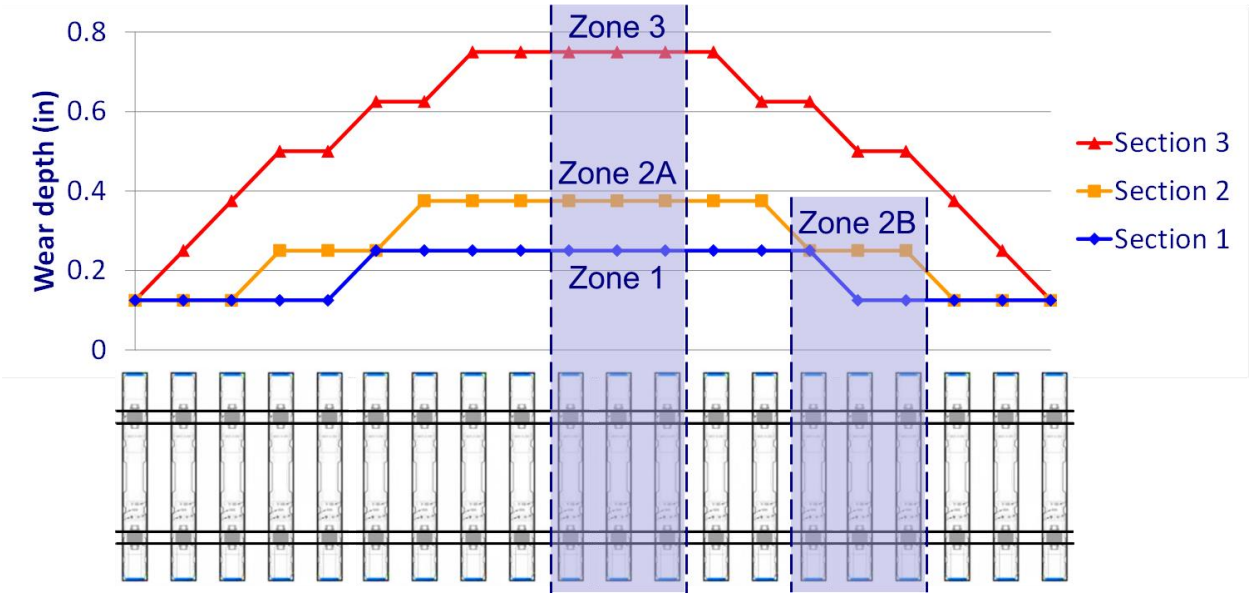

Figure 3.1 Wear depth profiles and location of instrumentation zones

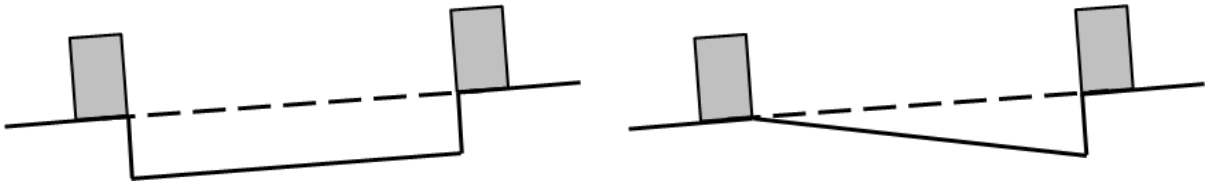

(a) Uniform Wear (Section 1) **(b) Triangular Wear (Sections 2 and 3)**

Figure 3.2 Illustration of uniform (a) and triangular (b) rail seat wear profiles

Four instrumentation zones were chosen, as shown in Figure 3.1. It was desired to capture all three target wear depths (Zones 1, 2A, and 3), but a fourth zone (Zone 2B) was chosen in Section 2 at a wear depth of 1/4 in (6.35 mm). This was the same wear depth as Zone 1, and was chosen to isolate the effect of rail seat wear profile (uniform or triangular) on the rail seat load distribution. Each instrumentation zone was comprised of three instrumented rail seats. Each rail seat was instrumented with MBTSS to capture the rail seat load distribution, as well as with linear potentiometers to capture the rail base vertical displacement on both the field and gauge side of the rail. The potentiometers were mounted on displacement fixtures attached to the crosstie with anchored screws and were used to calculate rail base rotation.

Loads were applied to the track structure using the FRA's T-18 Gage Restraint Measurement Vehicle. The vehicle is designed to evaluate the health of crossties and fastening systems by utilizing a gauge restraint measurement system (GRMS), a deployable axle which can be used to apply controlled vertical and lateral loads to the track structure (Bloom and Lee 2005). Testing consisted of both static and dynamic application of load at each zone. The vertical wheel load was kept constant at 20,000 lbf (89 kN), comparable to the wheel loads of Amtrak long-distance passenger equipment, for all static and dynamic experiments. The lateral wheel load was varied to generate L/V force ratios ranging from 0 to 0.8. For static experiments, the L/V force ratio was increased at 0.2 increments; for dynamic experiments, the L/V force ratio was increased at 0.4 increments. Dynamic experiments were conducted at 5 and 15 mph (8 and 24 kph).

In order to provide a control case, the results from this experimentation were compared to data gathered at TTC as part of the field experimentation further detailed in Chapter 2 of this thesis. The

control rail seats were untreated, with the original rail seat geometry intact, and tested in tangent track on TTCI's RTT. The control experiments were conducted at 20,000 lbf (89 kN) vertical wheel load with increasing lateral loads, such that the L/V force ratios applied to the track structure ranged from 0 to 0.6.

3.3. Results of Field Experimentation

The discussion of results for this chapter is based on a comparison of average results for each instrumentation zone. Figures and graphs illustrating the behavior of individual rail seats within each zone are available in Appendices A and B. When experimentation results were analyzed, it was observed that Rail Seat 12 in Instrumentation Zone 3 exhibited abnormally low contact areas and, therefore, high pressures. Rail Seat 12 was a clear outlier in both the qualitative distribution of load and the quantitative data relative to the other two rail seats in Zone 3, to the extent that the average results for the zone were significantly skewed by including Rail Seat 12. Moreover, because of Rail Seat 12's greatly reduced contact area relative to adjacent instrumented rail seats, it was determined that the chosen rail seat load calculation method would result in unreasonably high rail seat pressures. It is hypothesized that the support conditions under Rail Seat 12 were poor relative to adjacent rail seats, resulting in a reduction of rail seat load. Rail Seat 12 was therefore omitted from analysis of the average results discussed in this paper, but is included for reference in the relevant figures in Appendices A and B.

To guide the analysis of these data, several hypotheses were generated to characterize the loading environment and the effect of RSD. These hypotheses can be broken into three primary areas: the effect of rail seat wear profile, the comparison of static and dynamic loading environments, and the characterization of loading environment by rail roll.

In order to achieve triangular rail seat wear profiles of increasing depth at the field side of the rail seat, the slope of the worn profile must increase. Because of this, the toe load applied to the rail base by the field side clips will be reduced, and the rail will be able to rotate more freely. As the rail rotates toward the field, increasing the negative rail cant, the area of the rail seat engaged in load transfer will be reduced. Therefore, it is hypothesized that contact area will be reduced by increasing the wear depth of a triangular rail seat wear profile. This loss of contact area will inherently result in increased average

pressures, and it is hypothesized that the maximum pressures exerted in each instrumentation zone will also be increased.

Associated experimentation on concrete crossties and fastening systems at UIUC has shown that increasing train speed tends to decrease vertical deflection of the rail relative to the crosstie (RailTEC 2015). In these cases, static load application serves as the upper bound of deflection. It is theorized that at higher speeds, the track structure does not have time to "settle" completely after each load application, as it does under static loads. It is hypothesized that this behavior will be mirrored by the contact area, and that an increase in speed will therefore yield a decrease in contact area, regardless of rail seat wear profile.

In attempting to make the findings of this experimentation applicable for industry use, it was desired to correlate the rail seat load distribution to a parameter that could be measured by track geometry cars such as the T-18. Of the geometry data gathered by the T-18, rail cant was identified as the parameter most directly affecting the rail seat load distribution. It was therefore determined that the linear correlation between maximum pressure and rail cant should yield an R^2 value of 0.8 or higher to be considered a reliable relationship.

3.3.1. Effect of Rail Seat Wear Profile

Figure 3.3 shows the qualitative effect of wear depth on the rail seat load distribution under static load application. In the figure, all rail seats are oriented such that the field side of the rail seat is towards the top of the page. As wear depth increases from left to right across the figure, the severity of load concentration on the field side of the rail seat increases, indicating reduced contact areas and higher contact pressures. As predicted by the hypothesis, a significant reduction in contact area from 3/8" to 3/4" triangular wear can be observed.

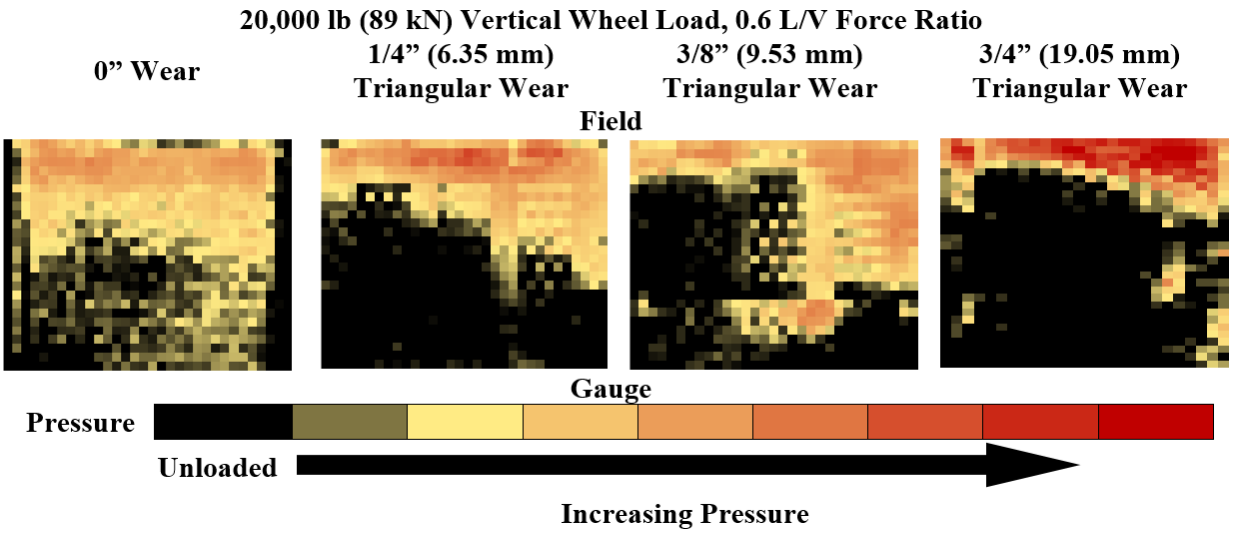

Figure 3.3 Rail seat load distribution under increasing wear depth

The qualitative effect of increased L/V force ratio of the applied static load on the rail seat load distribution is presented in Figure 3.4. In this figure, the vertical load and rail seat wear profile are held constant as the L/V force ratio varies. At low L/V force ratios, the rail seat load tends to distribute over a portion of the rail seat on both the gauge and field sides. Most of the rail seat wear profiles exhibit consistent behavior. As the rail rotates under increasing L/V force ratios the rail pad deforms under the rail base, distributing a reduced portion of the rail seat load on the gauge side. At L/V force ratios higher than 0.4, the rail continues to rotate, disengaging the gauge side of the rail seat entirely and concentrating the load across the entire width of the field side. It is hypothesized that a critical point of rotation is exceeded at 0.6 L/V, at which point the vertical wheel load no longer provides a moment resisting the tendency of the rail to roll to the field. This rail rotation behavior was observed in all rail seats to varying degrees. It is hypothesized that the differences in magnitudes of rotation can be attributed to variability in fastening system tolerances, and the resulting fatigue of clips during previous experimentation in the zone. Detailed results for individual rail seats can be found in Appendix A, Artificial RSD Rail Seat Load Distributions.

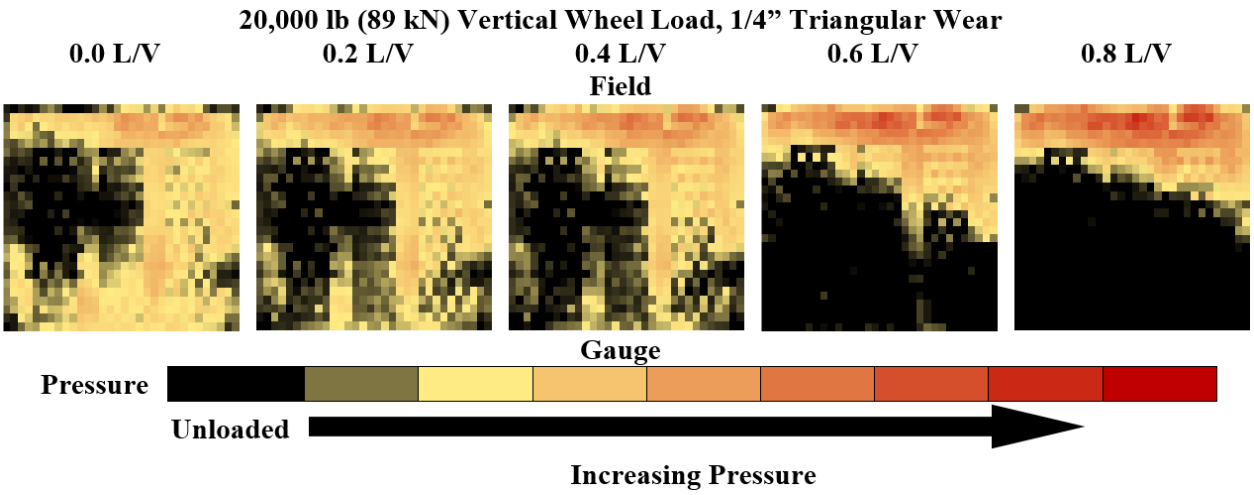

Figure 3.4 Rail seat load distribution under increasing L/V force ratio

The concentration of load described in Figure 3.4 due to rail rotation can be further explained by quantitatively examining the effect of L/V force ratio on rail rotation. Figure 3.5 compares the average rail rotation experienced in each Zone, calculated from measurements taken by the vertical potentiometers installed on each instrumented rail seat. If the deformation of the rail is neglected, this measurement is analogous to rail roll (the rotation of the rail relative to the in-situ, no-load case). Thus, rotation of the rail base toward the field side of the rail is considered as negative rotation. The results from all four instrumentation zones follow a consistent pattern of increasing rotation towards the field. The magnitude of this increase declines between 0.2 and 0.4 L/V, then increases again at L/V force ratios higher than 0.4. The rail base rotation observed in the 1/4" Triangular zone plots within 6% of that of the 1/4" Uniform zone at L/V force ratios less than 0.4; above this L/V, the rail base rotation experienced under the triangular wear profile was 30 to 40% higher than that under the uniform wear profile of the same depth. It is hypothesized that the more negative rail seat cant in the triangular wear case allowed for greater rail base rotation than the uniform wear case at high L/V force ratios.

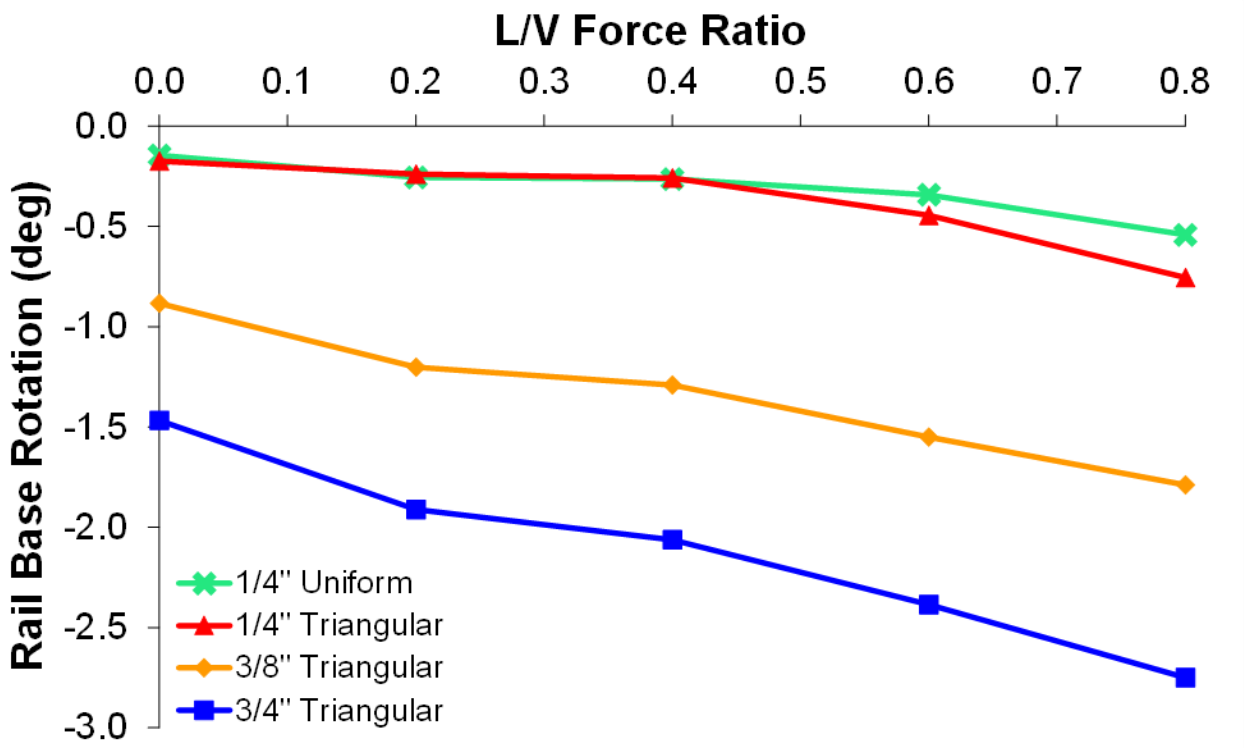

Figure 3.5 Rail base rotation under increasing L/V Force Ratio at 20,000 lbf (88.9 kN) Vertical Wheel Load

The reduction of contact area observed in Figures 3.3 and 3.4 is quantified in Figure 3.6, which shows the effect of increased L/V force ratio for all instrumentation zones at a constant vertical load. Error bars have been included in Figure 3.6 to show +/-1 standard deviation from the average for each rail seat wear profile. The majority of this variability is due to differences in the initial contact area of each rail seat within a given instrumentation zone at 0 L/V force ratio, and the relative behavior is consistent in each zone. For further detail on the quantitative performance of individual rail seats, refer to Appendix B, Rail Seat Contact Area and Pressure Graphs. The visual trend of reduced contact area in zones of greater wear depth is quantified in Figure 3.6, and the contact area resulting from 3/8” wear is consistently 75% larger than that resulting from 3/4" wear. The effect of rail seat wear profile is also quantified in Figure 8, which shows that the average contact area resulting from 1/4” uniform wear is 43% less than that resulting from 1/4" triangular wear below an L/V force ratio of 0.6. It is hypothesized that this is due to

reduced deflection of the clip toes leading to reduced clamping force applied to the rail base. This allows the rail to rotate more freely, leading to less contact between the rail base and rail pad.

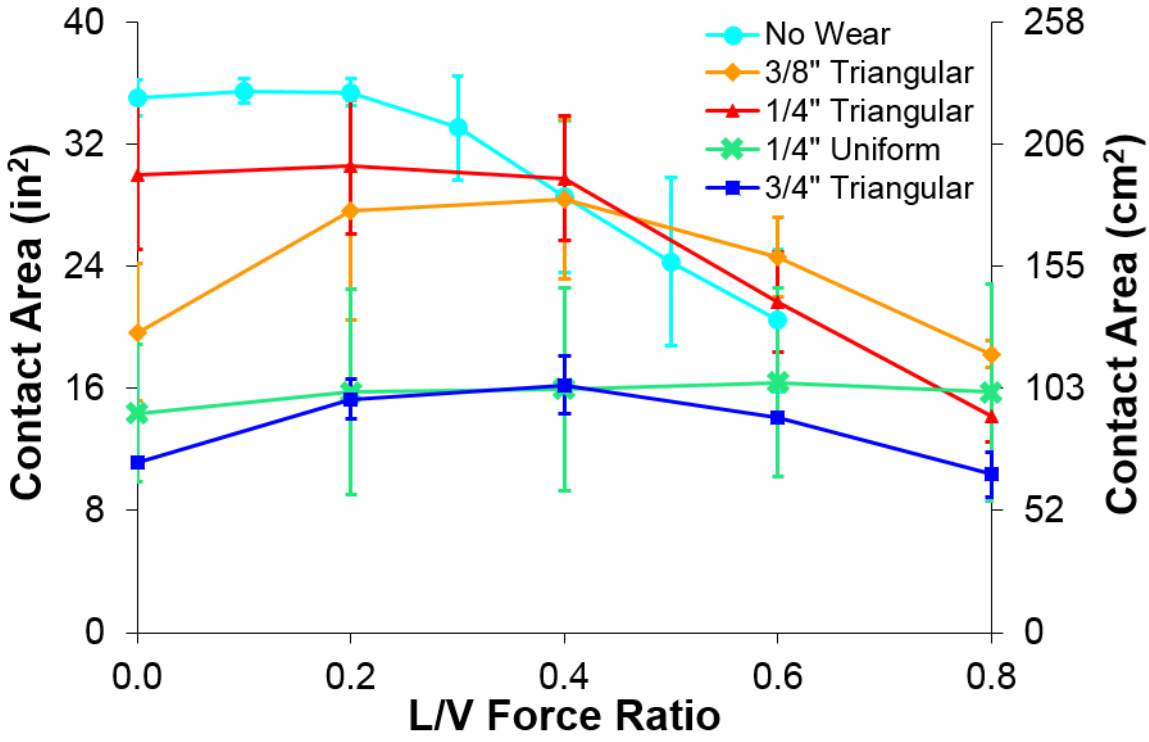

Figure 3.6 Behavior of contact area under increasing L/V at 20,000 lbf (89 kN) vertical wheel load

Figure 3.7 illustrates the effect that the rail seat load concentration has on the pressures exerted on the rail seat. Based on the findings of both a literature review of rail seat load calculation methodologies and of previous field experimentation, it is assumed that half of the vertical input load is transferred to the rail seat directly below the point of loading (RailTEC 2015). From this assumption, it is possible to determine two primary metrics for these pressures. Figure 3.7a illustrates the average pressure for each instrumentation zone at a given L/V force ratio, which is calculated by dividing the rail seat load by the contact area (the area of the rail seat engaged in load transfer) for each rail seat, and averaging all values at a given L/V force ratio. Figure 3.7b illustrates the maximum pressure observed in each instrumentation zone at a given L/V force ratio. Conventional design methodology approximates the rail seat load as uniformly distributed across the entirety of the rail seat area. This assumption is represented in both

Figure 9a and 8b by the data series “Uniform Pressure”. By definition, decreased contact area correlates to increased average pressure, which is reflected in Figure 3.7a. It is immediately clear that the uniform pressure distribution does not accurately describe the behavior of the average pressure: at extreme L/V force ratios, the average pressures from even the smallest amount of RSD, the 1/4” and 3/8” Triangular Zones, are twice the value of the uniform pressure assumption, and extreme cases of high RSD wear depth and high L/V force ratios may generate average pressures more than 3.5 times the hypothetical uniform pressure. Moreover, Figure 3.7b shows that in the same extreme cases, the actual pressure at discrete points on the rail seat may be as much as 16 times the same assumed uniform pressure. Even in areas of less severe wear, discrete points on the rail seat may be experiencing five times the uniform pressure. It is important to note that the 1/4" Uniform data series yields pressures consistently higher than those observed in the 1/4" Triangular data series. It is hypothesized that these higher, more damaging pressures will tend to alter the rail seat wear profile to one more similar to the triangular profile previously described.

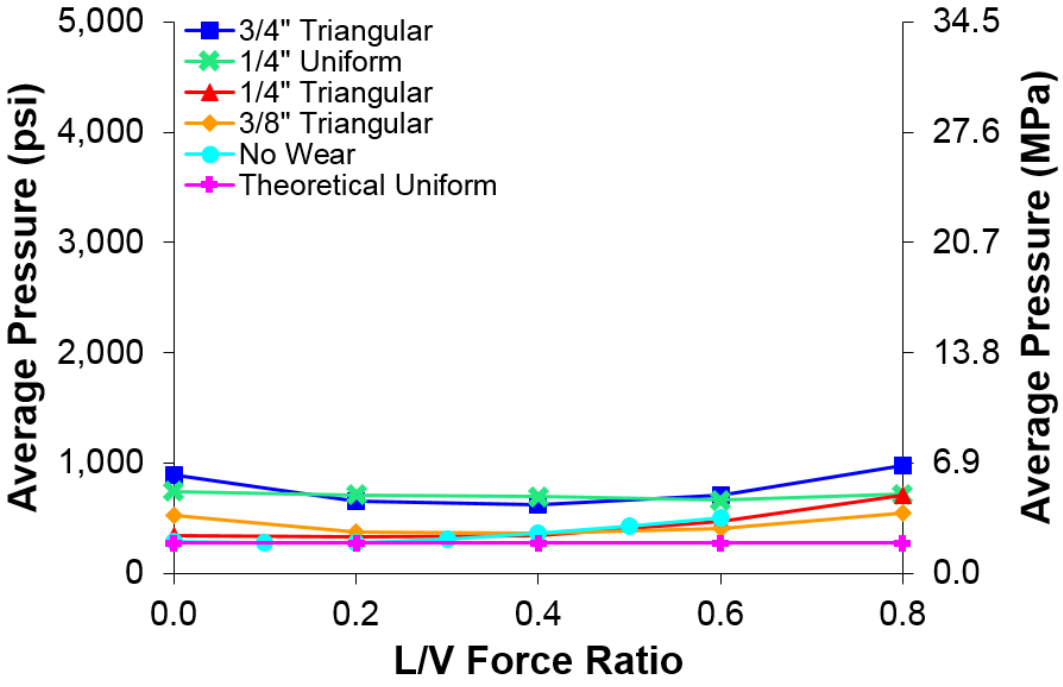

(a) Average pressure

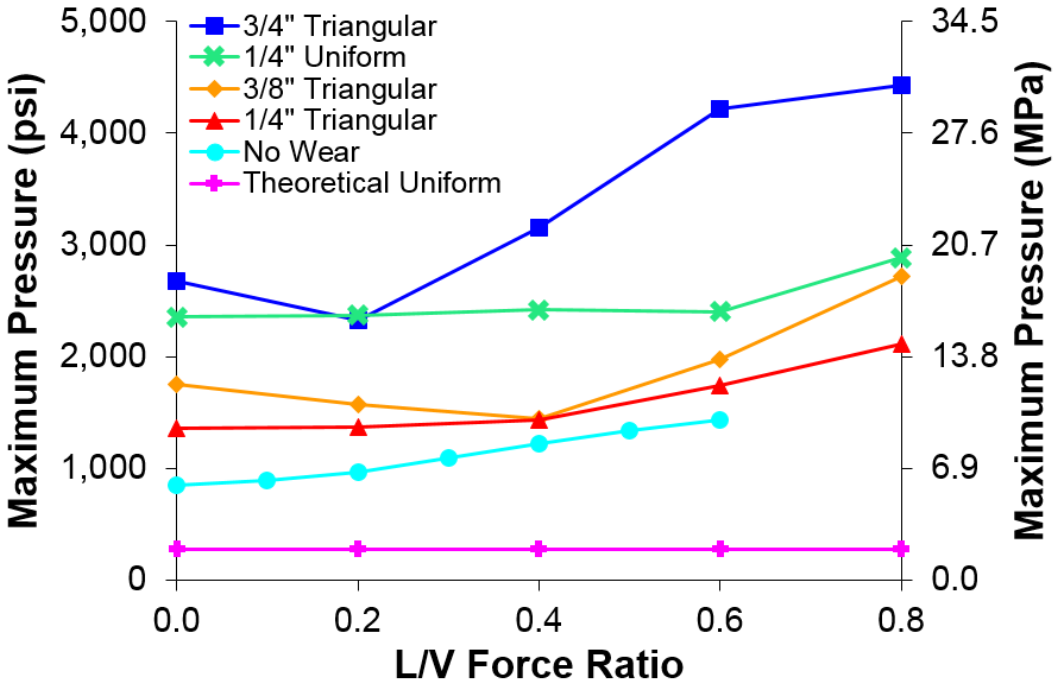

(b) Maximum Pressure

Figure 3.7 Changes in average (a) and maximum (b) rail seat pressure under increasing L/V at 20,000 lbf (89 kN) vertical wheel load

Although the pressures shown in Figure 3.7 do not exceed the recommended design strength of concrete crossties, 7,000 psi (48 MPa) (AREMA 2014), experimentation with 3/4" (19.05 mm) triangular wear at high L/V force ratios yielded pressures which may exceed the fatigue compressive strength of the concrete, estimated to be 50% of the ultimate compressive strength, or 3,500 psi (24 MPa) as described further in Chapter 4 of this thesis. In these extreme conditions, crushing of the rail seat due to a high number of repeated load applications may be feasible. In all cases, the increased pressures may change the characteristics of RSD failure mechanisms such as abrasion (increased normal load will generate higher frictional forces) and hydraulic pressure cracking (rapid application of high pressure may produce greater tensile stresses in the concrete (Zeman 2010)). Further, the observed pressures may be artificially lowered by restrictions of the experimental plan and its equipment. Although the T-18 was not able to apply loads simulating heavy-axle freight traffic, previous research has shown that the average pressure may increase by 500 psi (3.44 MPa), and that the maximum pressure can be expected to increase by 800 psi (5.52 MPa) under heavy axle loads.

3.3.2. Comparison of Static and Dynamic Loading

Figure 3.8 illustrates the effect of speed on contact area for each rail seat wear profile. It is important to note that although most of the data see a reduction in contact area when the speed is increased, the data collected at 0.0 L/V show that this trend is significantly reduced, or that there is even an increase in contact area with the application of speed. It is hypothesized that the lateral load may confound some dynamic effect contrary to the original hypothesis. Table 3.1 summarizes the relative reductions in contact area. While experimentation with triangular wear patterns revealed minimal effect due to train speed, which yielded an average contact area reduction of 3%, experimentation at Zone 1, with the uniform wear pattern, produced an average contact area reduction of 42% with the change in speed. It is hypothesized that this difference in behavior is due to the reduced rotational restraint of the rail due to reduced or nonexistent clamping force. On average, the contact area was reduced from the static load scenario by 13% with a standard deviation of 20%. Although this does not indicate a significant effect on

contact area, experimentation was constrained to relatively low speeds. In locations where trains operate at speeds two or three times those tested here, this effect may be more pronounced.

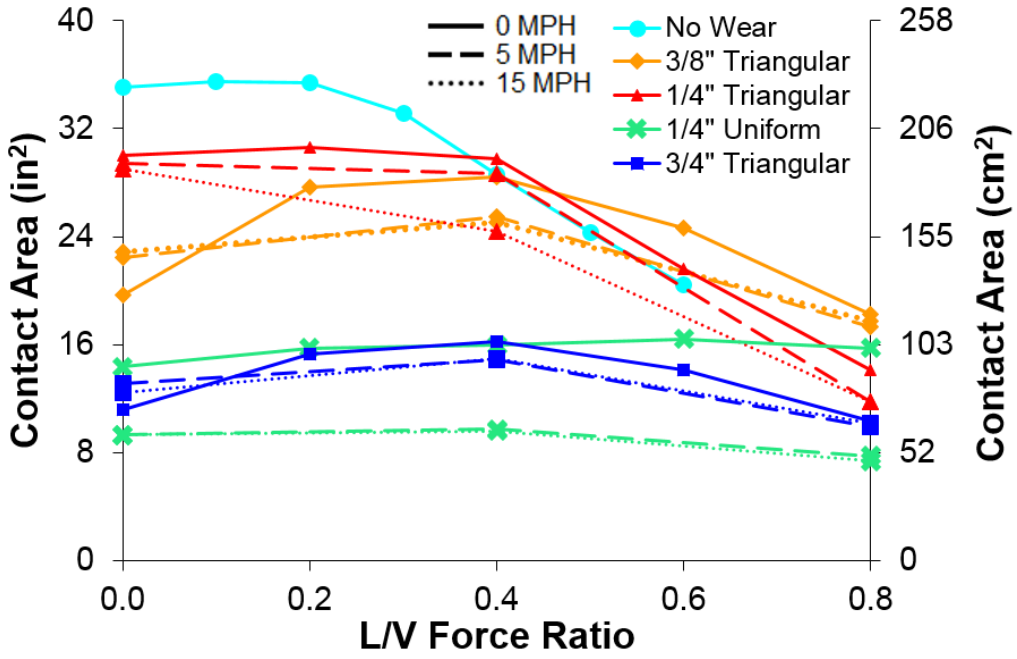

Figure 3.8 Reduction in contact area due to dynamic load application at 20,000 lbf (89 kN) vertical wheel load

Table 3.1 Average Reduction of Contact Area Due to Speed

Rail Seat Wear Profile	Speed (mph)	Speed (kph)	L/V Force Ratio 0.0	0.4	0.8
1/4" Uniform	5	8	35%	39%	51%
	15	24	35%	40%	53%
1/4" Triangular	5	8	-14%	10%	5%
	15	24	-16%	12%	3%
3/8" Triangular	5	8	2%	4%	17%
	15	24	3%	18%	17%
3/4" Triangular	5	8	-12%	8%	2%
	15	24	-18%	8%	4%

The reduction of contact area due to dynamic loading results in an increase in pressures exerted onto the rail seat. Because the reduction of contact area was determined to be negligible at low speeds, the effect of train speed on average pressure, which is calculated directly from contact area, is similarly negligible. Results for maximum pressure indicated a general trend of increased maximum pressure, with

an average increase of 10%, with a maximum increase of 32% in the case of uniform wear at high L/V force ratios. Appendix B, Artificial RSD Rail Seat Contact Area and Pressure Graphs, contains more detailed data for average and maximum pressures under dynamic load application.

3.3.3. Characterization of Loading Environment by Rail Cant

Figure 3.9 illustrates the relationship between maximum pressure and rail cant, using data gathered from dynamic runs of the T-18 over the instrumentation zones. These data have been separated by L/V force ratio and speed to isolate the effects of these variables. For rail seats with a typical 1:40 cant, the FRA has established cant exception thresholds at -1.8 degrees (Alert) and -2.8 degrees (Alarm), as measured from the horizontal (Clouse 2008). These thresholds have also been included in Figure 3.9. These data indicate a trend of increasing maximum pressure with decreasing rail cant. This agrees with the findings previously discussed in this paper, and is expected, as increased negative rail cant indicates greater rotation of the rail towards the field side, which decreases contact area. The majority of the data exhibit similar trends, with the notable exception of 0.8 L/V at 5 mph, in which a consistent outlier in the data collected on rail seats with 1/4" Triangular wear has distorted the linearity of the data. The pressures observed on rail seats with no RSD at equivalent vertical loads did not exceed 1,500 psi (10.3 MPa), while a vertical load of 40,000 lbf (178 kN) generated pressures less than 2,500 psi (17.2 MPa), as illustrated in Chapter 2 of this thesis. At rail cants measured above the Alert threshold, the maximum pressures observed at 0.8 L/V exceeded the highest pressures observed on an unworn rail seat under 40,000 lbf (178 kN), which is considered to be the nominal loading case for North American heavy axle load freight service.

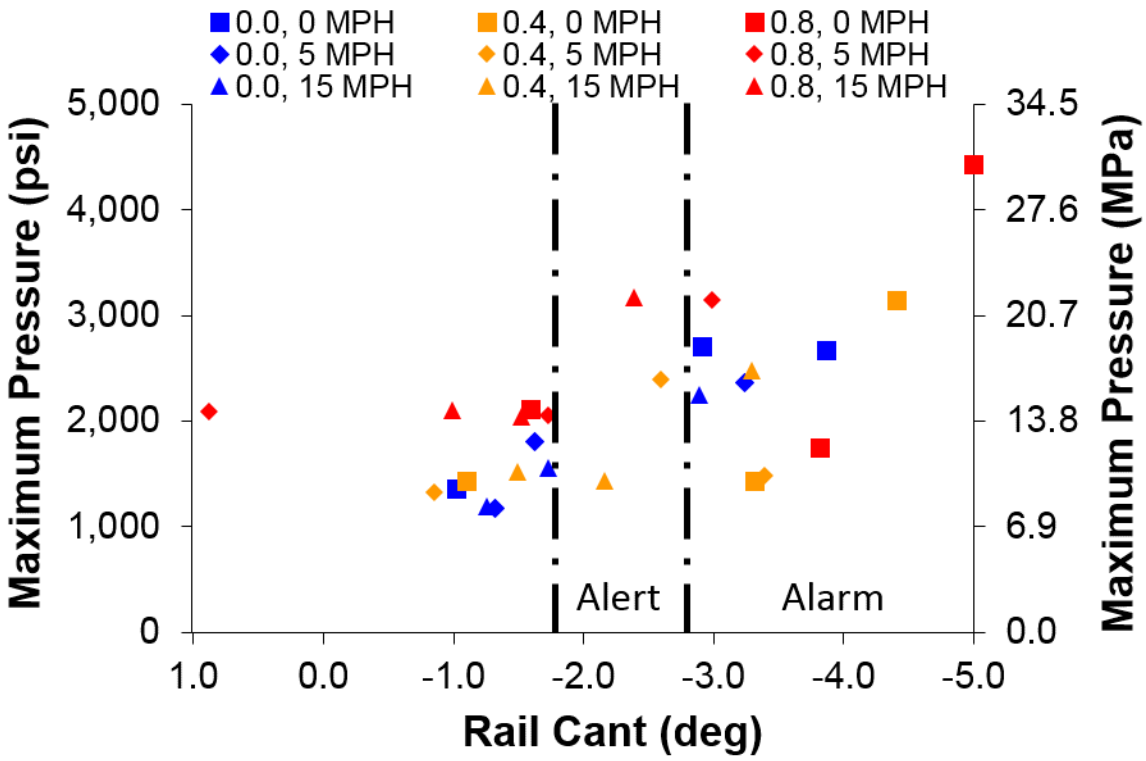

Figure 3.9 Correlation between maximum pressure and rail cant at 20,000 lbf (89 kN) vertical wheel load

The relationships described by Figure 3.9 are quantified in Table 3.2, which lists the equations and R^2 values corresponding to the linear regression for each data series. If the hypothesized limit of good correlation, 0.8, is considered, then a linear correlation appears to be most suitable at low L/V force ratios. Because GRMS typically operate between 0.5 and 0.8 L/V (FRA 2014), it is considered impractical to accurately predict maximum pressure from GRMS rail cant data based on this limited data set. Correlation was improved with increased speed, but this result is inconclusive based on this limited data set. It should be noted, however, that all instances of maximum pressures exceeding the aforementioned nominal loading case for heavy axle loads on healthy track were associated with rail cants exceeding the Alert threshold.

Table 3.2 Linear Fit Equations for Maximum Pressure – Rail Cant Relationship

L/V	Speed (mph)	Speed (kph)	Equation	R^2
	0	0	$y = -500.2x + 948.0$	0.877
0.0	5	8	$y = -528.2x + 688.2$	0.837
	15	24	$y = -633.9x + 419.0$	0.997
	0	0	$y = -443.7x + 699.7$	0.572
0.4	5	8	$y = -149.9x + 1395$	0.114
	15	24	$y = -500.2x + 948.0$	0.816
	0	0	$y = -572.3x + 778.9$	0.462
0.8	5	8	$y = -229.0x + 2137$	0.530
	15	24	$y = -814.0x + 1103$	0.823

3.4. Comparison to Field-Worn RSD

The artificially-worn rail seats used in this experimentation exhibited a smooth, planar surface, similar to a new and unworn rail seat. By comparison, Figures 1.1 and 1.2 in Chapter 1 of this thesis show several instances of RSD which exhibit exposed aggregate particles where the concrete paste has worn away, typical of most RSD. It is hypothesized that the less planar surface generated by field-worn RSD will yield reduced contact area when compared to artificially-worn rail seats, generating higher pressures than those observed in field experimentation.

3.4.1. Laboratory Experimental Design

Laboratory experimentation was performed at RailTEC's RAIL at Schnabel. Experiments were conducted using the Pulsating Load Testing Machine (PLTM), a bi-axial loading frame owned by Amsted RPS, further described in Chapter 4 of this thesis. Figure 3.10 shows the rail seat used for experimentation, which had experienced severe RSD as a result of use on a North American heavy-haul railroad. Unlike the artificially-worn rail seats instrumented at TTC, the field-worn RSD crosstie had developed a trapezoidal wear profile, as shown in Figure 3.11. The surface of the rail seat had been worn to expose numerous large aggregate particles, with wear depth increasing from 0.355 in (9.02 mm) at the gauge side shoulder to 0.628 in (15.95 mm) at the field side shoulder. Experimentation was conducted using a new Safelok I fastening system manufactured by Amsted RPS.

Figure 3.10 Rail seat with field-worn RSD used in laboratory experimentation

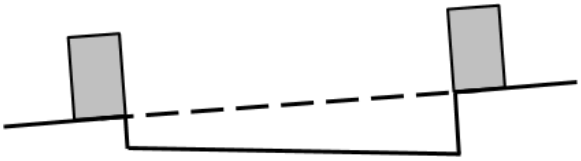

Figure 3.11 Illustration of trapezoidal rail seat wear profile

The magnitude of vertical load applied in this experimentation was varied to simulate different levels of load transfer from a single vertical wheel load to the crosstie directly below the point of loading. This value may vary under field conditions due to support conditions of the loaded crosstie relative to adjacent crossties (RailTEC 2015). Testing was conducted at 10,000 lbf (44.5 kN), 20,000 lbf (88.9 kN), and 30,000 lbf (133 kN). These values were chosen to represent 25%, 50%, and 75% of 40,000 lbf (178 kN), representing the 95th percentile nominal vertical wheel load for a loaded freight car in North American heavy haul service (Van Dyk 2014). At each magnitude of vertical load, the L/V force ratio was also varied from 0 to 0.6 to simulate varying degrees of curvature. Results from experimentation at 10,000 lbf (44.5 kN) vertical load were compared to data collected in Zone 3 during experimentation at TTCI, as the chosen artificial RSD wear profile and depth which most closely represented the field-worn RSD.

3.4.2. Results of Laboratory Experimentation

Figure 3.12 illustrates the qualitative differences between laboratory experimentation at 10,000 lbf (44.5 kN) vertical load with field-worn RSD and field experimentation conducted at TTC with artificially-worn RSD. It is immediately apparent that the presence of protruding aggregate on the field-worn rail seat leads to a significant reduction of contact area when compared to the artificially-worn rail seat tested at TTC. The field-worn RSD data show that although the amount of area engaged in load transfer remains relatively constant with increasing L/V force ratio, the load tends to migrate towards the field side of the rail seat, leading to higher maximum pressures as denoted by warmer colors. These maximum pressures, often concentrated in regions 0.25 in^2 (1.61 cm^2) or smaller, are more isolated than those observed in artificially-worn RSD experimentation, which are more distributed in larger regions of elevated pressure. These "peaks" in the field-worn RSD distributions coincide with areas of exposed aggregate, which may protrude from the deteriorated surface of the rail seat as the concrete paste is worn away by RSD. Because a smaller portion of the rail seat in field-worn RSD experimentation is engaged in transferring the same magnitude of rail seat load as in artificially-worn RSD experimentation, it is expected that the pressures observed in the laboratory will be greater than those in the field.

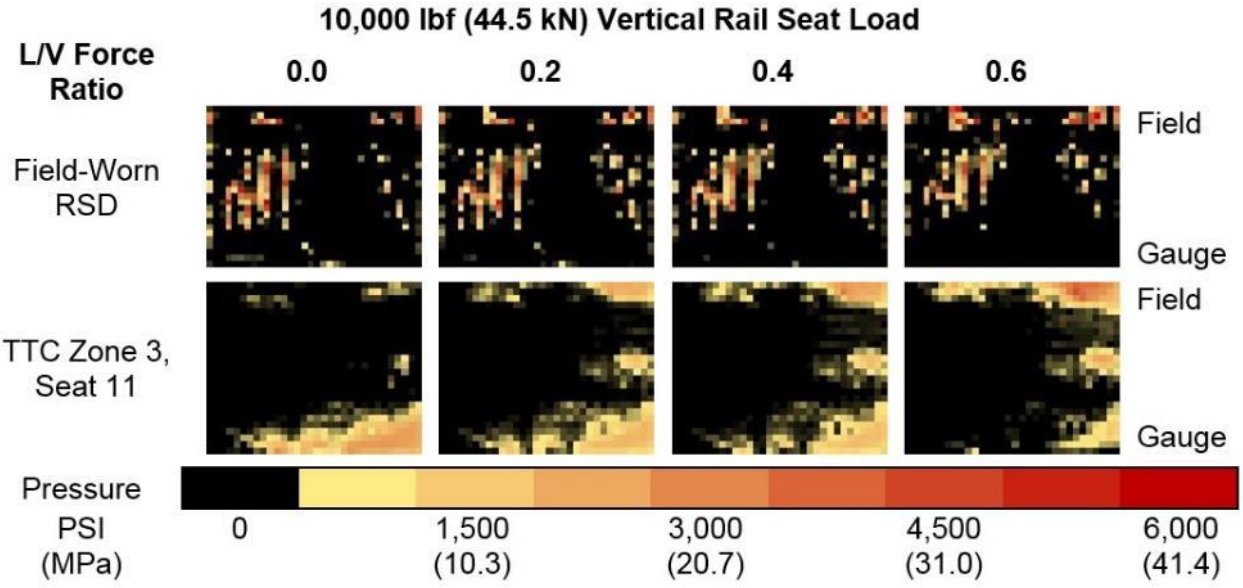

Figure 3.12 Qualitative comparison of field-worn and artificial RSD wear profiles

Figure 3.13 illustrates the relationship between contact area and L/V force ratio at the three experimental loading magnitudes. Contrary to data from Zone 3 at TTC, field-worn RSD experimentation yielded contact areas which either remained relatively constant or decreased, depending on the magnitude of vertical and lateral loads applied. Field-worn RSD experimentation at 10,000 lbf (44.5 kN) yielded negligible change in contact area from 0.0 to 0.6 L/V force ratio, compared to the 13% reduction in contact area from 0.4 to 0.6 L/V force ratio observed in artificially-worn RSD experimentation. As illustrated in Figure 3.12, the exposed aggregate at the rail seat surface led to a significant reduction in contact area when compared to artificially-worn RSD experimentation, ranging from 71% of field contact area at 0.0 L/V force ratio to 56% at 0.6 L/V force ratio. 20,000 lbf (88.9 kN) and 30,000 lbf (133 kN) field-worn RSD experimentation resulted in contact area reductions of 9% and 22%, respectively, from 0.0 to 0.6 L/V force ratio.

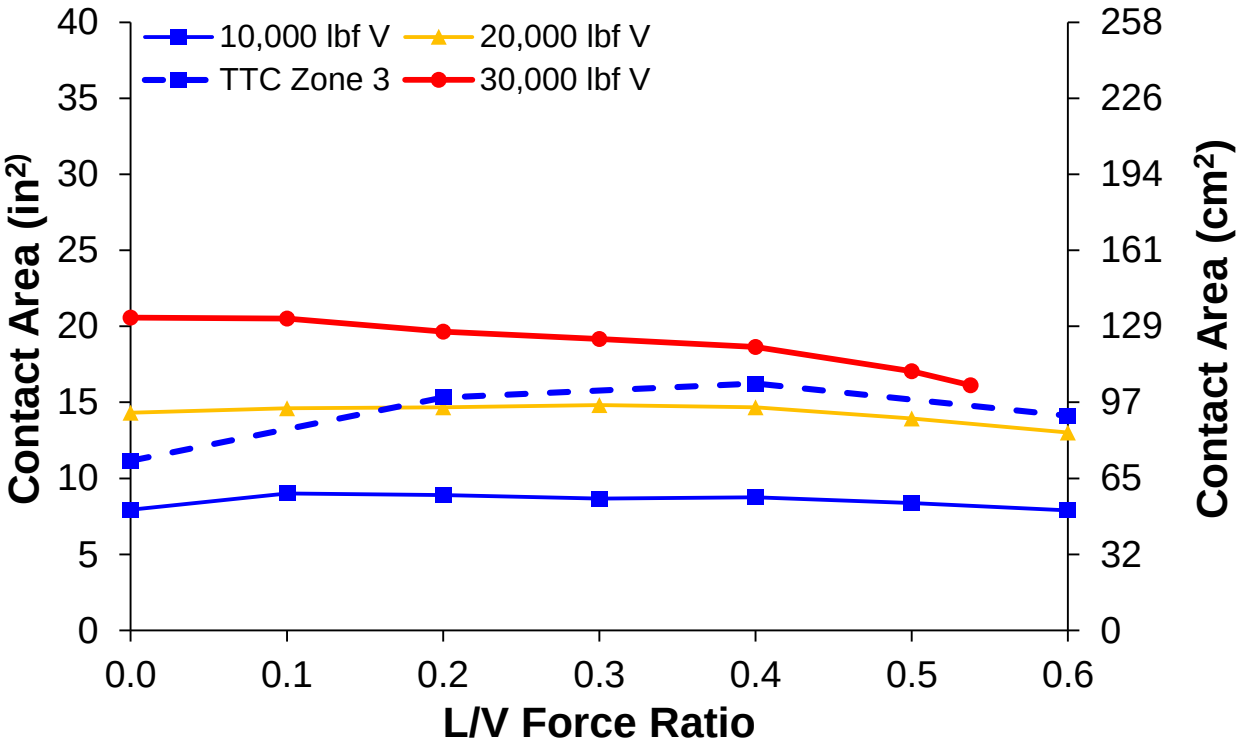

Figure 3.13 Behavior of contact area under increasing L/V

Figures 3.14 and 3.15 illustrate the effect of L/V force ratio on the rail seat pressures at the three experimental loading magnitudes. It should be noted that in both Figure 3.14 and 3.15, the pressures

observed during artificially-worn RSD experimentation at TTC serve as a lower bound for the pressures observed during field-worn RSD experimentation. This is expected, given the higher vertical rail seat loads of 20,000 lbf (88.9 kN) and 30,000 lbf (133 kN) applied to the field-worn rail seat, as well as the reduced contact area observed at 10,000 lbf (44.5 kN) vertical rail seat load, which is estimated to be comparable to the experimental loading environment in artificially-worn RSD experimentation.

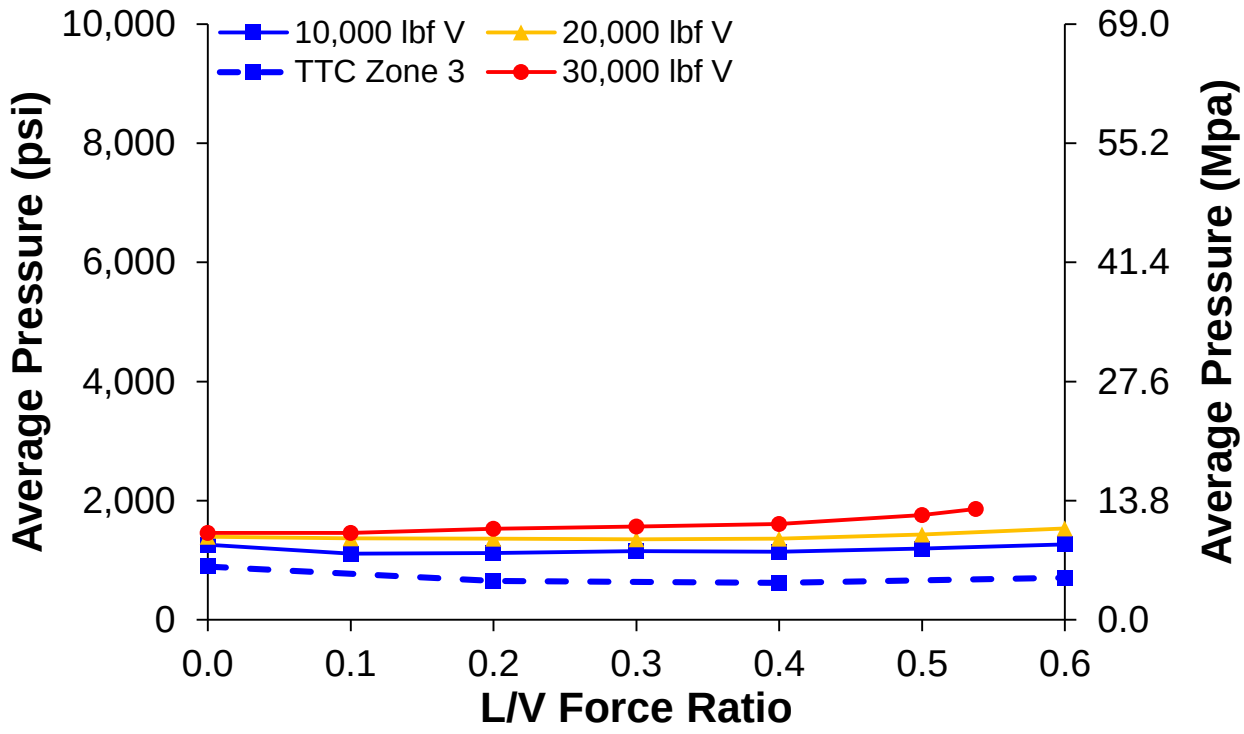

Figure 3.14 Change in average pressure under increasing L/V

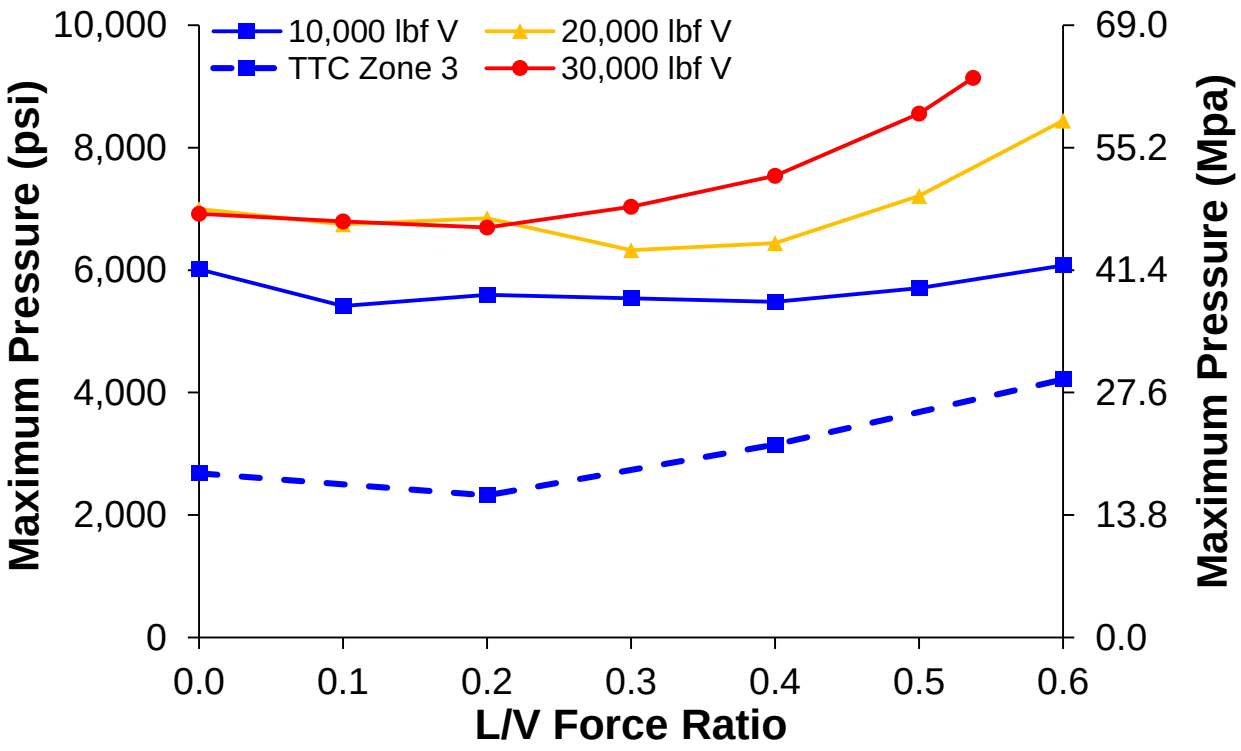

Figure 3.15 Change in maximum pressure under increasing L/V force ratios

Figure 3.14 shows the change in average pressure as a result of increasing L/V force ratio. As previously described, average pressure is derived from the measured contact area, and thus an inverse relationship between contact area and average pressure is observed at a constant loading magnitude. The largest change in average pressure was a 28% increase from 0 to 0.54 L/V force ratio at 30,000 lbf (133 kN) vertical rail seat load. Figure 3.15 shows the change in maximum pressure as a result of increasing L/V force ratio. As with the contact area and average pressure, the effect of L/V force ratio becomes more pronounced at higher vertical load magnitudes, with 1%, 21%, and 32% increases in maximum pressure from 0.0 to 0.6 L/V force ratio for 10,000 lbf (44.5 kN), 20,000 lbf (88.9 kN), and 30,000 lbf (133 kN) vertical rail seat loads, respectively. Field-worn RSD experimentation at 10,000 lbf (44.5 kN) yielded maximum pressures consistently higher than those observed in artificially-worn RSD experimentation, ranging from 124% higher at 0.0 L/V force ratio to 44% higher at 0.6 L/V force ratio. This agrees with the qualitative assessment of the rail seat load distribution images in Figure 3.12, in

which a few, distinct "peaks" can be seen in images taken from field-worn RSD experimentation, versus the more distributed regions of higher pressure observed in artificially-worn RSD experimentation.

Lastly, it is important to note that under combinations of high vertical rail seat loads and high L/V force ratios, the recorded maximum pressures may exceed the design compressive strength of the concrete, defined previously in this chapter as 7,000 psi (48 MPa) (AREMA 2014). This indicates that crushing of the rail seat due to a single load application may be feasible in advanced stages of RSD. Furthermore, all maximum pressures observed in field-worn RSD experimentation exceeded 3,500 psi (24 MPa), which was previously described as the estimated fatigue compressive strength of the concrete as described further in Chapter 4 of this thesis. This indicates that crushing of the rail seat due to a high number of repeated load applications may also be feasible in advanced stages of RSD.

3.5. Conclusions

Data from this experimentation have shown that the presence and severity of rail seat deterioration has a significant effect on the rail seat load distribution. A correlation between increased wear depth and reduced contact area was observed for triangular wear profiles; this reduction of contact area resulted in significant increases in both the average and maximum pressures imparted to the rail seat, which are both drastically underestimated by conventional design methodology. Further, although there did appear to be a reduction of contact area with the addition of speed, it was determined that the effect was negligible at low speeds, or may even be reversed at low L/V force ratios. A direct correlation between rail seat load distribution and traditional GRMS measurements could not be made with the limited data collected in this experiment. However, a general trend of maximum pressures exceeding 2,500 psi (17.2 MPa) occurring only with rail cants above the FRA rail cant Alert level was observed. Lastly, experimentation with field-worn RSD showed that the presence of aggregate at the worn rail seat surface can significantly increase the magnitude of rail seat pressures. Field-worn RSD experimentation revealed maximum pressures exceeding the estimated fatigue compressive strength of the concrete at all combinations of vertical rail seat loads and L/V force ratios, and maximum pressures exceeding the design ultimate compressive

strength of the concrete at combinations of both extreme vertical rail seat loads and extreme L/V force ratios.

CHAPTER 4: THE EFFECT OF PARTICLE INTRUSION AT THE RAIL SEAT INTERFACE[3]

4.1. Introduction

Crushing is defined as damage to the crosstie rail seat resulting from pressures exceeding the strength of the concrete material (Zeman 2010). In North America, the minimum recommended design 28-day compressive strength is 7,000 psi (48 MPa) (AREMA 2014). However, practical experience has shown that the achieved 28-day compressive strength can exceed 11,000 psi (76 MPa) (Zeman 2010).

Experimentation conducted at Volpe suggests that crushing may be a feasible failure mechanism for RSD. To investigate several passenger train derailments caused by RSD, Volpe utilized a NUCARS™ model to obtain the magnitudes of vertical and lateral load and location of the wheel/rail contact patch. This information was then applied to an empirical model which treats the rail as a footing on an elastic foundation. The findings of this research suggest that pressures exceeding 16,000 psi (110 MPa) may be possible (Choros et al. 2007). However, the analysis was performed under several "worst-case" assumptions. The analysis neglected the rotational restraint provided by the elastic fasteners, and assumed that the rail pad provided no distribution of load from the rail. These assumptions may therefore not accurately represent typical field conditions, and may simulate only the most extreme cases of RSD and fastening system deterioration. Further, the research detailed in the preceding chapters of this thesis has not revealed evidence of rail seat pressures exceeding 4,400 psi (30 MPa), far below the minimum theoretical threshold for crushing, 7,000 psi (48 MPa). Experimentation was therefore undertaken with MBTSS to generate extreme rail seat pressures via particle intrusion at the crosstie rail seat.

4.2. Laboratory Experimentation

Experimentation was conducted at UIUC's RAIL at Schnabel utilizing the PLTM, which is owned by Amsted RPS. The PLTM is a bi-axial loading frame designed to perform AREMA Test 6, a Wear and Abrasion test, on a single rail seat with a complete fastening system assembly. The PLTM is equipped with one vertically-oriented 55,000 lbf (245 kN) actuator and one laterally-oriented 35,000 lbf (156 kN)

[3] Chapter 4 was originally published in the Proceedings of the 2015 International Heavy Haul Association Conference in Perth, Western Australia, Australia (Greve et al. 2015c)

actuator. The actuators can be controlled independently by either force or displacement. For these experiments, force control was used.

In order to develop an experimental matrix which would generate extreme rail seat pressures, the size and amount of particles applied to each rail seat were varied. Locomotive sand was used to represent typical particle intrusion, as practical experience and the AREMA Test 6 procedure indicate that particles typically found at the rail pad-rail seat interface are of comparable size. To generate more extreme pressures, virgin Class B crushed stone ("B-Stone") aggregate from the UIUC concrete laboratory was used to simulate debris from deterioration of the concrete at the rail seat. Figure 4.1 shows the grain size distribution of the aggregate after all material retained at or above the #4 sieve was removed (14% of the total sample by weight).

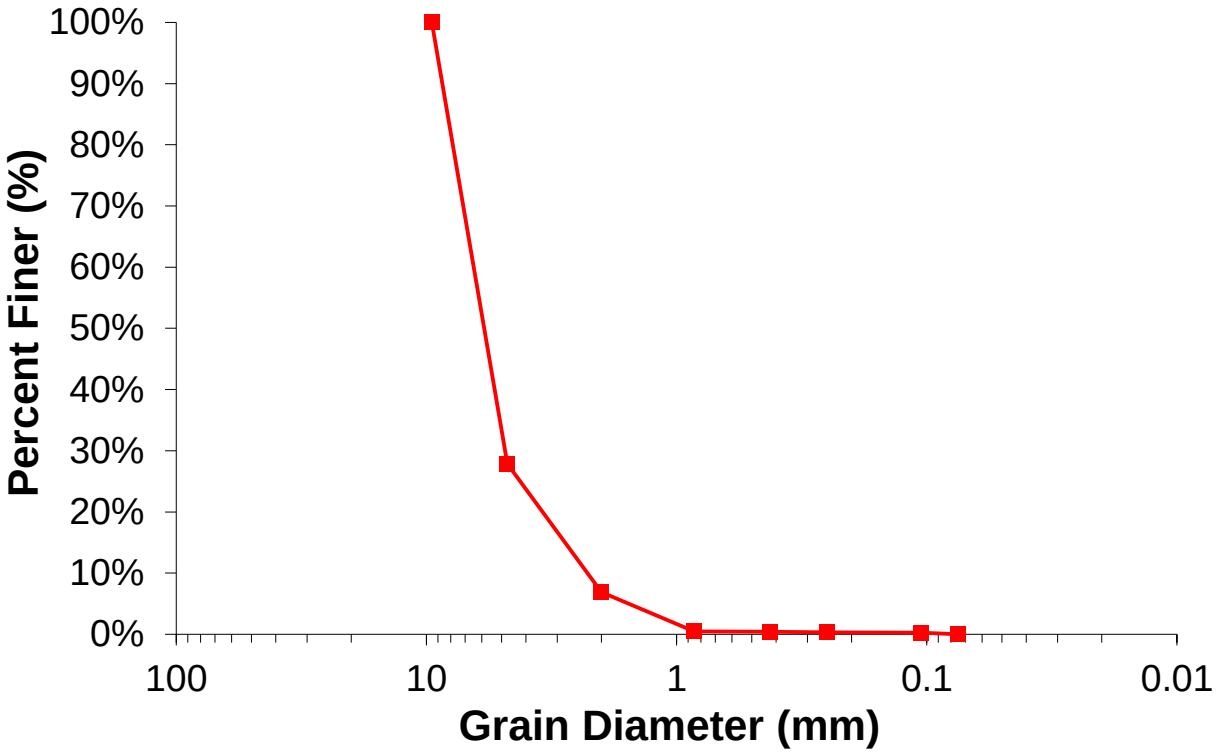

Figure 4.1 Concrete aggregate grain size distribution

As further detailed in Chapter 5 of this thesis, experimentation has shown that the portion of the rail seat not more than 1 inch (2.54 cm) from the field side shoulder is the region of the rail seat which is most sensitive to changes in the rail seat load distribution. Therefore, it was decided to also vary the

portion of the rail seat over which the particles were applied. To represent typical particle intrusion, 3 teaspoons (15 mL) of material were distributed evenly over the entire rail seat.

To simulate a more extreme case, 0.5 teaspoons (2.5 mL) of material were distributed evenly over the 1 inch (2.54 cm) of the rail seat closest to the field side, as described above. It was hypothesized that this uneven distribution of particles would create an effective difference in height across the rail seat, resulting in a greater proportion of the rail seat load imparted on the area of the rail seat already known to be most sensitive to changes in rail seat load. This combination of particle size and region of intrusion leads to five experimental cases: No Fines (the control case), 1" Sand (sand applied to the field-side inch of the rail seat), Full Sand (sand applied to the entire rail seat), 1" Aggregate (B-Stone aggregate applied to the field-side inch of the rail seat), and Full Aggregate (B-Stone aggregate applied to the entire rail seat).

In field conditions, it is rare that a single rail seat will carry the entire vertical load applied by a single wheel. Instead, the vertical wheel load is often distributed across five or more crossties, with the rail seat directly below the point of loading carrying the largest proportion of the load (Hay 1982). An extensive literature review and previous field experimentation have shown that average values for the rail seat load directly below point of loading are typically close to 50% of the total vertical wheel load. However, this value may vary significantly, predominately due to the support conditions under the rail seat in relation to that of neighboring rail seats (RailTEC 2015). The magnitude of vertical load applied in this experimentation was therefore varied to capture this behavior, with testing conducted at 10,000 lbf (44.5 kN), 20,000 lbf (88.9 kN), and 30,000 lbf (133 kN). These values were chosen to represent 25%, 50%, and 75% of 40,000 lbf (178 kN), which represents a 95^{th} percentile nominal vertical wheel load in North American heavy haul freight service (Van Dyk 2014). At each magnitude of vertical load, the L/V Force Ratio was also varied from 0.0 to 0.6, to simulate varying degrees of curvature.

The Amsted RPS P2000 fastening system was used in this experimentation. All clips were applied new, and discarded when removed to eliminate variability due to reduced toe load from fastener wear. The same two-part pad assembly and insulators were used for all experimentation to eliminate

thickness variations within manufacturing tolerances. The rail pad assembly and insulators were lightly used in previous experimentation but were undamaged prior to installation. Before each application of particles, the rail seat was cleaned with a handheld broom to prevent contamination from the prior particle intrusion case (e.g. removing sand prior to experimentation with aggregate). Three separate trials were conducted for each combination of particle size, intrusion region, vertical load, and lateral load. The results presented in this paper represent an average of the three corresponding data points, except as noted. Replicates were collected to assess the variability induced by particle intrusion, but the rail seat load distribution was found to behave consistently for repeated trials with identical experimental conditions.

4.3. Results

During experimentation, researchers noted that the presence of aggregate at the rail seat significantly increased the difficulty of assembling the fastening system. Due to the effective increase in height of the rail base above the rail seat, the insulators developed a tendency to become unseated during clip application. Additional rotational restraint of the rail was required to enable the application of both fasteners. Upon disassembly of the fastening system following experimentation with the crushed stone aggregate, the particles were found to have been pulverized during experimentation, resulting in reduced particle size as shown in Figure 4.2. Despite the pulverization of the aggregate, the qualitative behavior of the rail seat load distribution did not appear to change as a result of the effective decrease in particle size. Due to the small sample size, a sieve analysis was not run on the pulverized material.

In order to prevent failure of the fastening system, experimentation was halted when the rail seat load became concentrated solely on the half of the rail seat closest to the field side shoulder (i.e. if the gauge side of the rail seat was completely unloaded). Experience has shown high lateral loads tend to result in this concentration, which precedes the plastic yield-failure of the gauge side clip. This threshold was reached at approximately 0.56 L/V force ratio under a 30,000 lbf (133 kN) vertical load during experimentation both with no fines present and in the Full Sand case. When aggregate was placed on the field side of the rail seat, the target 0.6 L/V force ratio was achieved at all three tested vertical load

magnitudes. It is hypothesized that the improved tolerance of high lateral loads was due to an effective increase in rail cant caused by the aggregate elevating the field side of the rail base. When aggregate was placed on the entire rail seat, experimentation was halted at 0.58 L/V under a 20,000 lbf (88.9 kN) vertical load and 0.5 L/V under a 30,000 lbf (133 kN) vertical load due to the previously described unloading of the gauge side. It is hypothesized that the effective increase in height of the rail base, which led to the aforementioned difficulty with assembling the fastening system, may have changed the magnitude and direction of the resultant force applied by the fastener toe load, leading to a decrease in rail rotational restraint.

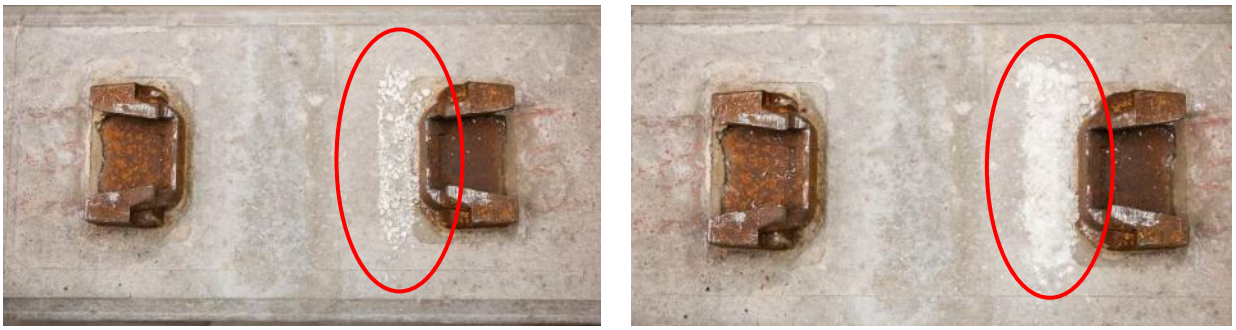

(a) (b)

Figure 4.2 Aggregate (circled) before (a) and after (b) 1" aggregate experiments

4.3.1. Qualitative Analysis

Figure 4.3 compares the qualitative effect of both L/V force ratio and particle intrusion on rail seat load distributions. The first series represents the common design assumption that the rail seat load is distributed uniformly across the entirety of a clean crosstie rail seat. By definition, this assumption does not account for changes in L/V force ratio. The remaining five series illustrate each of the experimental cases for particle intrusion: clean rail seat (no particle intrusion), sand intrusion on the field side of the rail set, sand intrusion on the entire rail seat, aggregate intrusion on the field side of the rail seat, and aggregate intrusion on the entire rail seat.

A non-uniform distribution of load was observed in all five experimental cases, with the variation in particle size and extent of intrusion affecting the magnitude of non-uniformity. The primary effect of particle size was on regularity of the load distribution. Larger aggregate particles produced greater

variation in measured load at adjacent sensing locations, as represented by the "peaks" of warmer colors evident in the Full Aggregate case. The primary effect of the extent of particle intrusion was on the portion of load applied to the region of the rail seat not more than 1 inch (2.54 cm) from the field side shoulder. The intrusion of particles exclusively in this region leads to a gap in the load distribution at lower L/V's that is not present under the intrusion of particles across the entire rail seat. Moreover, experimentation with sand particles suggests that in the 1" Sand case, a greater portion of the rail seat load was applied to the field side of the rail seat than in the Full Sand case.

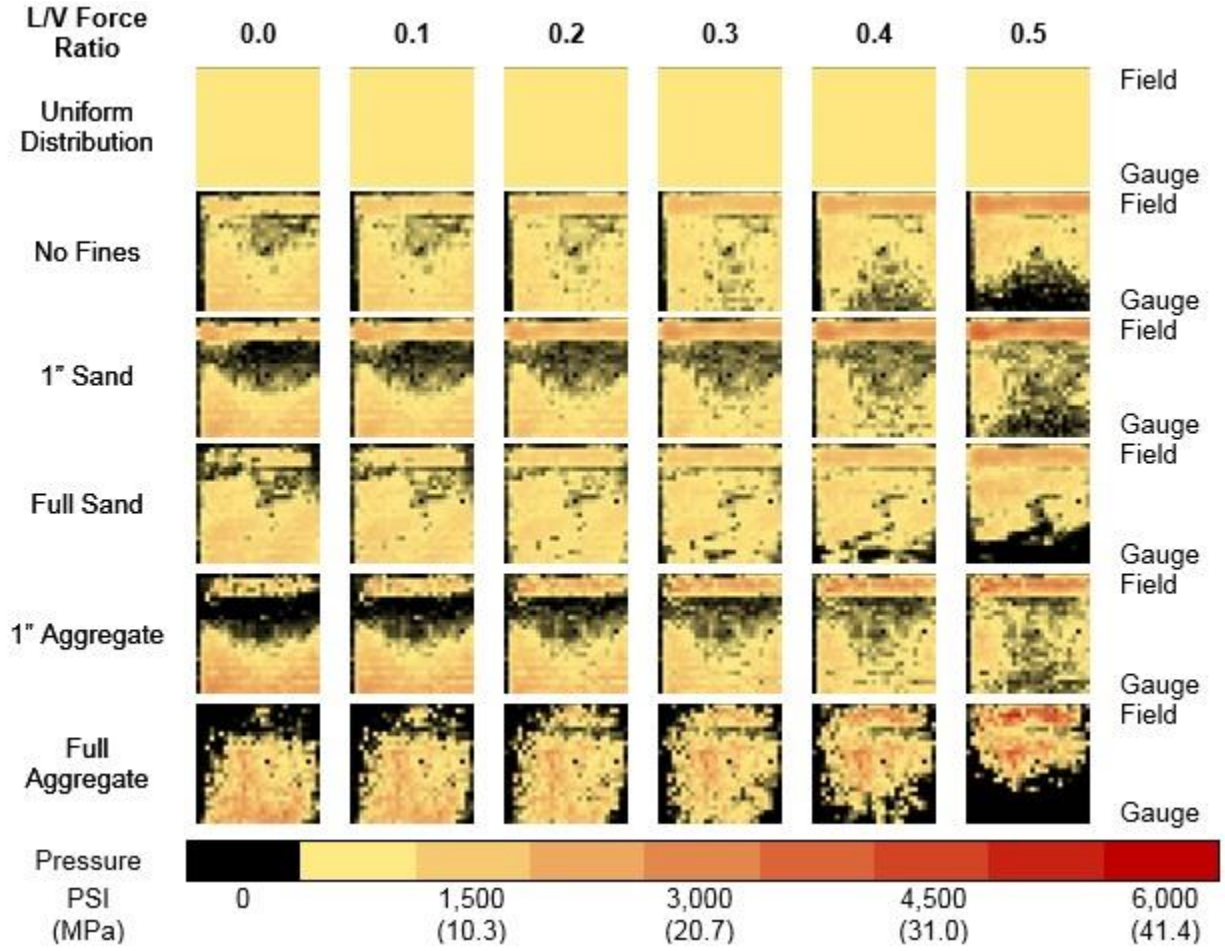

Figure 4.3 Qualitative comparison of rail seat load distributions under 30,000 lbf (133 kN) vertical wheel load at varying L/V force ratios

4.3.2. Quantitative Analysis

Figure 4.4 summarizes the effect of particle intrusion on contact area (the area over which the rail seat load is distributed) when subjected to increasing L/V force ratio under a constant 30,000 lbf (133 kN)

vertical load. In the No Fines, 1" Sand, and Full Sand cases, more than 90% of the rail seat is engaged at low L/V force ratios. The contact area remains relatively constant until 0.4 L/V force ratio is reached, with the presence of sand introducing slightly higher contact areas than the No Fines case. Beyond 0.4 L/V force ratio, the three cases experienced a rapid loss of contact area. When experimentation was halted at approximately 0.56 L/V force ratio, the No Fines, 1" Sand, and Full Sand cases exhibited a 38%, 33%, and 43% reduction in contact area, respectively, relative to the contact area observed at 0.0 L/V force ratio for each case.

As shown qualitatively in Figure 4.3, the presence of aggregate at the concrete crosstie rail seat generates an overall reduction in contact area. Both aggregate cases exhibited a lower initial contact area at 0.0 L/V force ratio. Only 80% of the total rail seat area was loaded in the 1" Aggregate case, and only 69% was loaded in the Full Aggregate case. Both aggregate cases then showed a gradual increase in contact area before reaching a critical L/V force ratio. Beyond this threshold, both experimental cases exhibited rapid reductions in contact area. In the 1" Aggregate case, contact areas comparable to those observed in the No Fines case were achieved between 0.3 and 0.5 L/V force ratio. As previously mentioned, the 1" Aggregate case was the only experimental case to achieve the target L/V force ratio of 0.6 L/V under a 30,000 lbf (133 kN) vertical load, at which point the contact area was measured to be 37% less than that at 0.5 L/V force ratio. The Full Aggregate case, by comparison, achieved a maximum contact area 21% lower than the contact area observed on a clean rail seat. When experimentation was halted at 0.5 L/V force ratio, the Full Aggregate case exhibited 44% less contact area than that observed at 0.0 L/V force ratio in the No Fines case.

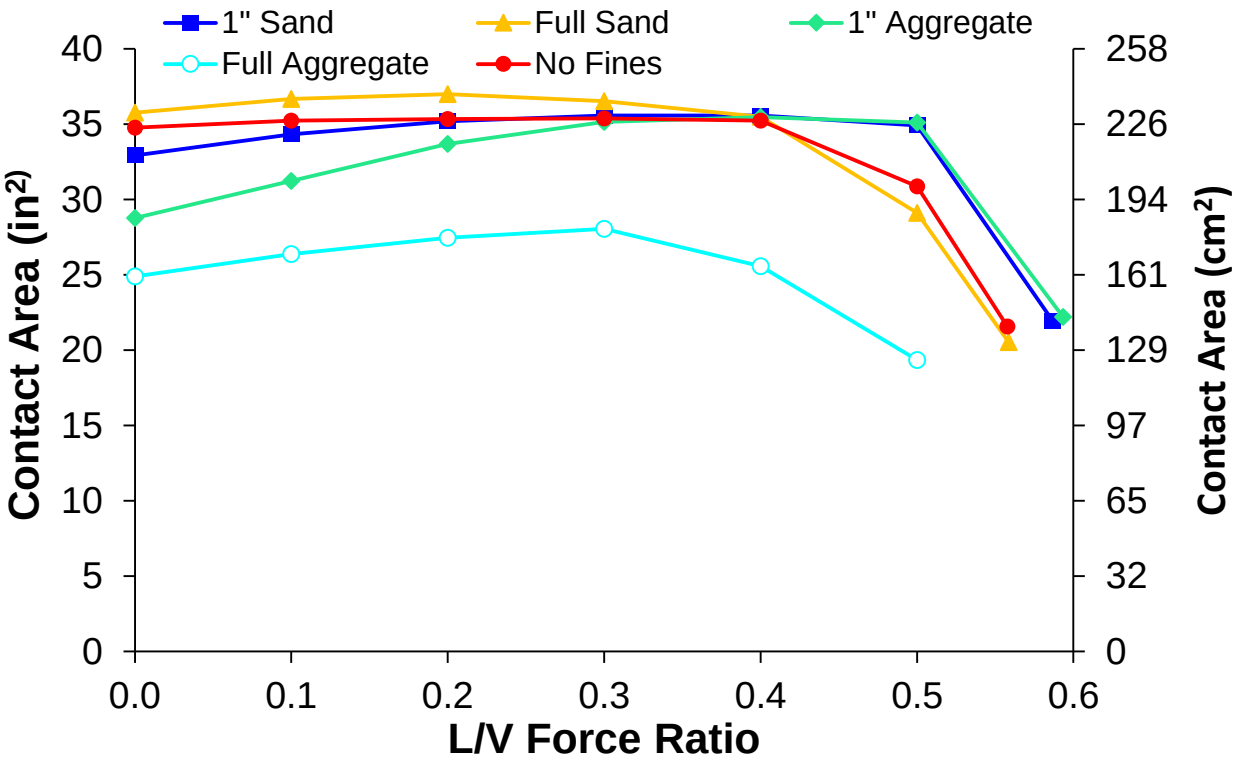

Figure 4.4 Loss of contact area under 30,000 lbf (133 kN) vertical load

Figures 4.5 and 4.6 quantify the change in pressure as a result of the experimentation. There are three primary metrics by which rail seat pressures are typically analyzed: theoretical uniform pressure, average pressure, and maximum pressure. The theoretical uniform pressure is obtained by dividing the total rail seat load by the total rail seat area, and represents the common design assumption that the rail seat load is uniformly distributed across the entirety of the crosstie rail seat. The theoretical uniform pressure is included in both Figures 4.5 and 4.6, and serves as a comparison between the data and the theoretical, uniform case. The average pressure is obtained by dividing the total rail seat load by the measured contact area, rather than the total rail seat area as used to calculate the theoretical uniform pressure. The maximum pressure is the highest pressure recorded by the MBTSS at any combination of vertical load and L/V force ratio.

Figure 4.5 illustrates the effect of particle intrusion and L/V force ratio on the average rail seat pressure. Because average pressure is derived from contact area, the data series exhibit inverse behavior when compared to the contact area data illustrated in Figure 4.4 (i.e. higher contact areas correlate to

lower average pressures). Because the No Fines, 1" Sand, and Full Sand cases result in almost the entire rail seat being engaged in load transfer at low L/V force ratios, the average pressures plot very close to the theoretical uniform pressure. Below the aforementioned threshold of 0.4 L/V force ratio, the three cases yielded average pressures within 10% of the theoretical uniform pressure. As contact area decreased above this threshold, the No Fines, 1" Sand, and Full Sand cases experienced an increase in average pressure of 61%, 51%, and 75%, respectively, resulting in average pressures 67%, 65%, and 77% higher than the theoretical uniform pressure, respectively.

Due to the reduced contact area measured in the presence of aggregate at the crosstie rail seat, the 1" Aggregate and Full Aggregate cases exhibited slightly higher pressures than those observed on a clean rail seat or in the presence of sand. As contact area increases from 0.0 to 0.3 L/V force ratio for the 1" Aggregate case, the average pressure was reduced from 25% higher than the theoretical uniform pressure to just 3% higher. Following the loss of contact area from 0.5 to 0.6 L/V force ratio, the average pressure increased 59%, resulting in an average pressure 30% higher than the theoretical uniform pressure. In the Full Aggregate case, the average pressure at 0.0 L/V force ratio was 45% higher than the theoretical uniform pressure before experiencing a reduction as increasing L/V force ratio resulted in a greater portion of the rail seat engaged in load transfer. At 0.3 L/V, the average pressure observed in the Full Aggregate case was 30% higher than the theoretical uniform pressure, before again increasing as contact area was lost. At 0.5 L/V force ratio, when experimentation was halted, the Full Aggregate case had experienced an overall increase in pressure of 31%, resulting in values 90% higher than the theoretical uniform pressure.

Figure 4.6 illustrates the effect of particle intrusion and L/V force ratio on the maximum rail seat pressure. While the presence of sand resulted in contact areas slightly higher than those observed in the No Fines case, Figure 4.3 shows significant areas of the rail seat engaged in load transfer at lower pressures in the 1" Sand case. This therefore leads to higher maximum pressures than those seen in the No Fines and Full Sand cases. While maximum pressures in the Full Sand case are comparable to those observed in the No Fines Case, increasing from 2.6 to 5 times the theoretical uniform pressure between

0.0 and 0.56 L/V force ratio, maximum pressures recorded in the 1" Sand case ranged from 3.1 to 7.1 times the theoretical uniform pressure at 0.0 and 0.58 L/V force ratio, respectively. The 1" Aggregate case resulted in behavior similar to the 1" Sand case, with maximum pressures ranging from 3.7 to 7.3 times the theoretical uniform pressure at 0.0 and 0.6 L/V, respectively. The Full Aggregate case consistently exhibited the highest maximum pressures at any given L/V force ratio, ranging from 4.8 to 7.7 times the theoretical uniform pressure at 0.0 and 0.5 L/V, respectively.

The highest pressure recorded during experimentation were observed in the Full Aggregate case, with a maximum pressure of approximately 6,400 psi (44 MPa), achieved at 0.5 L/V force ratio, respectively. It is hypothesized that crushing of the B-Stone aggregate occurred at these high L/V force ratios, leading to reduced particle size which, in turn, led to similar results to the 1" Sand case at high L/V force ratios. Had the aggregate particles not failed, it is feasible that higher maximum pressures could have been observed. Further experimentation with stronger aggregate is needed to evaluate this hypothesis. The sensing resolution of the MBTSS also presents a limitation. Each sensing location is 0.22 inches (0.56 cm) square. It is possible that there may be regions smaller than the size of a single sensing location where the applied pressure may be higher than those observed in this study. Due to the limitations of the instrumentation, however, the data reflect the average pressure applied to each 0.0484 $inch^2$ (0.31 cm^2) sensing location. Nonetheless, because the observed maximum pressures fall short of the design compressive strength of concrete used in the manufacture of concrete crossties in North America (7,000 psi), crushing damage due to a single load application is not expected in the presence of particle intrusion on a concrete rail seat with a new fastening system.

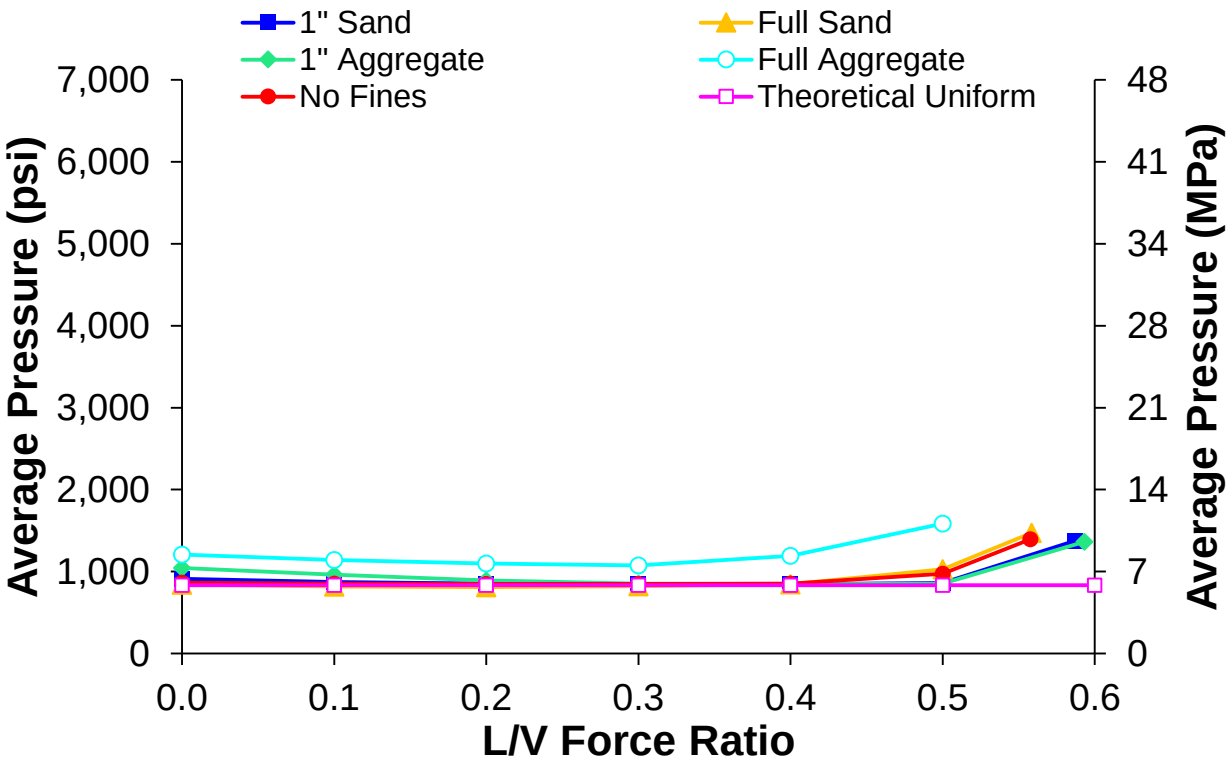

Figure 4.5 Increase in average pressure under 30,000 lbf (133 kN) vertical load

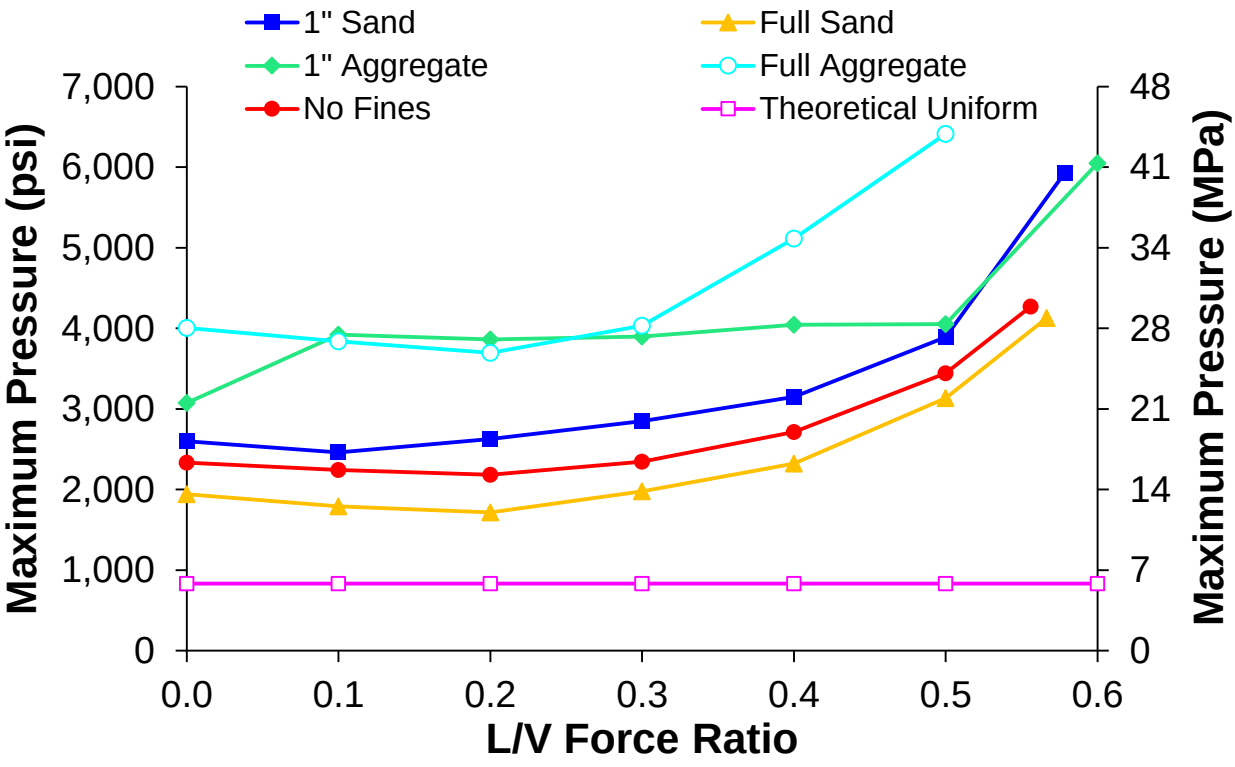

Figure 4.6 Increase in maximum pressure under 30,000 lbf (133 kN) vertical load

While this experimentation did not generate pressures exceeding the design compressive strength of the concrete, crushing damage as a result of repeated load applications may be feasible. The fatigue compressive strength of concrete is generally regarded as ranging from 50 to 60% of the ultimate compressive strength for high-load cycle applications (El Shahawi and Batchelor 1986, ACI Committee 215 1992). A conservative estimate of the design fatigue compressive strength of concrete would therefore be 3,500 psi (24 MPa), or half of the design compressive strength. Figure 4.6 shows that at high L/V force ratios (above 0.4), the maximum pressures observed in the 1" Sand, 1" Aggregate, and Full Aggregate cases exceeded this threshold. This indicates that crushing damage to the concrete rail seat as a result of repeated load applications may indeed be feasible in cases of extreme particle intrusion and high rail seat loads.

Practical experience has shown that the actual compressive strength achieved in the manufacture of North American concrete crossties can exceed 11,000 psi (76 MPa), nearly twice the highest pressure observed in this experimentation. Further, the reported concrete compressive strength is obtained from compressive tests on unreinforced concrete cylinders (AREMA 2014). The confinement provided by the mass of concrete comprising the rail seat and the prestress provided by the crosstie reinforcement will further increase the actual compressive strength of the concrete at the crosstie rail seat, further increasing the pressure necessary to generate crushing. Although these factors further indicate that crushing due to a single load application may not be feasible, the data shown in Figure 8 suggest that crushing due to repeated load application may still be feasible in the most extreme cases (e.g. particle intrusion only on the field side of the rail seat). Further, as described in Chapter 2 of this thesis, fastener wear can lead to an increase in rail seat pressures. In such cases, the accumulation of crushing damage to the concrete rail seat may be accelerated by the increase in maximum pressures.

4.4. Conclusions

In this experimentation, particle size, extent of intrusion, vertical rail seat load, and L/V force ratio were varied to generate realistically demanding loading environments. The distribution of loads at the crosstie rail seat was collected using matrix-based tactile surface sensors, and the data were analyzed to determine

the effect of particle intrusion. While the presence of sand had little effect on the measured contact area, the presence of aggregate led to an average reduction of 23% at 0.0 L/V force ratio. An average 35% reduction in contact area due to high L/V force ratios was observed in all experimental cases. No average pressures were observed to be greater than 200% of the theoretical average pressure given a uniform distribution of rail seat load. While maximum pressures of 6,400 psi (44 MPa) were recorded, the minimum threshold to generate crushing, a proposed failure mechanism for RSD, as a result of a single load application, was not exceeded. In extreme loading cases, however, the estimated design fatigue strength of the concrete, 3,500 psi (24 MPa) was exceeded. These findings indicate that crushing damage may be generated as a result of a large number of repeated load applications. It was therefore concluded that although crushing damage of concrete crosstie rail seats due to a single load application is not expected, crushing damage due to repeated load applications may be feasible in the presence of particle intrusion.

CHAPTER 5: THE INTRODUCTION OF RAIL SEAT LOAD INDEX, A PROPOSED DESIGN METRIC[4]

5.1. Introduction

Historically, the process by which components of the track structure are designed has been largely reactive, based on performance failures and practical experience. This design process as presented in the *AREMA Manual for Railway Engineering* (2014) has been simplified greatly to allow easy and rapid application of the concepts contained therein. This has resulted in a design methodology that can be regarded as a "black box" in which critical design values are determined by graphical relationships and reduction factor tables, often presented without explanation of the equations, assumptions, or limit states from which these graphs and tables were determined.

A survey of railroad industry experts conducted by researchers at UIUC identified the following list of crosstie and fastening system failures as most critical in North America, ranked in order of criticality (adapted from RailTEC 2015):

- **Rail seat deterioration (RSD)**
- **Shoulder and fastening system wear and fatigue**
- **Cracking from dynamic loads**
- Derailment damage
- **Cracking from center binding**
- Tamping damage
- Other (e.g., manufactured defect)
- **Cracking from environmental or chemical degradation**

The five entries which are bolded represent failures which may be mitigated by improved design methodologies. Because so many critical failures can be affected by or are related to the design of the

[4] Chapter 5 was originally published as part of the 2010 FRA Tie and Fastener BAA Final Report by the University of Illinois at Urbana-Champaign (RailTEC 2015)

crosstie and fastening system, significant benefits may result from improvements to the fundamental philosophy by which concrete crossties and their fastening systems are designed.

As part of a larger study examining the design and performance of concrete crossties and fastening systems, researchers at UIUC have proposed a mechanistic design process framework for concrete crossties and fastening systems (RailTEC 2015). A mechanistic design approach utilizes measured relationships between inputs (wheel loads, material properties, etc.) and critical outputs (interface pressures, component displacements, etc.) to select the materials and geometry for each component, and to assure that components do not interact negatively. This allows for crosstie and fastening system designs to be optimized for the expected loading environment (e.g. designs for tangent track applications do not have to resist the same magnitude of lateral loads to which designs for high curvature applications are designed) (RailTEC 2015). The pad assembly-rail seat interface is regarded as one of the critical interfaces in this design approach, due to the role of rail seat pressures and relative displacement of the pad assembly and rail seat in the deterioration of the crosstie rail seat. Therefore, a mechanistic evaluation of the rail seat load distribution was considered as part of this mechanistic design process framework.

5.2. Overview of current design process – general case

AREMA Chapter 30 does not contain any design considerations for the distribution of load at the concrete crosstie rail seat. For design purposes, the rail seat load is regarded as uniformly distributed across the entire rail seat. This assumption, however, does not accurately describe the behavior of the rail seat load at high L/V force ratios, as further detailed in Chapter 2 of this thesis. Figure 5.1 shows the distribution of rail seat load in the worn fastener case as a function of the distance from the field side shoulder, collected using MBTSS. The data series were calculated by summing the load applied to each sensor row, which are 0.22 inches (5.59 mm) in width, at each L/V force ratio. As the L/V force ratio increases, the data show significant concentration of the rail seat load on the field side of the rail seat, and an unloading of the gauge side of the rail seat, which agrees with the rail seat load behavior observed in this thesis. The area of the rail seat that is 1 inch (25.4 mm) or less from the field side shoulder, illustrated by the area left

of the dashed line in Figure 5.1, exhibits the highest sensitivity to changes in the L/V force ratio, and consistently exhibits significantly higher loads than the remainder of the rail seat. Figure 5.1 also shows the effect of the rail pad texture. The micro-level variations in each data series are due to studs on the bottom of the rail pad designed to allow water to drain from the rail pad-abrasion frame interface, with higher loads occurring under the studs. Although the variation in load due to rail pad texture is not as significant as that due to changes in the loading environment, it is interesting to note that the effect of rail pad texture does have an observable impact on the rail seat load distribution.

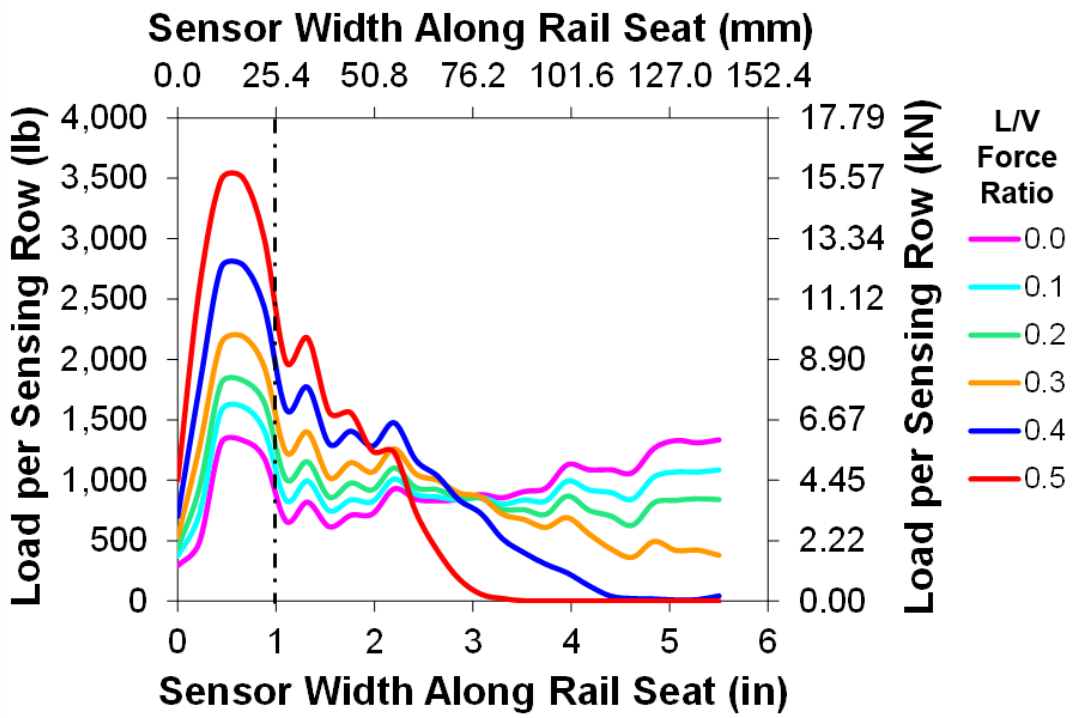

Figure 5.1 Lateral distribution of rail seat load at varying L/V force ratio (40,000 lbf (178 kN) vertical wheel load)

It is important to note that although none of the pressures observed in Figure 5.1 approach the design compressive strength of the concrete (i.e. 7,000 psi (AREMA 2014)), the increase in pressure will change the characteristics of failure mechanisms associated with RSD (e.g. increased frictional force leading to more severe abrasion). It is hypothesized that RSD first develops in regions of extreme pressure and then spreads as the loss of material becomes more severe. Therefore, a design check

ensuring that the rail seat load distribution does not generate these critical higher pressures would lead to fastening systems with a greater inherent resistance to RSD.

5.3. Overview of New Design Process – General Case

The Rail Seat Load Index (RSLI) is proposed as a quantifiable design value which describes the sensitivity of the rail seat load distribution to changes in the L/V force ratio. The RSLI of a rail seat describes the portion of the total rail seat load that is imparted onto a critical region of the rail seat, normalized to a theoretical uniform distribution, i.e.,

$$RSLI = \frac{\frac{P_{crit}}{P}}{\frac{1}{6}} = 6 \times \frac{P_{crit}}{P}$$

where, RSLI = Rail Seat Load Index

P_{crit} = Vertical load applied to critical area of rail seat

P = Total vertical rail seat load

Because the RSLI is calculated from a ratio of loads, RSLI can be applied to any units of load, provided that the same units are used for both the vertical load applied to the critical area and the total vertical rail seat load. This critical region is defined as the area of the rail seat not more than 1 inch (25.4 mm) from the field side shoulder. As illustrated in Figure 5.1, this region of the rail seat is the most sensitive to changes in the L/V force ratio. Therefore, for a 6 inch (152.4 mm) rail base, one sixth of the total rail seat load will be imparted onto the critical region in a uniform loading case.

To further explain this metric, RSLI values can be calculated for the data presented in the preceding chapters of this thesis. Figure 5.2 illustrates the average effect of increasing L/V force ratio on RSLI for both the new and worn fastener cases (further detailed in Chapter 2 of this thesis), considering a constant 40,000 lbf (178 kN) vertical wheel load. At 0.0 L/V force ratio, both the new and worn fastener cases achieve an RSLI near 1, indicating a proportionate amount of the rail seat load is imparted to the critical area. The new fastener RSLI increases to 1.4 at a 0.6 L/V force ratio; by the equation used to calculate RSLI, this indicates that slightly less than one quarter of the total rail seat load is applied to the

one inch closest to the field side shoulder. By contrast, the worn fastener case experiences a significant increase in RSLI, with a maximum RSLI of 3.1 at 0.55 L/V force ratio. This means that more than three times the load predicted by a uniform distribution—half of the rail seat load—is concentrated in the critical area of the rail seat, indicating a severely non-uniform load confirmed by the analysis detailed in Chapter 2 of this thesis. Figure 5.2 also includes RSLI data from joint experimentation with TTCI examining the effect of rail seat deterioration on the rail seat load distribution (further detailed in Chapter 3 of this thesis), considering a constant 20,000 lbf (88.9 kN) vertical wheel load. The data shown are representative of extreme RSLI values that may be observed in the field as a result of 0.75 inches (19.1 mm) of RSD: at 0.0 L/V force ratio, the data show an RSLI of 1.75 and increases to 4.37 under a 0.6 L/V force ratio. This represents four times the load predicted by a uniform distribution—nearly three quarters of the rail seat load—applied to the one inch closest to the field side of the rail seat. Lastly, Figure 5.2 also includes RSLI data from laboratory experimentation examining the effect of particle intrusion on the rail seat load distribution (further detailed in Chapter 4 of this thesis), considering a constant 30,000 lbf (133 kN) vertical rail seat load. The data represent RSLI values which may be observed in the field as a result of sand intrusion in the previously defined "critical area" of the rail seat, which produced the highest RSLI values of all particle intrusion experimentation. The observed values are similar in magnitude to those recorded during experimentation with artificial RSD: at 0.0 L/V force ratio, an RSLI of 1.58 was recorded, and at 0.58 L/V force ratio, a maximum RSLI of 4.16 was recorded. This represents 4.2 times the load predicted by a uniform distribution—more than two thirds of the total vertical rail seat load—applied to the most sensitive area of the rail seat. These extreme RSLI values correlate with maximum pressures approaching 6,000 psi (41.4 MPa), which will inherently increase the severity of failure mechanisms associated with RSD, as previously discussed in Section 5.1 of this chapter.

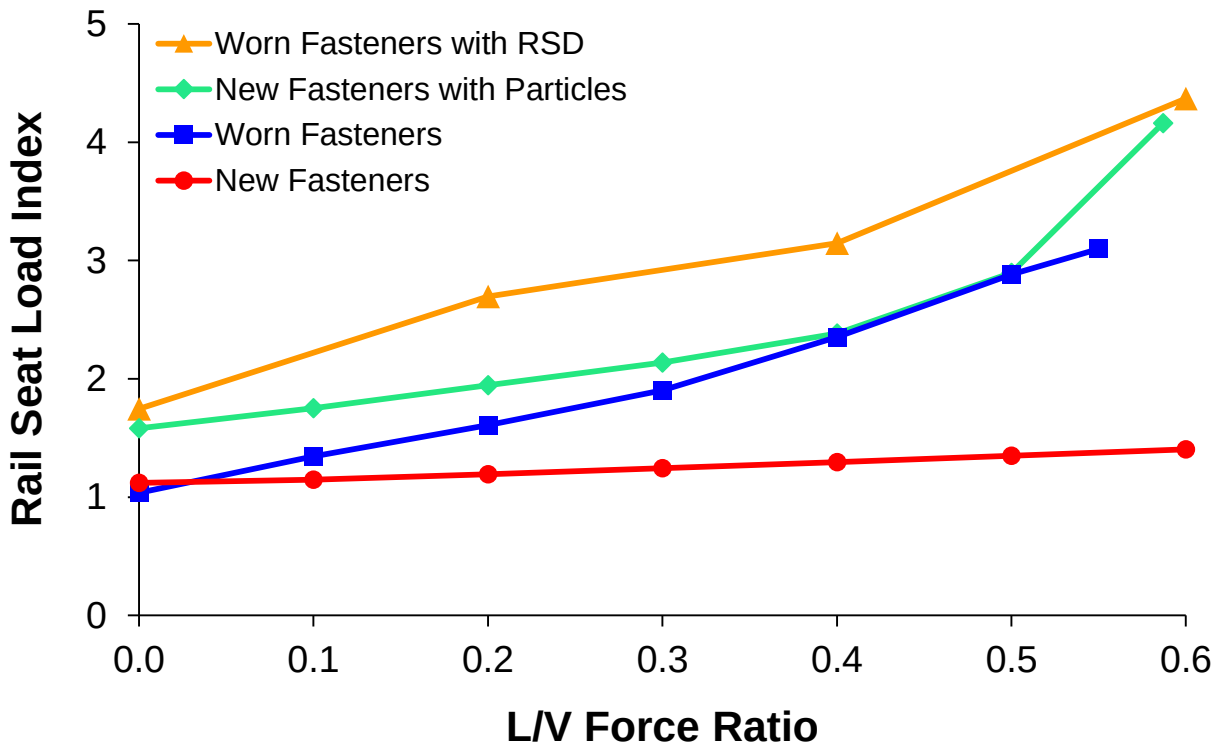

Figure 5.2 Effect of L/V force ratio on RSLI for varying cases of crosstie and fastening system wear

While RSLI clearly illustrates the non-uniformity of the rail seat load distribution on a macroscopic level (e.g. when considering the concentration of load towards the field side of the rail seat), it may not directly correlate to high maximum pressures. In Figure 5.2, the RSLI data representing worn fasteners with RSD are higher than those representing new fasteners with particle intrusion. If, however, the maximum pressures are considered, the latter data generate significantly higher pressures than the former (6,000 psi (41.4 MPa) versus 4,400 psi (30 MPa)). Further, Figure 5.3 illustrates RSLI calculated from data collected during experimentation to determine the effect of particle intrusion (further detailed in Chapter 4 of this thesis). The 1" Sand data series is equivalent to the New Fasteners with Particles data series in Figure 5.2, which yielded maximum pressures of approximately 4,100 psi (28.3 MPa) at an L/V force ratio of 0.5. By comparison, the Full Aggregate data series shown in Figure 5.3 correlates to pressures exceeding 6,400 psi (44 MPa) at a 0.5 L/V force ratio, but shows a comparable level of overall rail seat load non-uniformity as the 1" Sand data series. This highlights a potential shortcoming of RSLI,

and other such cases may exist where rail seats with higher maximum pressures may yield lower values of RSLI. However, RSLI is intended to describe the broad performance of a fastening system, rather than the maximum pressures generated by a specific combination of inputs. It is believed that a simpler alternative to a full analysis of the rail seat load distribution is more beneficial for the design process, and any such approach necessarily sacrifices "resolution" of the data for ease of comprehension.

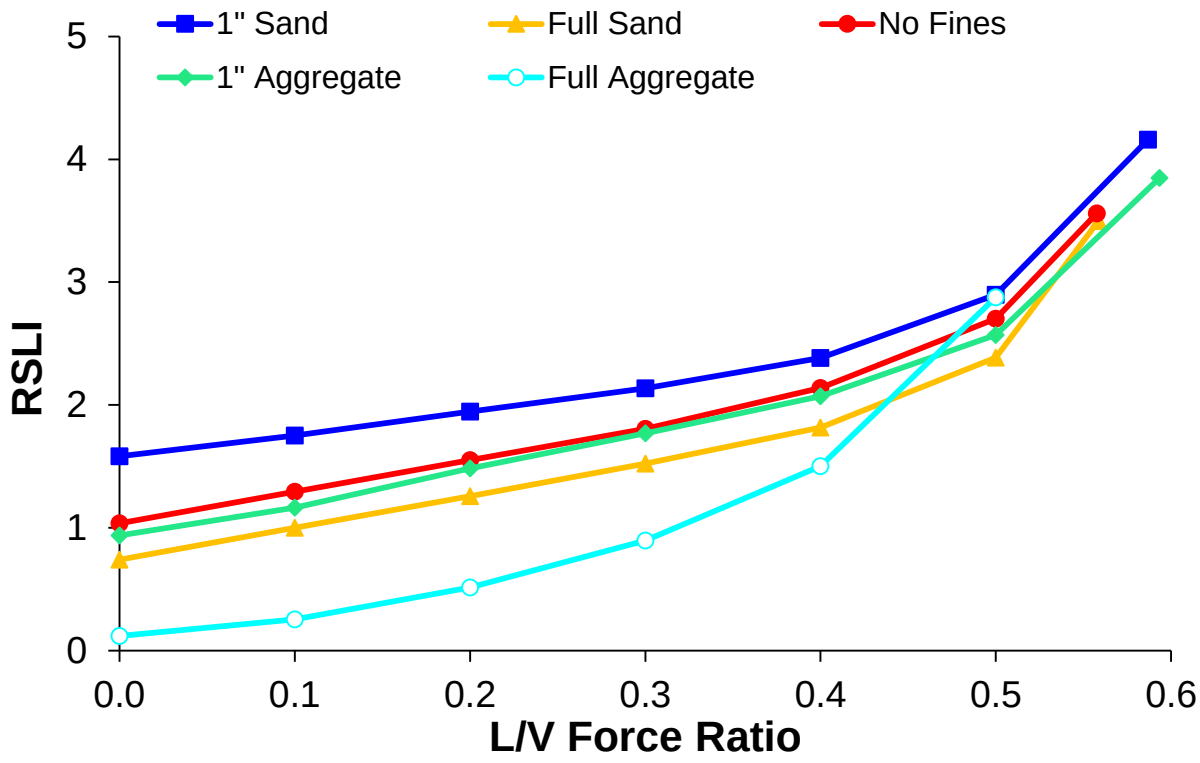

Figure 5.3 Effect of L/V force ratio on RSLI for varying cases of particle intrusion (30,000 lbf (133 kN) rail seat load)

5.4. Hypothetical RSLI Test Procedure

To determine the maximum RSLI of a fastening system, an experimental testing procedure has been developed. This RSLI test would be performed on a single rail seat in conjunction with AREMA Test 6 (Wear and Abrasion) to examine both new and worn fastening system component conditions. The test utilizes a loading frame capable of applying controlled vertical and lateral loads of independently varying magnitude to the rail head. A section of 136RE rail 18 inches (457 mm) in length should be affixed to a single rail seat with a typical fastening system, with an MBTSS installed between the fastening system

and crosstie rail seat as shown in Figure 5.4. The assembly should then be subjected to the design vertical load. Once the design vertical load is reached, the lateral load should be increased until the design L/V force ratio is achieved. The MBTSS is then removed, and the same fastening system components are reassembled and subjected to AREMA Test 6. Following Test 6, the fastening system is disassembled, the MBTSS is reinstalled, the fastening system is reassembled once more, and is then again subjected to the design loading environment. Failure criteria for the test would be established based on both the change in RSLI as a result of AREMA Test 6, and the absolute maximum RSLI recorded during the RSLI test.

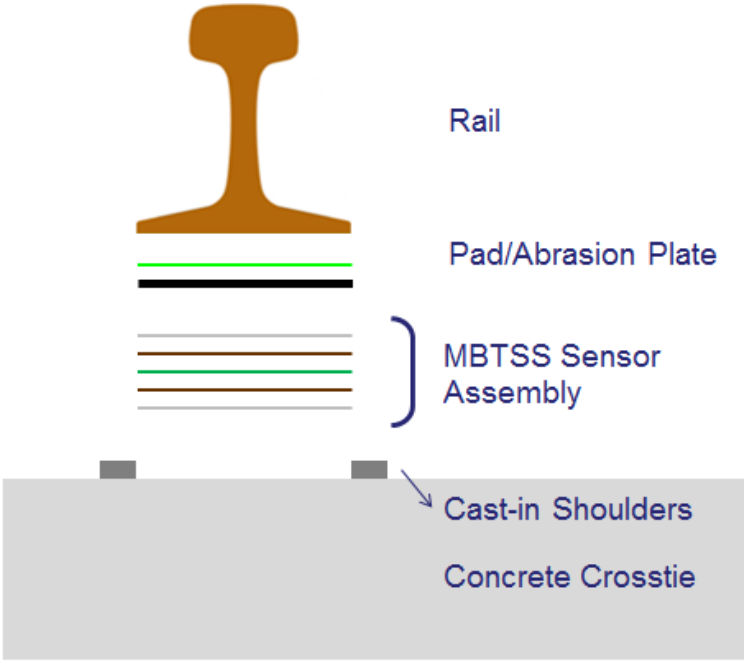

Figure 5.4 Profile view of example sensor installation for RSLI test

Although no criteria for maximum permissible RSLI has been established, it is theorized that a maximum RSLI exists which permits limited concentration of the rail seat load, but prohibits excessive loading on the field side of the rail seat. This excessive loading would result in accelerated wear of the fastening system and an increased potential for RSD. Figure 5.5 illustrates this hypothetical range, which is not affected by L/V force ratio. Instead, the fastening system should be designed to meet the maximum permissible RSLI at the design L/V; this will result in stiffer fastening system designs for loading environments in which high L/V force ratios are common. Further, this allows for fastening systems to be

optimized for their design application, rather than forcing all fastening systems to conform to the same standard regardless of application.

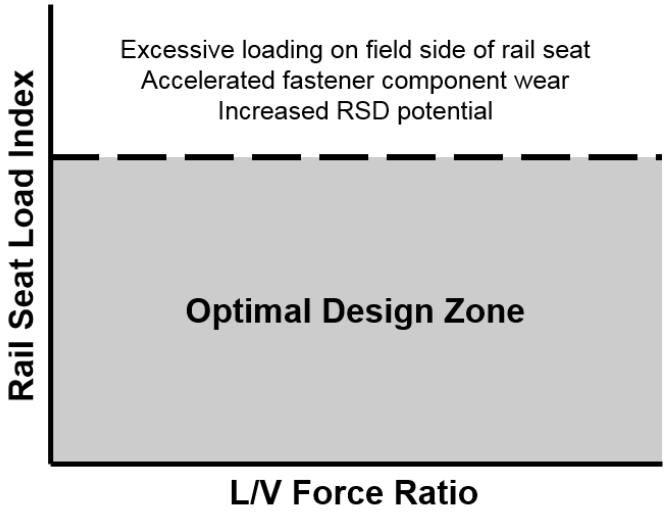

Figure 5.5 Conceptual RSLI design limit philosophy

5.5. Overview of New Design Process Using Safelok I – Sample Calculations

This section utilizes data from lab experimentation to perform a sample calculation of the RSLI at 0.6 L/V force ratio for an example rail seat with an Amsted RPS P2000 fastening system. Figure 5.6 shows the load distribution of a P2000 rail seat subjected to a vertical load of 32,500 lbf (144.6 kN) and a lateral load of 19,500 lbf (86.7 kN), equivalent to an L/V force ratio of 0.6. The critical portion of the rail seat is highlighted in blue, and the loads which will be used to calculate RSLI are tabulated below the figure.

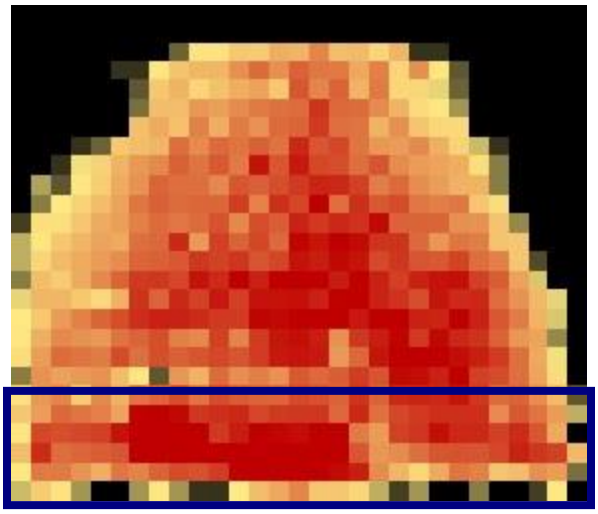

	Pounds	(kN)
Load in Critical Area	9,449	(42.0)
Total Rail Seat Load	32,500	(144.6)

Figure 5.6 Sample rail seat load distribution

The data given in Figure 5.6 can now be used to calculate the RSLI of the fastening system,

$$RSLI = 6 \times \frac{P_{crit}}{P} = 6 \times \frac{9{,}449}{32{,}500} = 1.74$$

Therefore, the RSLI of a new P2000 fastening system at a vertical load of 32,500 lbf (144.6 kN) and 0.6 L/V force ratio is 1.74 for this experimentation.

5.6. Path Forward for This Component

RSLI can be readily defined and evaluated for existing fastening systems with currently available testing equipment. However, a study comparing the RSLI of common fastening systems at varying stages of wear would further the understanding of the practical design zone for RSLI, and experimentation characterizing the relationship between RSD failure mechanisms and rail seat load non-uniformity would aid in the development of mechanistic thresholds for RSLI. Further, experimentation to establish a relationship between RSLI and a measurement presently obtained from AREMA Test 6 experiments would allow for more widespread adaptation of the concept behind RSLI without necessitating the acquisition of specialized instrumentation. Ultimately, the consideration of rail seat load non-uniformity

in the design of concrete crossties and fastening systems will lead to designs with a greater inherent resistance to RSD.

CHAPTER 6: CONCLUSIONS AND FUTURE WORK

6.1. Conclusions

The primary objective of this thesis was to quantify the distribution of rail seat loads on concrete crossties, in order to better understand the role of rail seat pressures in the formation of RSD. Experimentation was conducted in the laboratory and field using MBTSS to capture the rail seat load distribution in an array of loading environments. In Chapter 1 of this thesis, the following four questions were posed to guide the data analysis discussed in the body chapters of this thesis:

1. How do input load and fastener health affect the magnitude of rail seat pressures? (Chapter 2)
2. How does the presence and severity of RSD affect the distribution of loads at the crosstie rail seat? (Chapter 3)
3. Is crushing a feasible failure mechanism by which RSD may be initiated? (Chapter 4)
4. How can the findings of this thesis be applied to further the design methodology for crossties and fastening systems in the context of a framework for mechanistic design? (Chapter 5)

The following sections will summarize the primary findings related to each of these questions.

6.1.1. The Effect of Input Load and Fastener Health

In a purely vertical loading environment (i.e. no lateral load applied to the wheelset), the distribution of load on a new rail seat with a healthy fastening system can be noticeably non-uniform. With the addition of lateral load, the rail seat load tends to concentrate on the field side of the rail seat, which may lead to an increase in maximum pressure relative to the purely vertical case. An increase in pressures may increase the severity of failure modes associated with RSD, and the concentration of load on the field side of the rail seat correlates with the triangular wear pattern associated with RSD found in curved track.

The health of the fasteners has a significant effect on the extent to which the load concentrates on the field side of the rail seat in the presence of lateral loads. Reapplication of the fastening system will lead to a decrease in clamping force at a given fastener deflection, which reduces the ability of the fastening system to restrict rail rotation. In the presence of high L/V force ratios, repeated fastening system reapplication may lead to an unloading of the gauge side of the rail seat, further concentrating the

load on the field side. This behavior will exacerbate the trends of increased pressures and more severe RSD failure mechanisms that may be observed on a rail seat with a healthy fastening system.

6.1.2. The Effect of RSD Presence and Severity

The presence of RSD increases the rotation of the rail base at a given combination of vertical load and L/V force ratio. This rail rotation is proportional to the depth of wear, and is greater at a given wear depth with a triangular wear pattern than that with a uniform wear pattern. Further, this rotation leads to a reduction of contact area, the area through which the load is transferred, and an increase in rail seat pressures. These trends of reduced contact area and increased pressures also exhibit a positive correlation to wear depth.

6.1.3. The Effect of Particle Intrusion

Particle intrusion on the field side of the rail seat may lead to significantly higher maximum pressures than those recorded on a clean rail seat. Although these maximum pressures are lower than the design compressive strength of the concrete comprising the crosstie rail seat, they may exceed the fatigue compressive strength of the concrete. Because of this, crushing damage to the crosstie rail seat is not expected as a result of a single load application, but it may be feasible as a result of a high number of repeated load applications.

6.1.4. Application of Findings

RSLI provides a mechanistic evaluation of the uniformity of the rail seat load distribution. Higher values of RSLI have been shown to correlate to poorly-performing rail seats (i.e. rail seats with high observed pressures), and values of RSLI close to 1 have been shown to correlate to well-performing rail seats (i.e. rail seats with low observed pressures). Application of RSLI to crosstie and fastening system design methodologies may therefore result in fastening systems which are more inherently resistant to excessive load concentration, component wear, and RSD.

6.2. Future Work

This study has quantified rail seat pressures on concrete crossties and considered several factors which affect the distribution of load at concrete crosstie rail seats. Additional research to further the findings of

this study may better define the thresholds at which RSD occurs, and offer insight into design methodologies to modify these thresholds (e.g. increased clamping forces, alternative rail seat materials or inserts, or rail seat treatments).

6.2.1. Understanding RSD Failure Mechanisms

The experimentation detailed in Chapter 2 of this thesis offers a preliminary correlation between fastener reapplications and increases in rail seat pressures. A targeted study in which rail seat load distributions and clamping forces are recorded between successive clip reapplications could better define this relationship, and offer guidance for fastening system renewal strategies on heavy haul freight railroads. Further, research correlating rail seat pressures to wear rate or severity, similar to the research performed by Kernes (2013), could offer a correlation between rail seat load non-uniformity and the formation of RSD. Lastly, research into the effect of support conditions at the crosstie-ballast interface on the rail seat load distribution may be beneficial. Such a study would determine whether the effect of poor support conditions at adjacent crossties differs significantly from the effect of increasing the vertical rail seat load at a constant support condition.

6.2.2. Development of RSLI

The work described in Chapter 5 of this thesis defines RSLI and provides a theoretical framework in which it may be applied for industry use. However, additional research is required to establish maximum permissible values before RSLI can be adapted as an industry-standard design metric. Additional insight could be gained by conducting the proposed RSLI test, as described in Chapter 5, on both the Safelok I fastening system and other common fastening systems, such as an e-clip system or an Skl-type system. Such experimentation would help establish acceptable ranges of RSLI and may allow the correlation of RSLI to a measurement or set of measurements already recorded in AREMA Test 6. Lastly, the proposed research detailed in section 6.2.1 would also help to establish the maximum allowable RSLI.

As a result of experimentation conducted for Chapter 2 of this thesis, Chapter 30 of the AREMA Manual (Ties) was amended in 2015 to include a section which qualitatively describes the non-uniformity of the rail seat load distribution. Following the establishment of mechanistically-determined design

criteria for RSLI, it is anticipated that this section of Chapter 30 will be expanded to include design recommendations based on RSLI, and be accompanied by a suitable test to determine the degree of non-uniformity of rail seat load distribution for a given fastening system. The introduction of RSLI in the design of crosstie and fastening system design practices will promote designs with inherent resistance to RSD, extended life cycles, and improved safety.

REFERENCES

ACI Committee 215, 1992. *Considerations for Design of Concrete Structures Subjected to Fatigue Loading*. American Concrete Institute, Detroit, MI.

American Railway Engineering and Maintenance-of-Way Association, 2014. *AREMA Manual for Railway Engineering*. AREMA, Landover, Maryland.

Bakharev, T. and L.J. Struble. 1997. Microstructural features of railseat deterioration in concrete ties. *Journal of Materials in Civil Engineering* 9 (3): 146-153.

Bloom, J.A. and S. Lee. 2005. The Deployable Gage Restraint Measurement System - Description and Operational Performance. In: *Proceedings: Joint Rail Conference*, Pueblo, Colorado, March 2005.

Clouse, A. Rail cant measurements of concrete crossties (part 2 of 2). *Interface Journal - The Journal of Wheel/Rail Interaction*, 2008.

Choros, J., M.N. Coltman, and B. Marquis. Prevention of Derailments due to Concrete Tie Rail Seat Deterioration. In: *Proceedings: Joint Rail Conference & International Combustion Engine Spring Technical Conference*, Pueblo, Colorado, March 2007.

El Shahawi, M. and Batchelor, B.dV. 1986. Fatigue of partially prestressed concrete. *Journal of Structural Engineering* 112 (3): 524-537.

Federal Railroad Administration. 2006. *Federal Railroad Administration Office of Safety Headquarters Assigned Accident Investigation Report HQ-2006-08*. Federal Railroad Administration, Washington, D.C.

Federal Railroad Administration. 2014. *Track and rail and infrastructure integrity compliance manual, safety standards Volume II, Chapter 1, Section 213.110*. Federal Railroad Administration, Washington, D.C.

Greve, M.J., M.S. Dersch, J.R. Edwards, C.P.L. Barkan, J. Mediavilla, and B. Wilson. 2014. Analysis of the Relationship between Rail Seat Load Distribution and Rail Seat Deterioration in Concrete Crossties. In: *Proceedings: 2014 Joint Rail Conference*, Colorado Springs, Colorado, April 2014.

Greve, M.J., M.S. Dersch, J.R. Edwards, C.P.L. Barkan, H.B. Thompson, T. Sussmann, and M.T. McHenry. 2015a. Examination of the effect of concrete crosstie rail seat deterioration on rail seat load distribution. *Accepted, Transportation Research Record – Journal of the Transportation Research Board*.

Greve, M.J., M.S. Dersch, J.R. Edwards, and C.P.L. Barkan. 2015b. Evaluation of Laboratory and Field Experimentation Characterizing Concrete Crosstie Rail Seat Load Distributions. In: *Proceedings: 2015 Joint Rail Conference*, San Jose, California, March 2015.

Greve, M.J., M.S. Dersch, J.R. Edwards, and C.P.L. Barkan. 2015c. The Effect of Particle Intrusion on Rail Seat Load Distributions on Heavy Haul Freight Railroads. In: *Proceedings: 2015 International Heavy Haul Association Conference*, Perth, Australia, June 2015.

Hay, W.W. 1982. *Railroad Engineering 2nd ed.*, John Wiley & Sons, Inc., New York, New York.

Kernes, R.G. 2013. The Mechanics of Abrasion on Concrete Crosstie Rail Seats. MS Thesis, Department of Civil and Environmental Engineering, University of Illinois at Urbana-Champaign, Graduate College, Urbana, Illinois.

National Transportation Safety Board. 2006. *Railroad Accident Brief RAB-06-03*. National Transportation Safety Board, Washington, D.C.

Railroad Transportation and Engineering Center. 2015. *FRA Improved Concrete Crossties and Fastening Systems for US High Speed Passenger Rail and Joint Passenger/Freight Corridors*. Railroad Transportation and Engineering Center, University of Illinois at Urbana-Champaign, Urbana, Illinois. <http://railtec.illinois.edu/CEE/Crossties/FRA_Final_Report.php>

Rapp, C.T., J.R. Edwards, M.S. Dersch, C.P.L. Barkan, B. Wilson, and J. Mediavilla. 2012. Measuring Concrete Crosstie Rail Seat Pressure Distribution with Matrix Based Tactile Surface Sensors. In: *Proceedings: 2012 Joint Rail Conference*, Philadelphia, PA, April 2012.

Rapp C.T., Dersch M.S., Edwards JR, Barkan C.P.L., Wilson B., and Mediavilla J. 2013. Measuring rail seat pressure distribution in concrete crossties: experiments with matrix-based tactile surface sensors. *Transportation Research Record – Journal of the Transportation Research Board* 2374: 190-200.

Schust, W.C., and J.A. Elkins. 1997. Wheel Forces during Flange Climb. In: *Proceedings: Joint Rail Conference*, Boston, Massachusetts, March 1997, pp. 137-147.

Shurpali, A.A. R.G. Kernes, J.R. Edwards, M.S. Dersch, D.A. and C.P.L. Barkan. 2013. Investigation of the Mechanics of Rail Seat Deterioration (RSD) and Methods to Improve Rail Seat Abrasion Resistance in Concrete Sleepers. In: *Proceedings: 10th International Heavy Haul Association Conference*, New Delhi, India, February 2013, pp. 127-133.

Stith, J.C. 2005. Railroad Track Pressure Measurements at the Rail/Tie Interface Using Tekscan Sensors. MS Thesis, University of Kentucky, Lexington, Kentucky.

Van Dyk, B.J. 2014. Characterization of Loading Environment for Shared-Use Railway Superstructure in North America. MS Thesis, Department of Civil and Environmental Engineering, University of Illinois at Urbana-Champaign, Graduate College, Urbana, Illinois.

Zeman, J.C. 2010. Hydraulic Mechanisms of Concrete-Tie Rail Seat Deterioration. MS Thesis, Department of Civil and Environmental Engineering, University of Illinois at Urbana-Champaign, Urbana, Illinois.

APPENDIX A: ARTIFICIAL RSD RAIL SEAT LOAD DISTRIBUTIONS

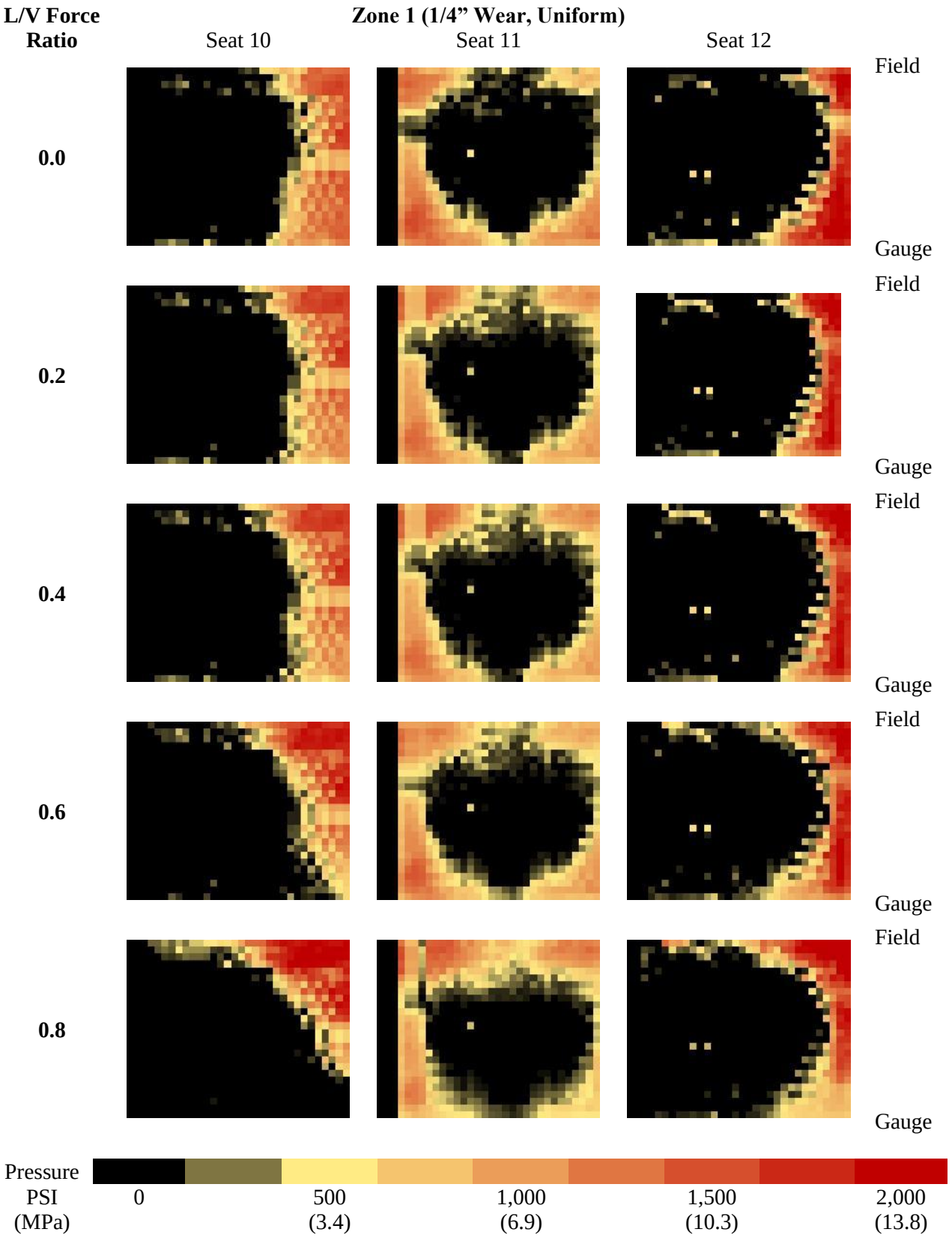

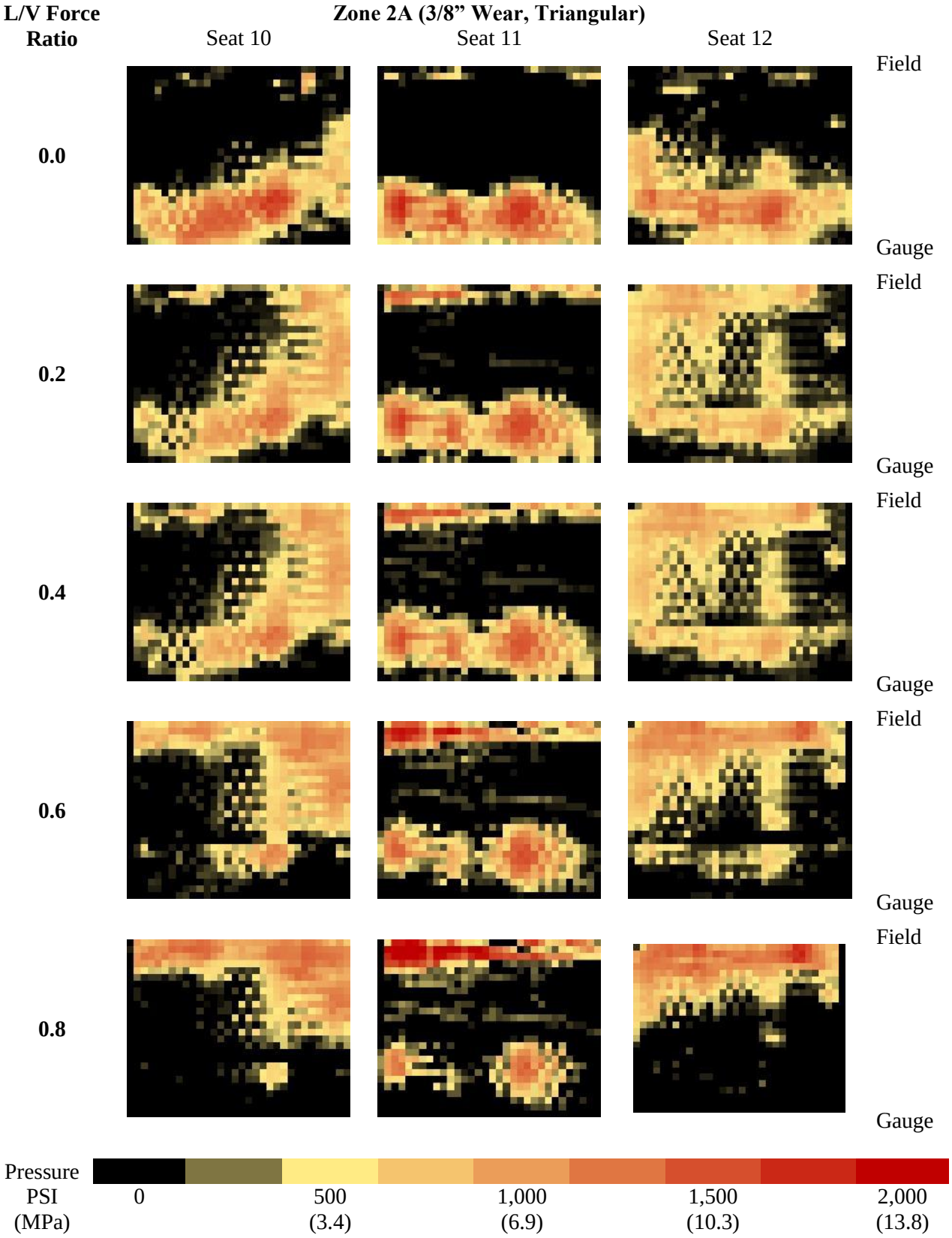
L/V Force Ratio
Zone 2A (3/8” Wear, Triangular)
Seat 10
Seat 11
Seat 12
Field
0.0
Gauge
Field
0.2
Gauge
Field
0.4
Gauge
Field
0.6
Gauge
Field
0.8
Gauge
Pressure
PSI
(MPa)
0
500
(3.4)
1,000
(6.9)
1,500
(10.3)
2,000
(13.8)
L/V Force

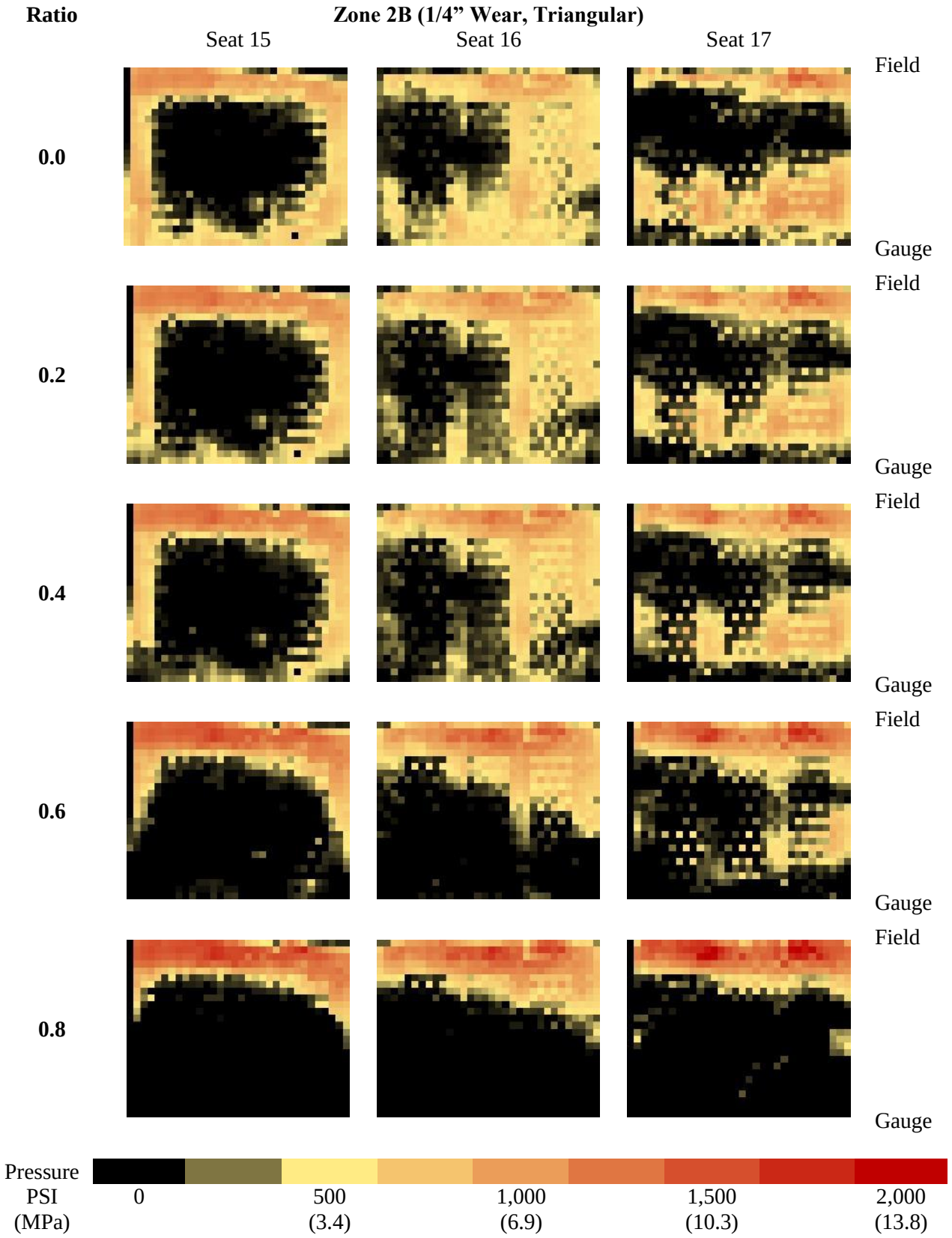
Ratio
Zone 2B (1/4” Wear, Triangular)
Seat 15
Seat 16
Seat 17
Field
0.0
Gauge
Field
0.2
Gauge
Field
0.4
Gauge
Field
0.6
Gauge
Field
0.8
Gauge
Pressure
PSI
(MPa)
0
500
(3.4)
1,000
(6.9)
1,500
(10.3)
2,000
(13.8)
L/V Force

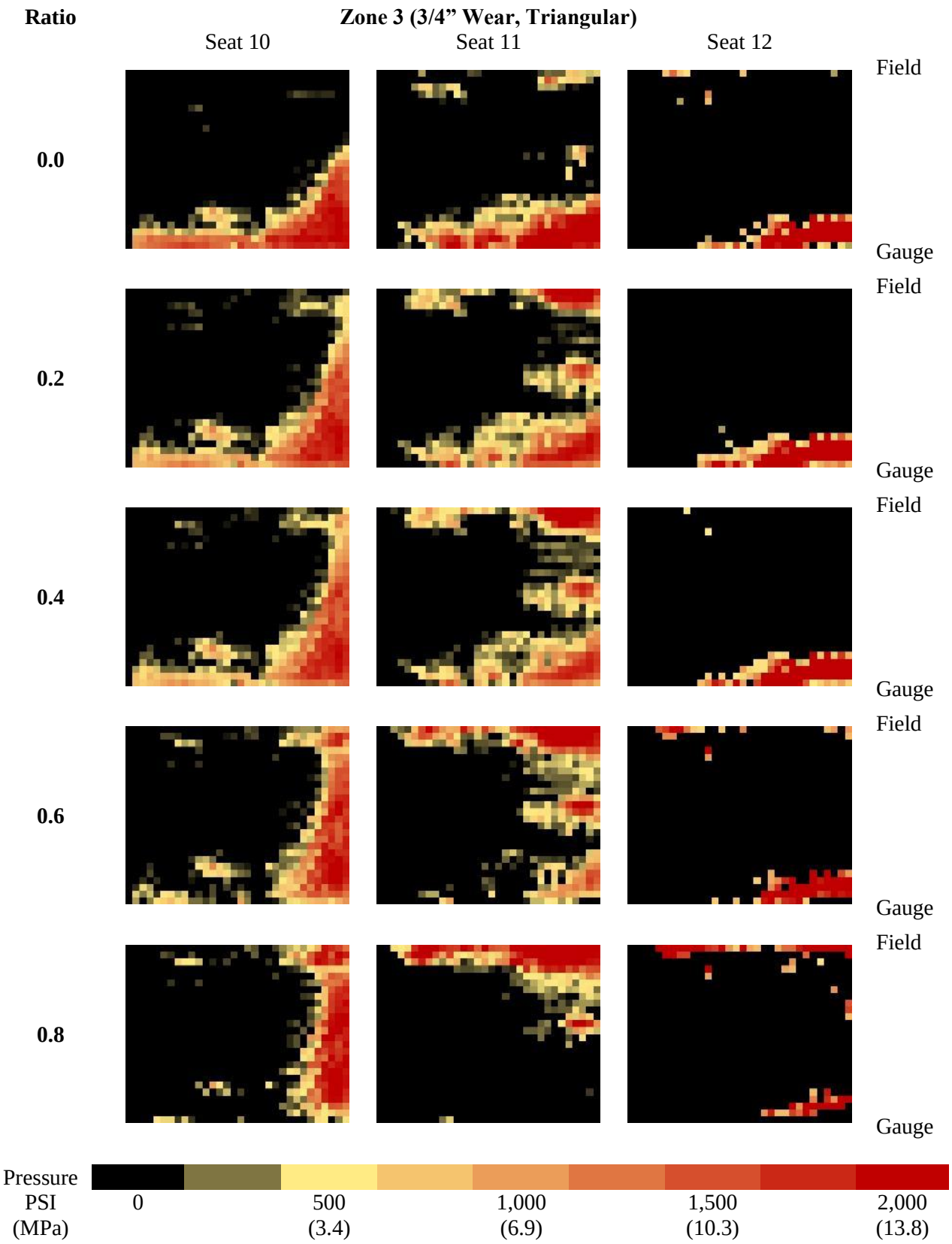
Ratio
Zone 3 (3/4" Wear, Triangular)
Seat 10
Seat 11
Seat 12
Field
0.0
Gauge
Field
0.2
Gauge
Field
0.4
Gauge
Field
0.6
Gauge
Field
0.8
Gauge
Pressure
PSI
(MPa)
0
500
(3.4)
1,000
(6.9)
1,500
(10.3)
2,000
(13.8)

APPENDIX B: ARTIFICIAL RSD RAIL SEAT CONTACT AREA AND PRESSURE GRAPHS

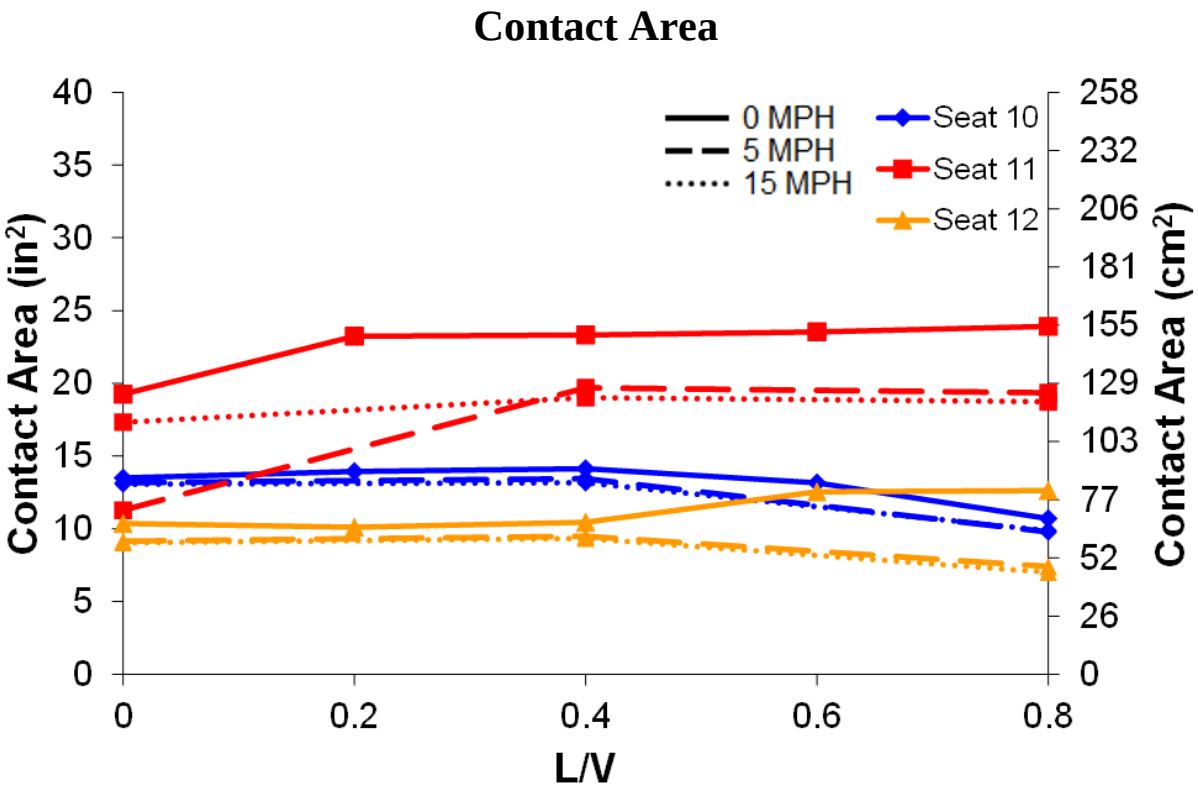

Zone 1

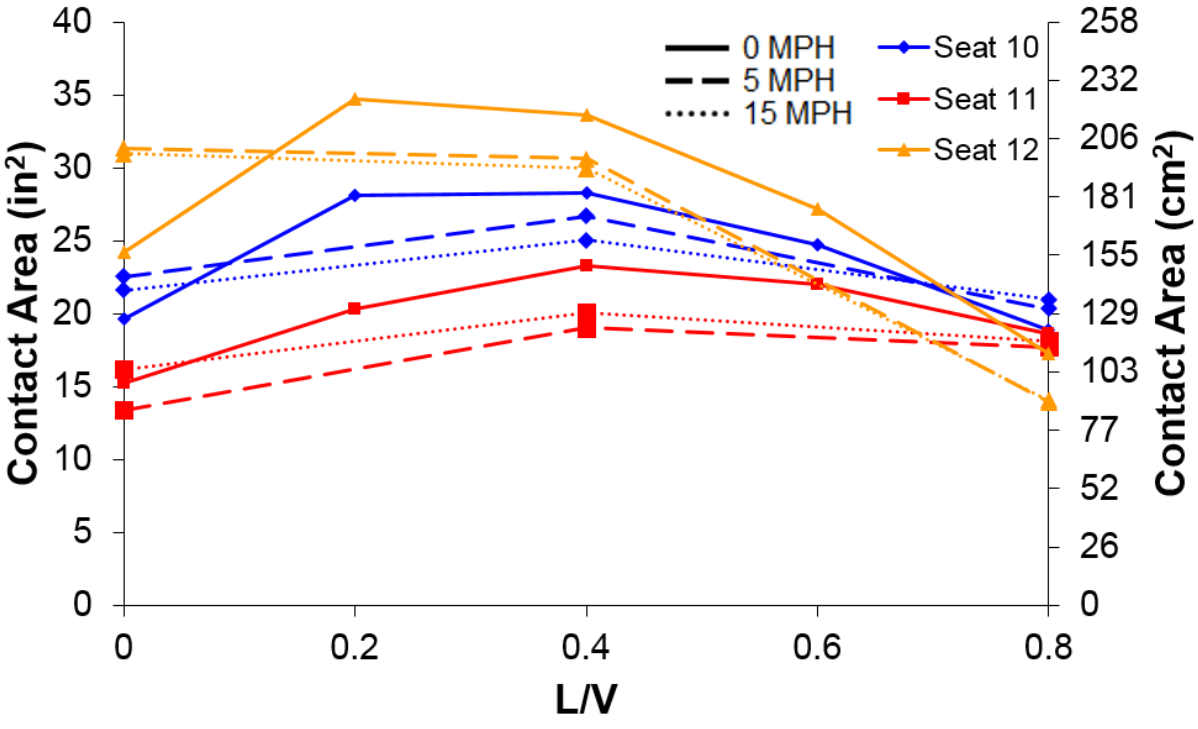

Zone 2A

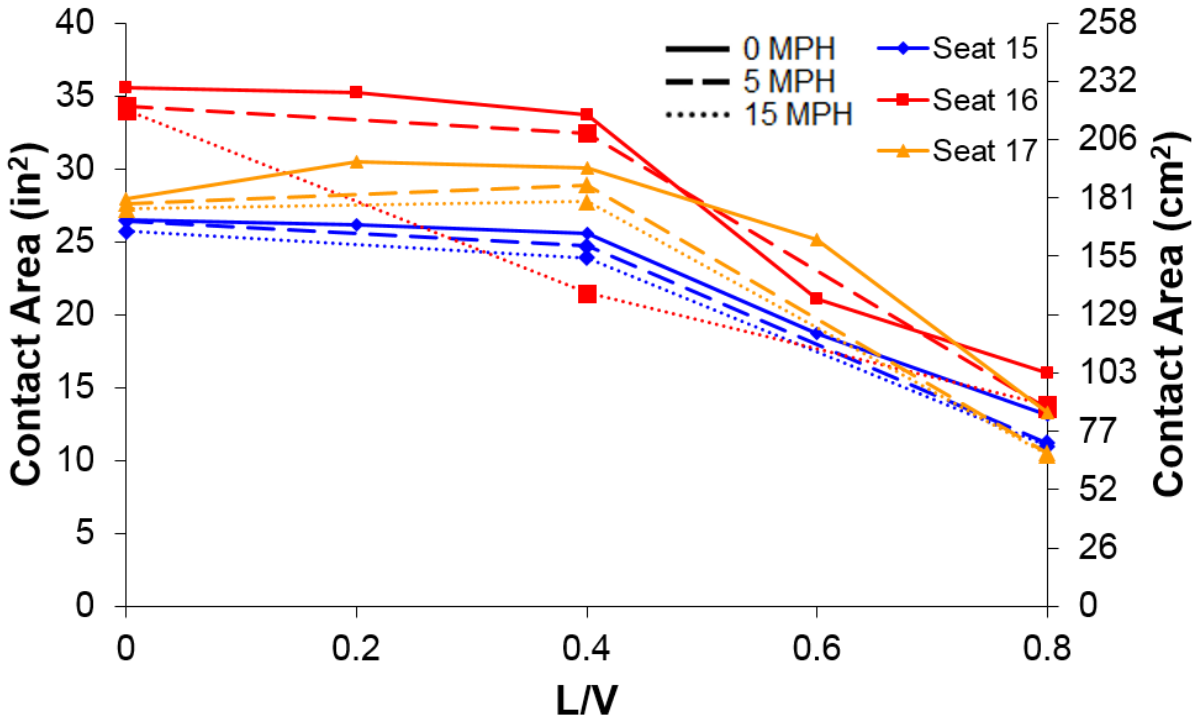

Zone 2B

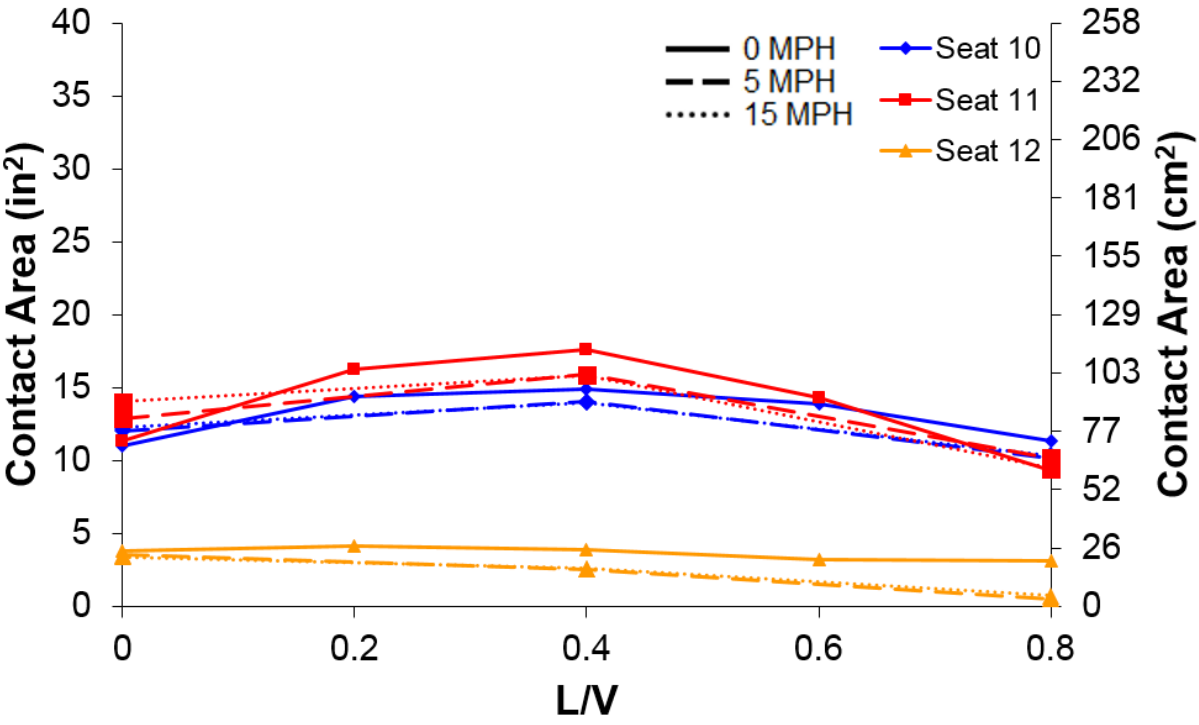

Zone 3

Average Pressure

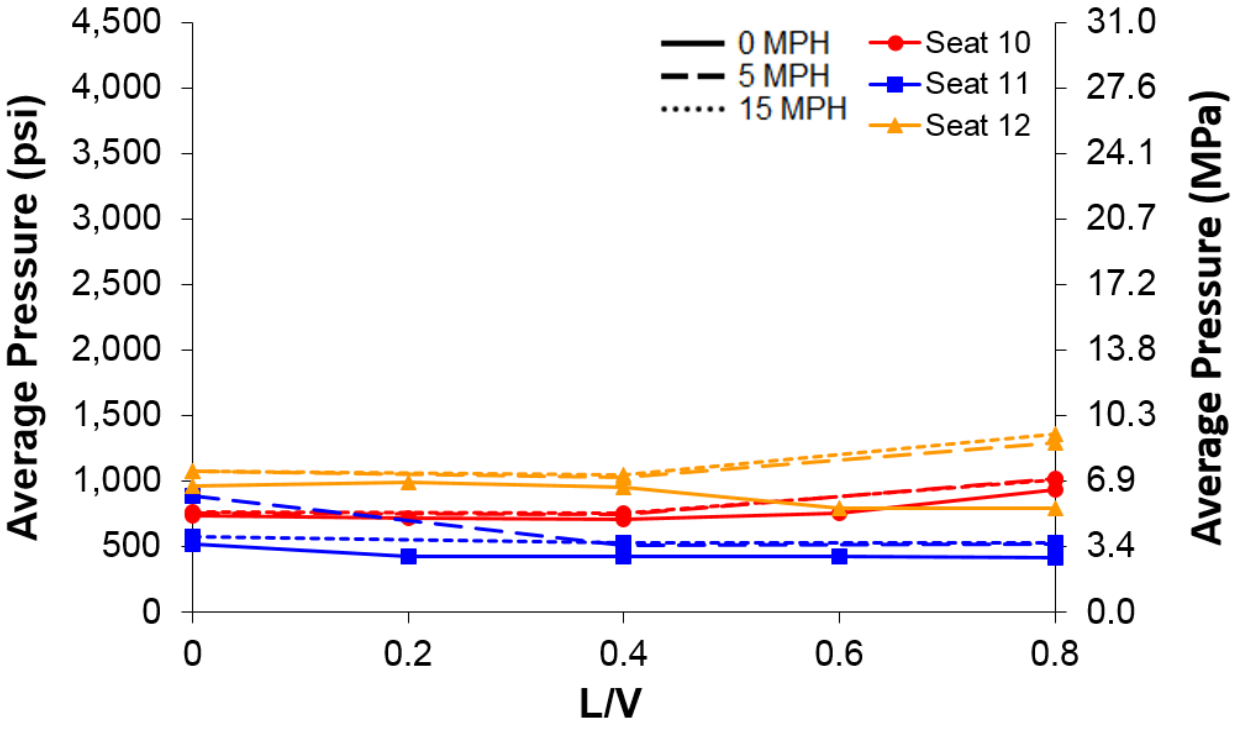

Zone 1

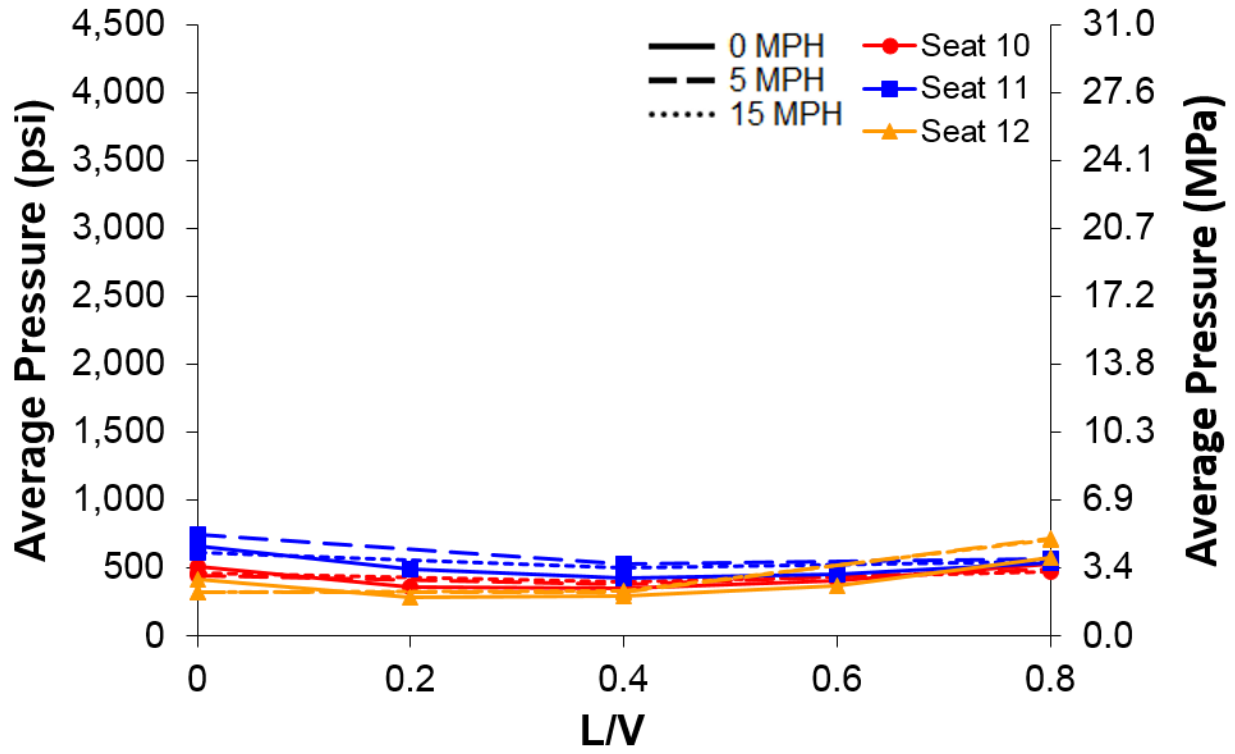

Zone 2A

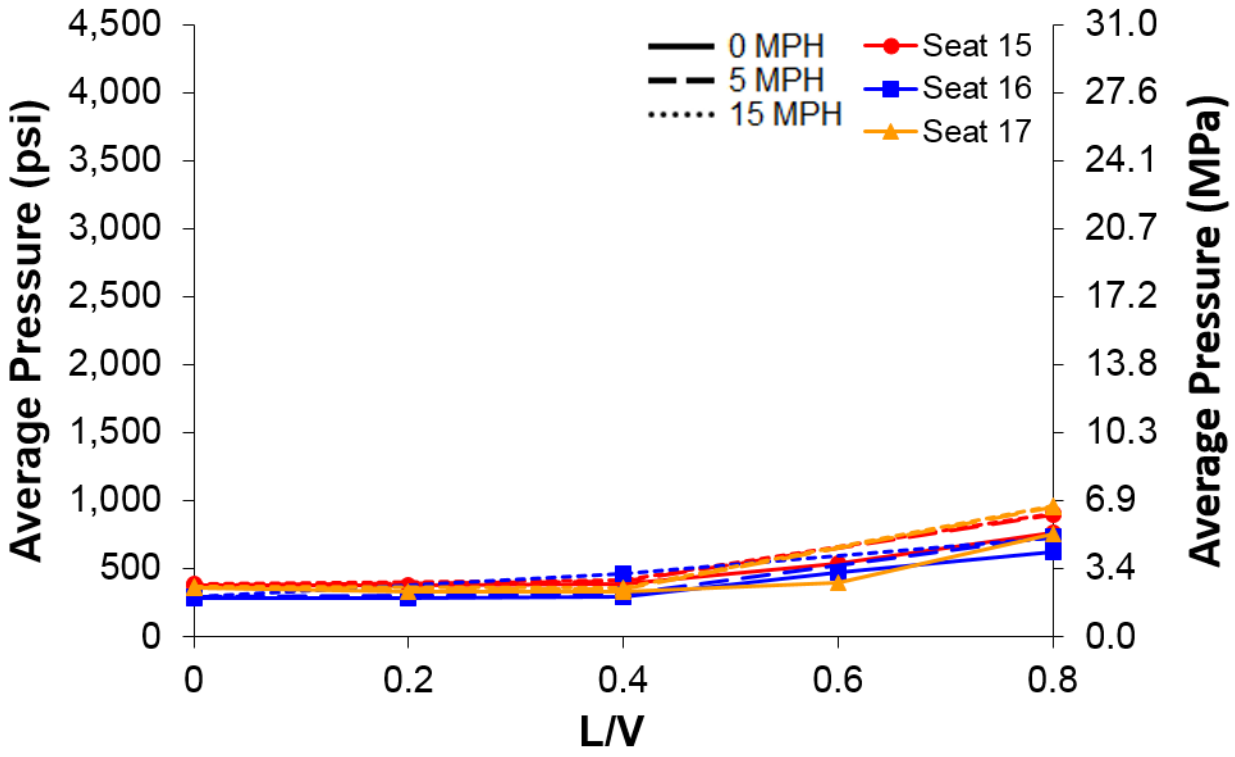

Zone 2B

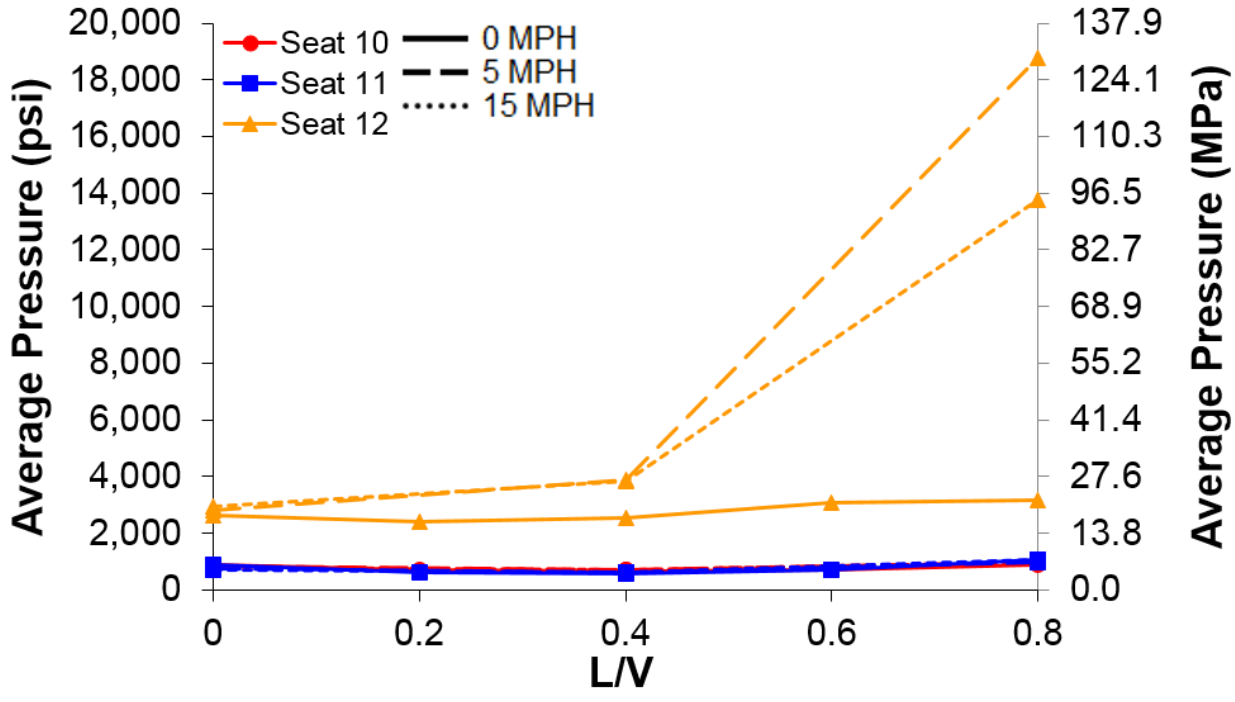

Zone 3

Maximum Pressure

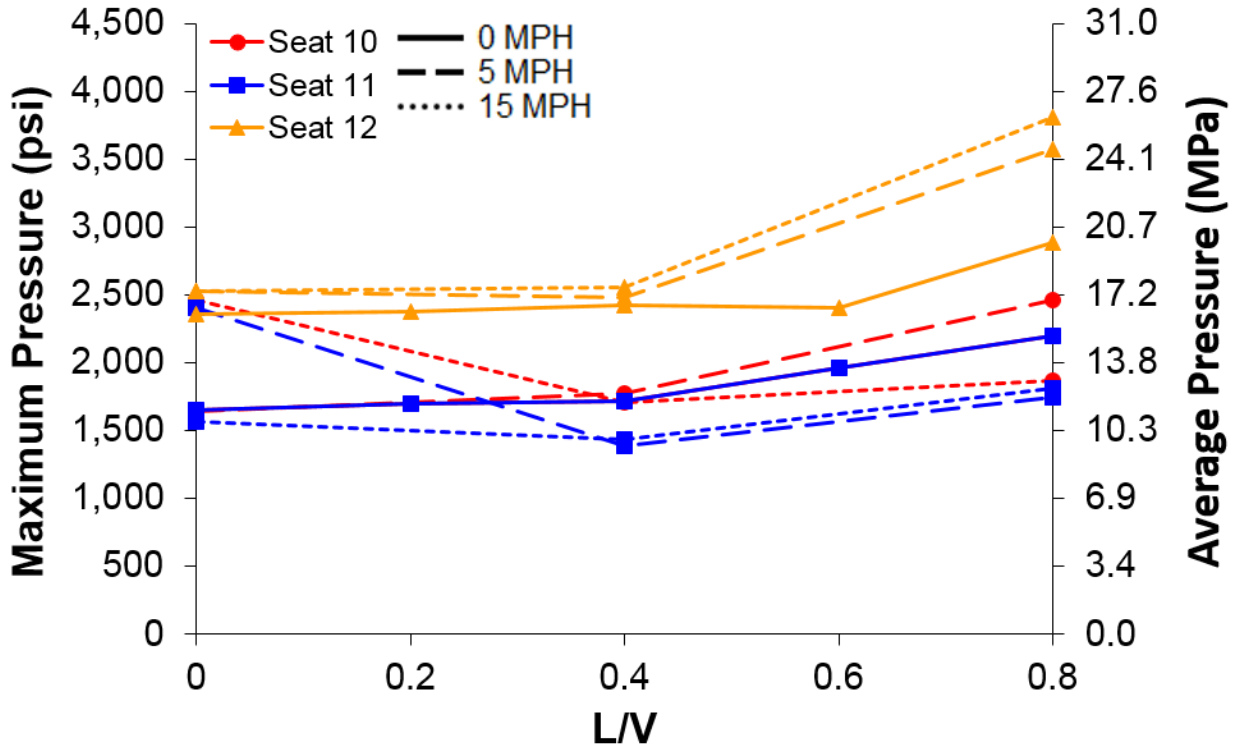

Zone 1

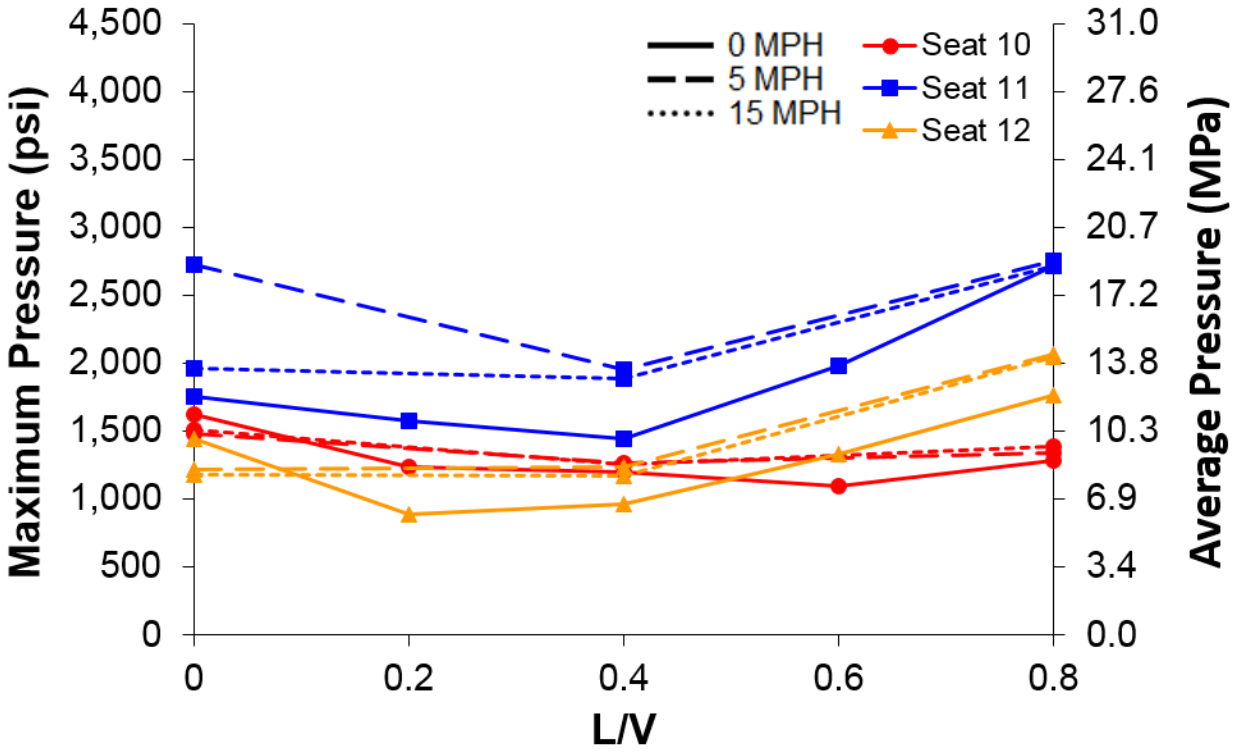

Zone 2A

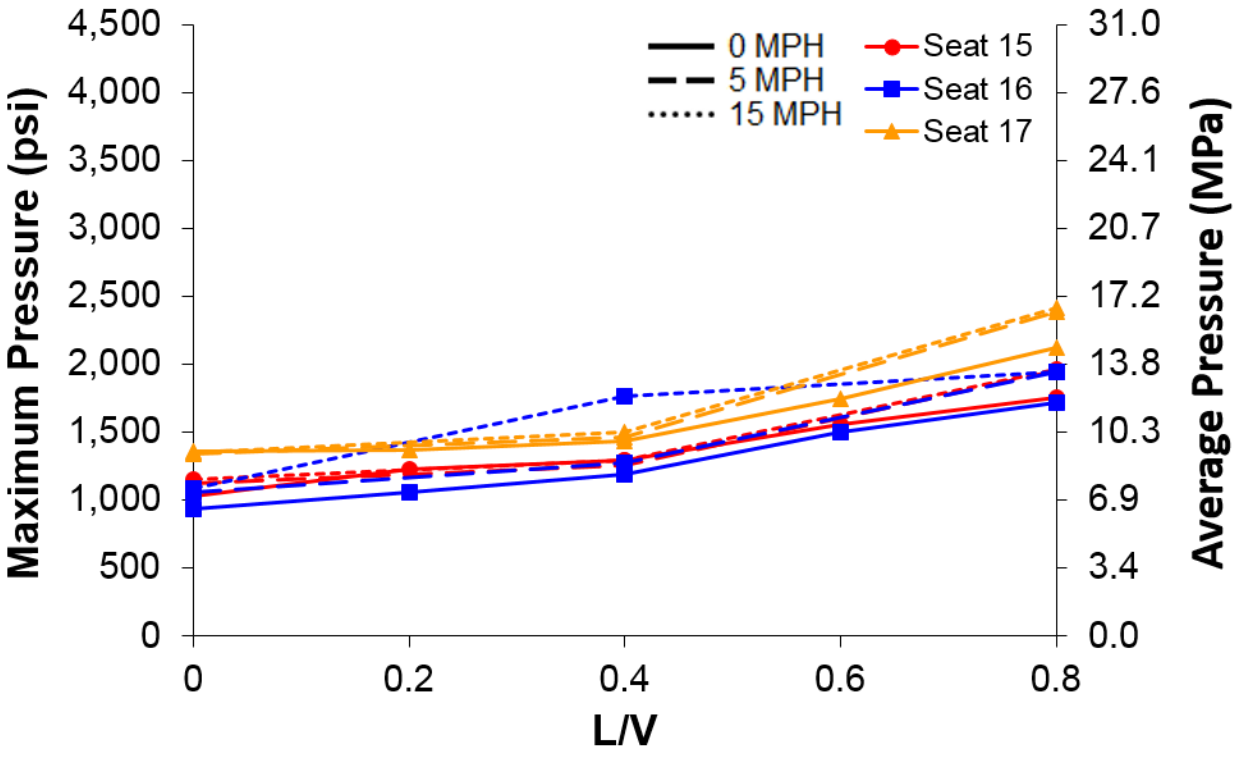

Zone 2B

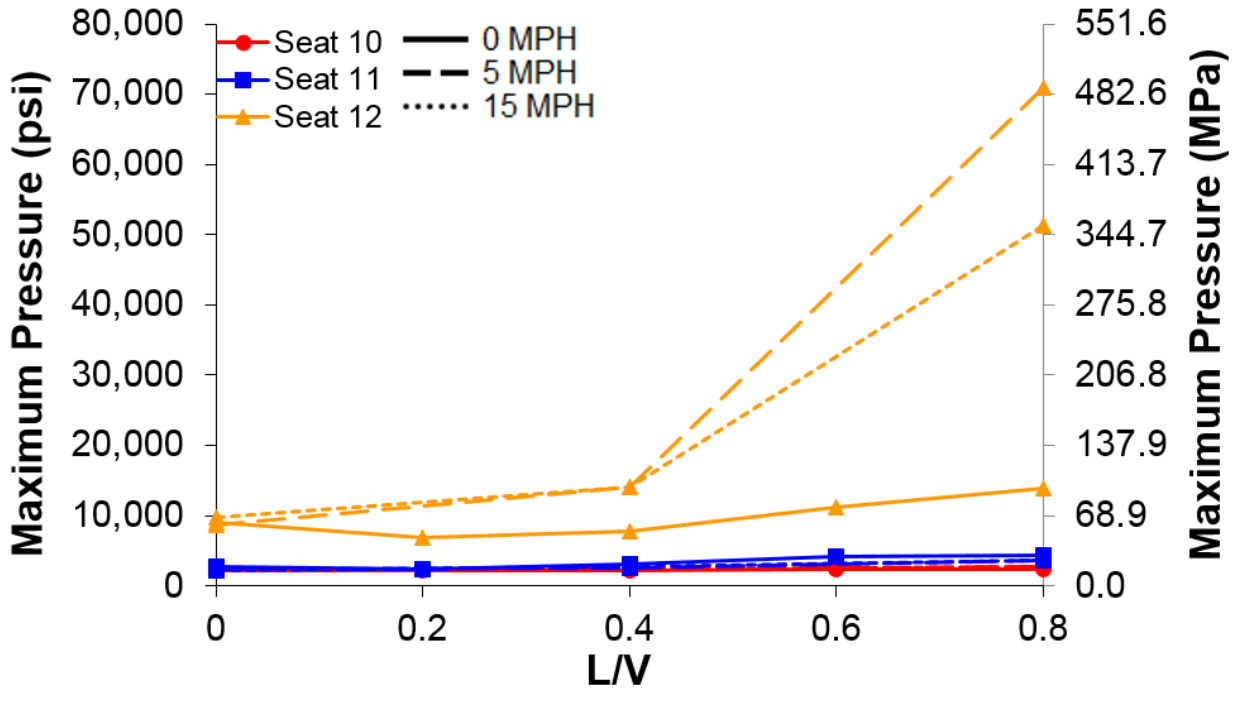

Zone 3